Design and Development of Unconventional pH Differential Fuel Cells

Thesis submitted to the Indian Institute of Science Education and Research in partial fulfilment of the requirements for the degree of

DOCTOR OF PHILOSOPHY

Submitted by

Zahid Manzoor Bhat

Reg. No.: 20163432

Thesis Supervisor: Prof. Muhammed Musthafa O. T.

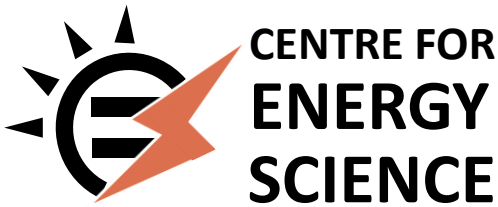

Indian Institute of Science Education and Research (IISER), Pune

May - 2021

भारतीय विज्ञान विक्षा एिं अनुसंधान संस्थान, पुणे

INDIAN INSTITUTE OF SCIENCE EDUCATION AND RESEARCH (IISER), PUNE

(An Autonomous Institution, Ministry of Human Resource Development, Govt. of India)

Dr. Homi Bhabha Road, Pune – 411 008.

Dr. Muhammed Musthafa O. T.

Associate Professor,

Department of Chemistry,

IISER Pune.

CERTIFICATE

This is to certify that this thesis entitled **"Design and Development of Unconventional pH Differential Fuel Cells"** towards the partial fulfilment of Ph.D. programme at the Indian Institute of Science Education and Research, Pune represents original research carried out by **Zahid Manzoor Bhat** at Indian Institute of Science Education and Research, Pune under the supervision of **Prof. Muhammed Musthafa O. T.,** Associate Professor, Department of Chemistry and Centre for Energy Science, IISER Pune during the academic years 2016 - 2021 and that no part of it has been included in any other thesis submitted previously for the award of any degree.

Signature of the Thesis Supervisor **Date: 18th May, 2021**

Dr. Muhammed Musthafa O. T.

Associate Professor,

Department of Chemistry and Centre for Energy Science,

IISER Pune.

भारतीय विज्ञान विक्षा एिं अनुसंधान संस्थान, पुणे

INDIAN INSTITUTE OF SCIENCE EDUCATION AND RESEARCH (IISER), PUNE

(An Autonomous Institution, Ministry of Human Resource Development, Govt. of India)

Dr. Homi Bhabha Road, Pune – 411 008.

DECLARATION

I hereby declare that the matter embodied in the thesis entitled **"Design and Development of Unconventional pH Differential Fuel Cells"** are the results of the investigations carried out by me at the Department of Chemistry and Centre for Energy Science of the Indian Institute of Science Education and Research, under the supervision of **Prof. Muhammed Musthafa O. T.,** Associate Professor, Department of Chemistry and Centre for Energy Science, IISER Pune and that no part of this thesis has been included in any other thesis submitted previously for the award of any degree.

Signature of the student **Date:** 18th May, 2021

Zahid Manzoor Bhat

Reg. No: 20163432

IISER Pune.

ACKNOWLEDGEMENT

First and foremost, all praises to the Almighty Allah for showering his blessing over me throughout my research journey. The Ph.D. journey became a very memorable journey of my life with a lot of memories. There were always some people who stood by me in every situation, without whom my journey could have been incomplete. So, before I discuss my Ph.D. journey, I would like to give my gratitude to them and sincerely apologize for any omissions.

I would like to give my sincere thanks to my thesis supervisor Dr. Muhammed Musthafa O.T for his constant support, encouragement and his priceless suggestions during my entire Ph.D. time. He always stood behind me in every odd and even situation. The freedom he provided me to execute my research projects in the best possible way is worth to remember. I have learned a lot about research planning and execution during discussions with him which has helped me to get an enhanced interest in pursuing research in the future. I can't forget the kind of inspirations and encouragements that he presented during the tough moments of my journey in his lab. Apart from the research the coffee time discussions with him in his cabin and friendly chats while exploring different cafés in pune require a special mention.

I would like to express my sincere gratitude to my research advisory committee (RAC) members, Dr. Manjusha V. Shelke (NCL, Pune) and Dr. Angshuman Nag (IISER Pune) for their valuable suggestions during the RAC meetings. Through their suggestions, it became possible for me to push my boundaries beyond my thinking. Sincere thanks to all the collaborators for being a part of this journey. I would like to express my gratitude to Prof. Stefan A. Freunberger (Institute of Science and Technology, Austria) and Prof. Shane Ardo (University of California, Irvine) for valuable discussions and support in shaping my experimental results in the best possible way. I would also like to thank Dr Muhammed Mamlouk (University of Newcastle, UK) for being the helpful host and allowing me to work in his lab. during my visit to the University of Newcastle under SPARC India program. A special mention to former lab member Dr Ravikumar (Research Associate Newcastle University) who has helped me through during the experimental design and operation throughout the Ph.D journey.

I am very much indebted to my current lab mates Dr. Alagar Raja, Manu, Soumodip, Neethu, Sanchayita, Ritwik, Vishnupriya, Muskan and Rahul who have provided me a healthy lab atmosphere and their supportive and friendly nature made my journey a lot more enjoyable and exciting. I am highly thankful to Alagar for being a nice friend and helping me a lot during this journey with his helpful inputs and friendly conversations both in and outside the lab. A special thanks to the partner in crime Neethu for all the fun fights, lovely moments and eatables I used to take from your room. Starting from the morning tea to the dinner parties it has been a wonderful set of memories that cannot be expressed in words. A word of thanks to Sanchayita for the fun filled company in the lab, late-night walks and the chats in and outside the lab.

I would like to convey my love and regards to all my past lab mates, Dr. Ravikumar T, Dr. Mruthyunjayachari. C. D., Dr. Shahid P Shafi, Dr. Chidananda, Dr. Rajkumar, Dr, Shateesh, Dr. Shambulinga, Sabbah, Swapnil, Siddhi, Abdul,

Fawaz, Pramod, Zeeshan, Heena, Balla, Digvijay, Sarvajith, Deepraj Thamaraichelvan, Giddaerappa, and Mahesh. A special mention to Siddhi for bring a very close buddy in and outside the lab and for the kind of positivity you bring to me all the time. I offer my special thanks to Dr. Mruthyunjayachari. C. D for being very helpful and friendly.

I would like to give my heartiest thanks and regards to all the academic and non-academic staff, especially Sandeep, Anil, Yatish, Tushar, Sayalee, Priyadarshini, Prabhas, Prabhakar, Mayuresh, Suresh, Meghna for being extremely helpful throughout my stay at IISER Pune. A special thanks to the housekeeping staff for keeping research laboratories and the institute clean and tidy all the time.

I am extremely thankful to the Council of Scientific and Industrial Research (CSIR) - India for providing me the Ph.D. fellowship and support to attend various national/international conferences. My appreciations also extend to American Chemical Society (ACS), Royal Society of Chemistry (RSC), John Wiley & Sons, Elsevier Science Ltd., Springer, etc. for accepting and publishing my research articles and also their permission to reprint the materials under copyright. I also thank SPARC india program for sponsoring my visit to the Newcastle university UK.

All the friends in and outside the IISER need a special mention as they have been there for me through my ups and downs. I spend joyful moments at IISER with my friends Saleem, Javid, Jabed Hossain, Danish, Nayeem bhai, Waseem Manzoor, Tariq, Habib, Motalib, Firdousi, Shabnam, Sarita, Dilsha, Rukhsana who made my stay at IISER pleasant and enjoyable. A special mention to Firdousi for the food and company outside the lab. You have been the kind of person I can count on anytime in life. Thanks to Sadhna Bansal (NCL pune) for being nice and supportive friend. Thanks to my friendzone outside IISER Feroz, Yaseen, Bilal, Zahid, Mohsin, Mudasir, Arjumand, Safiya, who have there even before the start of this journey. This acknowledgement will be incomplete without mentioning Saleem who is more of a brother than friend. I am highly thankful to my beloved Aalia Qureashi for being an important part of my life and this journey. She has been a constant support encouraging me all the time. I thank you for being so much understanding and managing my stress levels. Without your support and love this journey would have been much more difficult.

And most of all, I would like to share this moment of happiness with my loving, supportive, encouraging family for backing me up throughout my academic journey. The support of my guardians, parents, brother and sisters has been unconditional all these years and without their encouragement, prayers and understanding this journey would have been impossible. I very fondly acknowledge my brother-in laws for their love and support. It is my great pleasure to acknowledge my late guardian (Ab. Kabir Dar) to whom I owe the most. You bought me up and pampered me in every corner of my life. I miss you the most.

Zahid Bhat

Dedicated

to my guardian (late Ab. Kabir Dar)

Table of Contents

Synopsis of the thesis entitled "Design and Development of Unconventional pH Differential Fuel Cells"

21st century is witnessing serious energy crisis due to the depletion of fossil fuels and variability of renewable energy sources which in turn has increased the importance of electrochemical energy storage and conversion devices to level the mismatch between energy generation and demand. Proton exchange membrane fuel cells (PEMFCs) have been a forerunner in the domain of sustainable energy chain as they can convert the chemical energy stored in H_2 and O_2 into electrical energy at a higher efficiency. However, the issues with the production and storage of the H_2 fuel has led to the development of liquid fed fuel cells such as direct alcohol fuel cells (DAFC). But these DAFCs suffer from various issues mainly related to their cathodic interface like low oxygen reduction reaction kinetics, alcohol cross over, parasitic chemistry, depolarization losses, carbon corrosion etc. which impede their commercialization. Strategies like the development of alcohol tolerant cathodic electrocatalysts are being adopted to address these issues, however, the necessity of heavy loading of cathode catalysts and limited concentration range of alcohol tolerance still pose critical challenges to further develop DAFC.

Differing from the previous strategies, the primary aim of this thesis is to develop unconventional fuel cells by employing pH dependent/independent redox couples. In this thesis, by employing a pH independent outer sphere redox couple, issues related to the cathodic interface of the state of the art DAFCs is addressed. By employing a pH dependent redox couple, additional functionalities such as alcohol reformation could be integrated to a DAFC reaction pathway during electricity production. Thermodynamic calculations showed the participation of electrochemical neutralization in alcohol reformation and hence attempts were dedicated to harvest it directly using pH dependent hydrogen redox reaction. Electrochemical neutralization without a net

redox reaction, offered a unique pathway for desalination of saline water in a process that involves only gases, water, H^+ and OH^- with minimal chances of water contamination. The thesis is divided into following Chapters.

Chapter 1. Introduction: This chapter explains the working principle, architectural components and issues with the state of art hydrogen and alcohol fuel cells. The major issue with the hydrogen-based fuel cells is related to the hydrogen production which is discussed in detail in this Chapter. Major issues associated with the cathodic interface of a state of the art DAFC are highlighted with the current solutions available in the literature.

Chapter 2. A Direct Alcohol Fuel Cell Driven by a pH Independent Redox Couple: This chapter discusses the implications of modifying the cathodic interface of a direct alcohol fuel cell (DAFC) with a pH independent outer sphere redox couple. The modification of the cathodic interface with the outer sphere redox couple led to a DAFC with performance metrics ~8 times higher than Pt based DAFC-O_2 fuel cell, Figure 1. This Chapter also discusses in detail how the modification with an outer sphere redox couple can address the parasitic chemistry and depolarization losses associated with methanol crossover, Figure 1.

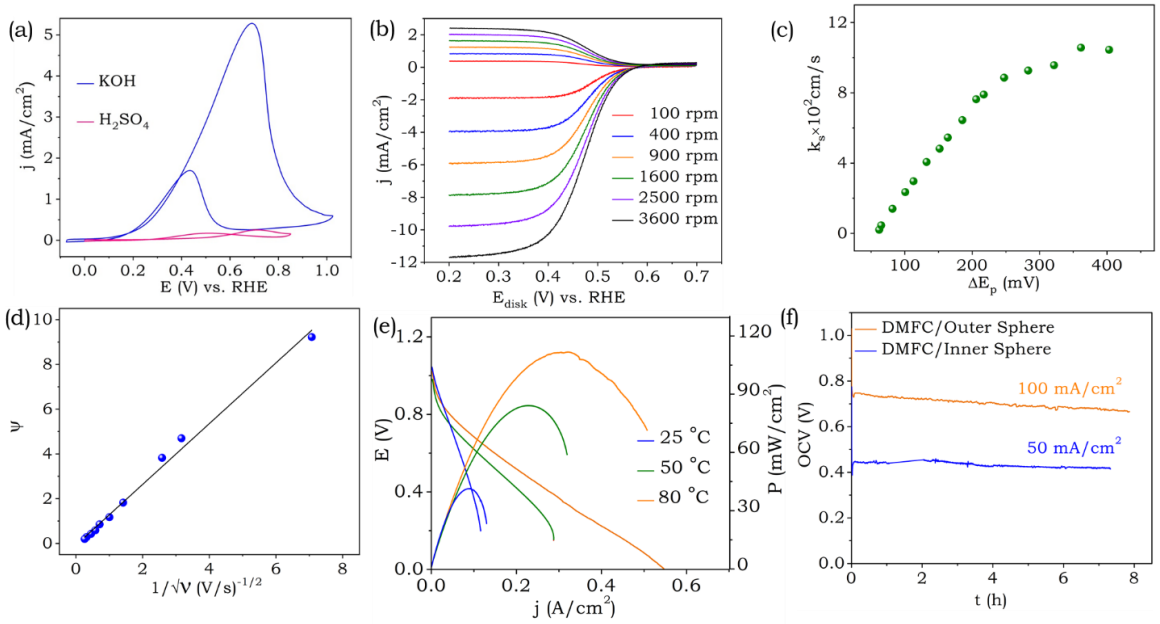

Figure 1. (a) Cyclic voltammograms of methanol (0.5 M) oxidation on a Pt/C electrode at a scan rate of 20 mV/s in 0.5 M H_2SO_4 and 1 M KOH, (b) rotating ring disk electrode measurements for potassium ferricyanide (10 mM) with a glassy carbon disk electrode and a platinum ring electrode. (c) Variation of heterogeneous rate constant with peak potential separation as per Klinger and Kochi method and (d) the plot for the Nicholson function vs. inverse square root of scan rate. (e) Polarization curves of DMFC-ferricyanide (3 M Methanol in 2 M KOH as anolyte and 0.6 M potassium ferricyanide in 2 M KOH as catholyte) fuel cell at different temperatures. Anode Pt loading was 0.5 mg/cm^2 and cathode carbon loading was 1 mg/cm^2. (f) Galvanostatic polarization curves for the DMFC-ferricyanide (at 100 mA/cm^2) and Pt based DMFC-O_2 (at 50 mA/cm^2) fuel cells at 80^{o}C.

Chapter 3. A Direct Alcohol Fuel Cell Driven by a pH Dependent Redox Couple: This chapter demonstrates how the cathodic interface modification with a pH dependent hydrogen redox couple could add new functionality to the DAFC reaction pathway. In this chapter, the design and performance of an alcohol reforming fuel cell (ARFC) wherein alcohol reformation is coupled with the electricity production is discussed in detail. The thermodynamic calculation showed that alcohol reformation which is otherwise a high temperature/pressure catalytic process can be driven at room temperature and pressure during electricity production with the simultaneous generation of pure hydrogen by utilizing the electrochemical neutralization reaction as the driving force. ARFC chemistry is unusual because of its distinctly positive entropic heat which allows ~56 % of the total available energy to be harvested from the surroundings leveraging a thermodynamic efficiency as high as 2.67. This ARFC demonstrates an energy density of ~253 Wh/kg with ~62 % of methanol to hydrogen conversion, Figure 2. Since the hydrogen fuel produced is free from carbon containing impurities, ARFC can be directly utilized as a fuel reservoir for a H_2-O_2 fuel cell in a tandem configuration, Figure 2.

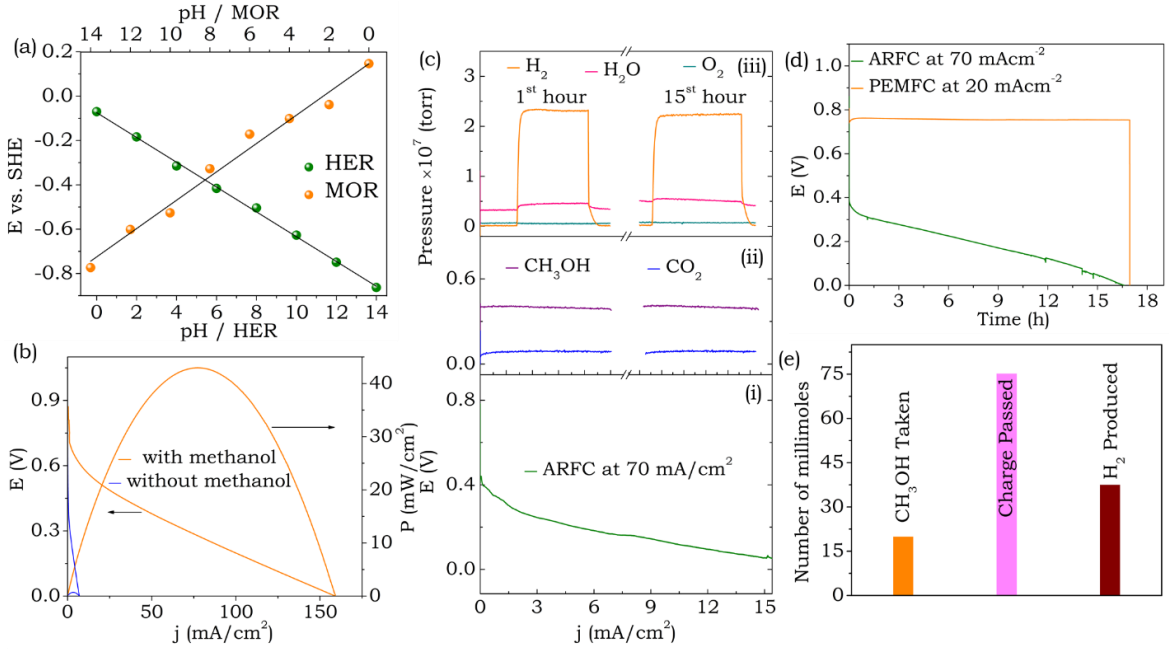

Figure 2. (a) Pourbaix diagrams for methanol oxidation reaction (MOR) and hydrogen evolution reaction (HER), (b) polarization curve for alcohol reforming fuel cell (ARFC) with methanol as the fuel (2 M methanol in 6 M KOH as the anolyte and 3 M H_2SO_4 as the catholyte), and (c) (i) Chronopotentiometry at 70 mA/cm^2, (ii) and (iii) are the corresponding in-situ electrochemical mass spectrometry from the (ii) anodic and (iii) cathodic half-cells of the ARFC during intermittent operation (1 h off/on). (d) Voltage versus time upon feeding an air breathing PEMFC at 20 mA/cm^2 with the cathodic exhaust of an ARFC at 70 mA/cm^2. This demonstrates electric power generation during H_2 production (from methanol-to-H_2 reforming) as well as H_2 utilization and (e) charge passed vs. H_2 produced and methanol consumed. For the ARFC, electrocatalyst loadings were 1 mg/cm^2 of Pt-Ru/C at the anodic half-cell and 1 mg/cm^2 of Pt on Ti mesh at the cathodic half-cell. For the air breathing PEMFC, electrocatalyst loadings were 1 mg/cm^2 of Pt/C at the anodic as well as cathodic half-cells.

Chapter 4. Direct Harvesting of Neutralization Energy as Electrical Driving Force: This chapter demonstrates a strategy for the direct harvesting of energy of neutralization as electrical driving force which is

otherwise impossible as acid base neutralization is not a redox reaction. In this Chapter, by utilizing a pH dependent hydrogen redox reaction, it is shown that energy of neutralization can be directly harvested as electrical driving force without a net redox reaction/consumption of fuel, Figure 3. This electrochemical neutralization cell employs H^+/H_2 redox couple to perform the neutralization reaction in an electrochemical pathway and the positive entropy change of the reaction allows nearly 30% of electrical energy to be harvested from the surroundings. The electrochemical neutralization cell (ENC) delivered a peak power density of ~70 mW/cm^2 at a peak current density of ~160 mA/cm^2 with a cathodic H_2 output of ~80 mL in 1 hour. In this Chapter, it is illustrated that the energy benefits from the same fuel stream can be amplified by directing it through ENC prior to a PEMFC in a tandem configuration.

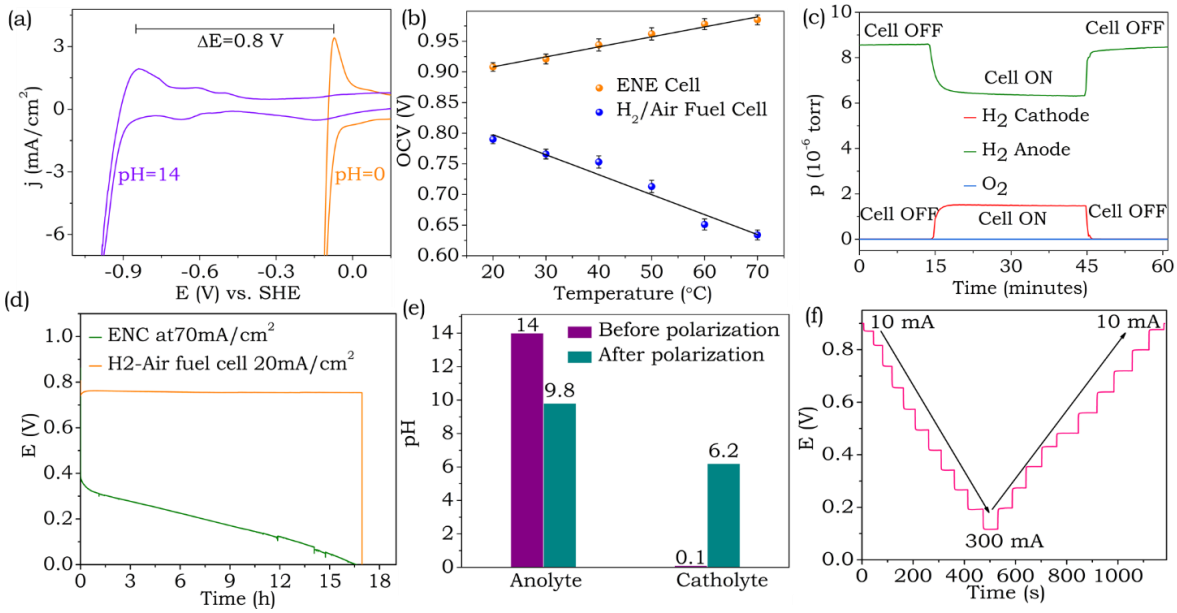

Figure 3. (a) Cyclic voltammograms for HER/HOR redox reactions at pH = 0 and pH = 14, and (b) plot of open circuit voltage vs. cell temperature for the electrochemical neutralization device (orange trace) and H_2/air fuel cell (blue trace). The lower OCV of H_2-air fuel cell could be due to the lower partial pressure of oxygen in air. (c) In-situ electrochemical mass spectrometry for the anodic and cathodic half-cells and (d) galvanostatic polarization of electrochemical neutralization cell at 160 mA/cm^2 when it

is connected to an air-breathing PEMFC (discharged at 20 mA/cm^2). (e) Corresponding pH measurements at anodic and cathodic half-cells before and after galvanostatic polarization and (f) step current discharge of ENC.

Chapter 5. An Electrochemical Neutralization Cell for Spontaneous Water Desalination: This chapter discusses the applications of direct harvesting of neutralization energy as electrical driving force for spontaneous water desalination. The chapter discusses the design, principle and performance of a 3-compartment electrochemical cell for simultaneous water desalination during electricity production. This pathway is unprecedented because desalination is achieved in the electrochemical neutralization cell without irreversibly consuming free energy stored in expensive metals as in redox flow batteries and metal ion batteries but by just interconverting the energy of neutralization as an electrical driving force. The device uses acid and alkali as fuels for desalination by performing reversible redox reactions involving only gases, water, H^+ and OH^- (Figure 4) such that the products and reactants of the redox reactions do not poison the desalinated water as in the state-of-the-art electrodialysis process. The electrochemical desalination cell driven by the electrochemical neutralization demonstrates performance metrics comparable to the state-of-the-art desalination processes reported in the literature (Figure 4).

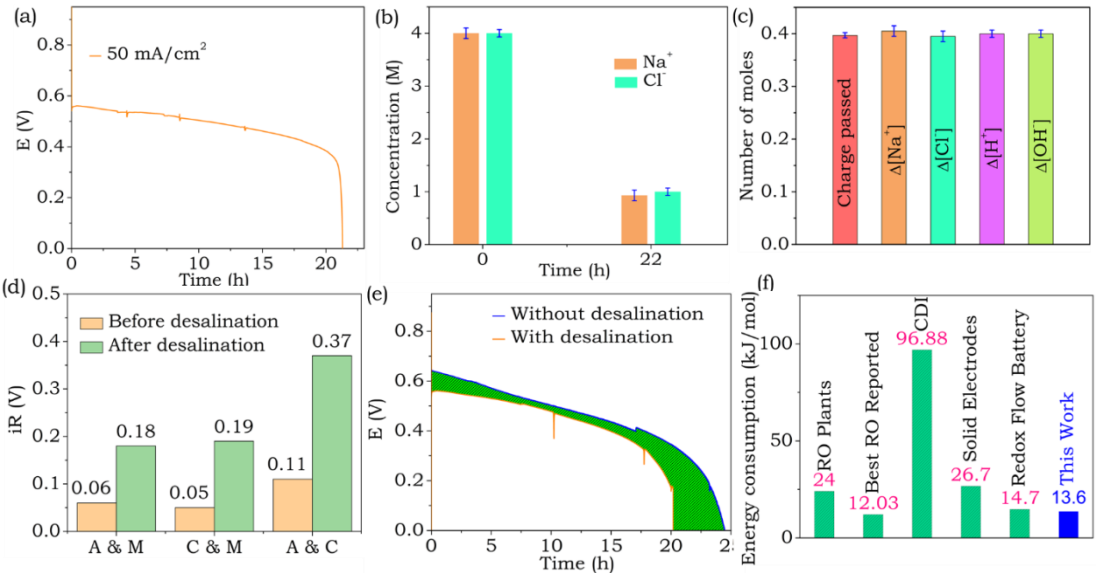

Figure 4. (a) Galvanostatic discharge of the electrochemical neutralization cell for water desalination at a current density of 50 mA/cm^2, (b) concentration of Na^+ ions measured by Microwave Plasma Atomic Emission Spectroscopy (MP-AES), and concentration of Cl^- ions measured by Mohr's titration method before and after long term discharge and (c) amount of charge passed vs. consumption of H^+ ions in the cathodic half-cell and OH^- ions in anodic half-cell and changes in the number of moles of Na^+ and Cl^- ions in the middle saline compartment, (d) comparison of *iR* drops before and after desalination (A, M and C represent anodic, middle and cathodic compartments, respectively). In panel d, *iR* drop is calculated by multiplying the area specific resistance with the current density of 50 mA/cm^2. (e) Galvanostatic discharge of the electrochemical neutralization cell at a current density of 50 mA/cm^2 with (orange trace) and without (blue trace) middle saline compartment and (f) comparison of the energy efficiency of desalination in the electrochemical neutralization cell with reverse osmosis, metal ion batteries and capacitive deionization.

Chapter 6. **Conclusions:** This chapter provides a brief summary and future outlook of the work reported in the thesis.

Taken together, the work outlined in the thesis on electrochemical neutralization provides a plethora of opportunities in electrochemical energy storage and conversion devices as outlined in Scheme 1

Scheme 1. Application of electrochemical neutralization for the development of unconventional fuel cells.

Chapter 1

Introduction

1.1. Introduction

The electricity is the foundation of the modern world which has proved to be a deciding factor in taking the world from dark age to the present developed modern age. The prime source for the electricity production has been the fossils fuels, but immoderate use of fossils fuels led to their depletion along with the global warming.[1-3] The present known reserves of oil, natural gas and coal will last for 41, 64 and 155 years respectively, if the consumption and production of this sources will continue at constant rate in the future.[1-3] The alarming rise in the energy demands with the growing population and environmental effects of the fossil fuel consumption have led to the search for alternative sources of energy. As such the world is moving from non-renewable sources to renewable sources of energy.[2-4] The sustainable and renewable sources for electricity production are hydroelectric, biomass, wind, solar, geothermal, and marine tidal. However, these sources of energy have got seasonal and geographical variations which demand their storage at the time of availability and conversion at the time of demand. Thus, there is a gap between the availability and demand with respect to these renewable sources of energy.[2-6] The electrochemical storage and conversion technologies such as batteries, supercapacitors, solar cells and fuel cells play important roles in sustainable energy landscape as these can bridge the existing gap between energy availability and energy demand.[5-7] Generally, these electrochemical energy devices offer high efficiency with low pollution to the environment and are also flexible with their construction. There are various types of electrochemical energy devices: fuel cells, batteries, supercapacitors and water electrolyzers. Fuel cells and water electrolyzers are considered to be electrochemical energy conversion devices whereas batteries and supercapacitors are energy storage devices which differ in their charge storage mechanisms.

1.2. Fuel Cells

Fuel cells are defined as electrochemical energy conversion devices which convert chemical energy of fuels directly into electrical energy. The

architectural components of a fuel cell are shown in Figure 1.1. It consists anodic electrocatalyst where the oxidation reaction takes place and a cathodic electrocatalyst where reduction reaction takes place.[8-10] These two half-cells are separated by an ion exchange membrane which conducts the ions during the redox reactions whereas electrons move through the outer circuit powering the load.[11-13]

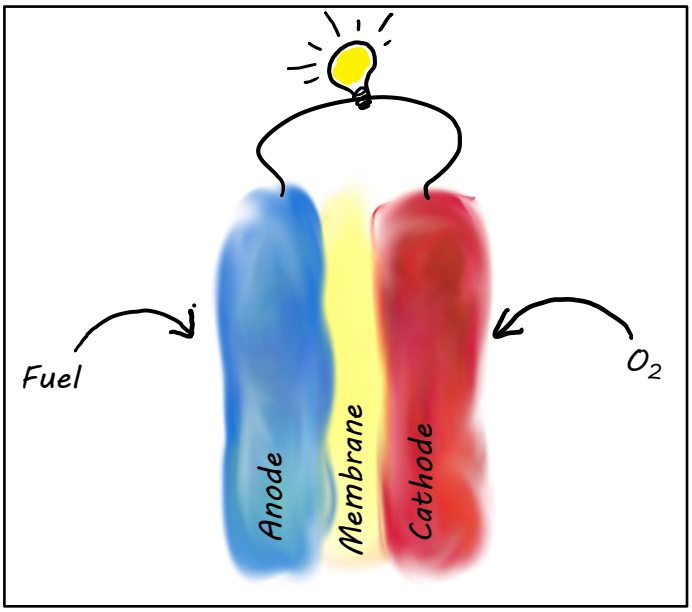

Figure 1.1. Schematic representation of a fuel cell.

The first fuel cell was discovered by Sir William Robert Grove, a Welsh judge, inventor, and physicist in 1839 which he named it as gas battery. He mixed hydrogen and oxygen in the presence of an electrolyte and produced electricity and water.[14,15] Although it didn't produce enough electricity to be useful but it paved a way for the future development of fuel cells. The term “fuel cell” was first coined by Ludwig Mond and Charles Langer in 1889, who attempted to build a working fuel cell using air and industrial coal gas.[16] There are also reports that William White Jaques was the first to use the term "fuel cell." Jaques was also the first researcher to use phosphoric acid in the electrolyte bath.[12,16] It was Francis T Bacon who in 1959 demonstrated a five-kilowatt working fuel cell that could power a welding machine. Francis T. Bacon, named his famous fuel cell design the "Bacon Cell."[17]

There are different types of fuel cells based on their electrolytes and operating temperatures (Table 1.1). Different types of fuel cells work at different operating temperatures. For example solid oxide fuel cell operates at 800-1000°C whereas polymer electrolyte membrane (PEM) fuel cells usually work at temperatures < 75° C. Anodic as well as cathodic reactions in these fuel cells are based on the feeding fuels to the electrodes. Generally, high temperature fuel cells such as solid oxide fuel cell and molten carbon fuel cell possess higher efficiency but due to the higher operating temperature, these fuel cells are suffering with the instabilities of the electrodes and electrolyte materials which are known to affect their overall output power density.[18-21]

Table 1.1. Different types of fuel cells and operating temperatures.

Fuel Cell Types	Anode Reaction	Cathode Reaction	Operating Temperature (°C)	Mobile Ion
Proton Exchange Membrane (PEM) Fuel Cell	$H_2 \rightarrow 2H^+ + 2e^-$	$\frac{1}{2} O_2 + 2H^+ + 2e^- \rightarrow H_2O$	< 75	H^+
Direct Methanol Fuel Cell	$CH_3OH + H_2 \rightarrow CO_2 + 6H^+ + 6e^-$	$\frac{1}{2} O_2 + 2H^+ + 2e^- \rightarrow H_2O$	< 75	H^+
Alkaline Fuel Cell	$H_2 + OH^- \rightarrow 2H_2O + 2e^-$	$\frac{1}{2} O_2 + H_2O + 2e^- \rightarrow 2OH^-$	80	OH^-
Phosphoric Acid Fuel Cell	$H_2 \rightarrow 2H^+ + 2e^-$	$\frac{1}{2} O_2 + 2H^+ + 2e^- \rightarrow H_2O$	200	H^+
Molten Carbonate Fuel Cell	$H_2 + CO_3^{-2} \rightarrow H_2O + CO_2 + 2e^-$	$\frac{1}{2} O_2 + CO_2 + 2e^- \rightarrow CO_3^{-2}$	650	CO_3^{-2}
Solid Oxide Fuel Cell	$H_2 + O^{-2} \rightarrow H_2O + 2e^-$	$\frac{1}{2} O_2 + 2e^- \rightarrow O^{-2}$	800-1000	O^{-2}

1.2.1. Hydrogen Fuel Cell

Hydrogen fuel cell belongs to the class of polymer electrolyte membrane fuel cells consisting of anodic and a cathodic half-cells separated by a polymer electrolyte membrane which performs the dual functions of separator and the electrolyte. H_2 fuel is continuously fed at the anode where it gets oxidized with the simultaneous reduction of O_2 at the cathode leading to the production of electricity by powering the external load. The basic electrochemical redox reactions of hydrogen fuel cell are:[13-22]

At anode:

$$H_2 \rightarrow 2H^+ + 2e^- \quad (E^0 = 0\ V) \quad (1.1)$$

At cathode:

$$\tfrac{1}{2}\ O_2 + 2H^+ + 2e^- \rightarrow H_2O \quad (E^0 = 1.23\ V) \quad (1.2)$$

Total cell reaction:

$$H_2 + \tfrac{1}{2}\ O_2 \rightarrow H_2O \quad (E^0_{cell} = 1.23V) \quad (1.3)$$

Both the anodic reaction i.e hydrogen oxidation reaction (HOR) as well as the cathodic reaction i.e. oxygen reduction reaction (ORR) are catalyzed by the platinum-based benchmark catalyst. As evident from the net cell reactions, the only by-product during the operation of these hydrogen-based fuel cells is water that is why they are considered as the clean energy conversion devices. The H_2-O_2 fuel fells have attracted much interest as they are in the state of development for transport applications as well as for power generators ranging from a few Watts to tens of kilo Watts. Despite the fact that fuel cells have many advantages, such as a high conversion efficiency, clean exhaust gases, modular design and low noise, still the major hindrance in the path to a hydrogen-based economy is the production and storage of hydrogen and the use of expensive platinum catalysts.[12,13,22]

1.2.1.1. Hydrogen Production

Although abundant on earth as an element, hydrogen is almost always found as part of another compound, like water (H_2O), hydrocarbons like methane (CH_4), alcohols (ROH) etc., and must be separated into pure hydrogen (H_2) for use in fuel cells. Hydrogen can be produced from resources including fossil fuels, biomass, and water.[23-26]

1.2.1.2. Hydrogen Production From Hydrocarbons

Steam reforming is currently one of the most widespread and commercially developed process for the hydrogen production. The most frequently used raw materials are natural gas and lighter hydrocarbons such as methane, methanol, and other oxygenated hydrocarbons. During the process, steam from the steam system and hydrocarbon raw material are pumped to to a reformer, where a catalyst activates the following endothermic reactions:[25-27]

$$C_mH_n + mH_2O\ (g) \rightarrow mCO + (m + 0.5\ n)\ H_2$$

$$C_mH_n + 2mH_2O\ (g) \rightarrow mCO_2 + (2m + 0.5\ n)\ H_2$$

$$CO + H_2O\ (g) \longleftrightarrow CO_2 + H_2\ (g)$$

$$CH_3OH + H_2O\ (g) \longleftrightarrow CO_2 + 3H_2$$

The steam reforming process takes place in two stages. In first stage the hydrocarbon/steam mixture is converted into syngas (H_2/CO) mixture. In the 2nd stage by passing more O_2/air to the reformer the CO is converted to CO_2. The steam reforming process require very high temperature (> 200 ^{0}C) and is driven by a catalyst. The catalytic systems employed for steam reforming can be divided into 2 parts; Precious catalysts and non-precious catalysts.[28,29]

Partial oxidation (POX) and catalytic partial oxidation (CPOX) of hydrocarbons have been proposed in hydrogen production for automobile fuel cells and some other commercial applications.[30,31] Here the gasified raw material often can be methane and biogas but primarily heavy oil fractions are used (e.g., vacuum remnants, heating oil), whose further

treatment and utilization are difficult.[31] POX is a non-catalytic process, in which the raw material is gasified in the presence of oxygen and possibly steam at temperatures in the 1300–1500°C range and pressures in the 3–8MPa range.[32-34] In comparison with the steam reforming (H_2 : CO= 3 : 1), in POX more CO is produced (H_2 : CO =1 : 1 or 2 : 1). The process is therefore complemented by the conversion of CO with steam into H_2 and CO_2.

In the case of plasma reforming, the network of reforming reactions is the same as that in conventional reforming. However, energy and free radicals used for the reforming reaction are provided by plasma typically generated with electricity or heat.[35–38]. When water or steam is injected with the fuel, H·, OH·, and O·radicals in addition to electrons are formed, thus creating conditions for both reductive and oxidative reactions to occur. The major disadvantages of plasma reforming are the dependence on electricity and the difficulty of high-pressure operation. High pressure also increases electrode erosion due to decreased arc mobility which in turn decreases electrode lifetime.

Till date much of the hydrogen is produced from the methane and alcohols like methanol through stream reforming processes and much of the focus has been devoted to the development of different catalytic systems to bring down the temperature and pressure requirements of the dehydrogenation process. Different catalytic systems based on noble and non-noble metals have been investigated. Among the noble metals (Ru, Rh, Pd, Ir, and Pt), Ru and Rh exhibited high reforming activities and low carbon formation rates.[39-42] Jones et al. proposed the activity order as Ru > Rh > Ir > Pt, indicating Pt catalyst as the least active among the other metals whereas Wei and Iglesia showed that C–H bond activation by Pt is more efficient than Ir, Rh, and Ru.[39-42] Although all these noble metal catalysts show high catalytic activity but their high cost hinders their practical applications. Among the non-noble metals Group VIII non-noble metals are also highly active for the catalytic reforming of hydrocarbons like

methane.[43-45] However, it was found the iron gets rapidly oxidized under reaction conditions whereas cobalt was found to be intolerant to high partial pressures of steam.[43-45] That is why nickel-based catalysts are the most studied and commonly used SMR catalysts at industrial scale mostly owing to their low cost.[46-48] Nieva et al., stated that the catalytic activity of Ni-based catalysts mainly depends on the support.[49] The activity order of Ni-based catalysts with different supports was observed as: $Ni/MgAl_2O_4$ > $Ni/ZnAl_2O_4$ > Ni/Al_2O_3 > Ni/SiO_2.[49] Moreover, at 500°C under ambient pressure the utilization of ZrO_2 support was found to stabilize Ni particles and allowed for higher methane conversion than aforementioned supports.[48,49] The addition of other metals was also found to promote the steam reforming of the methane on the nickel based catalysts.[50,51] Rezaei, Meshkani and co-workers investigated the catalytic properties of the La, Ce, Co, Fe and Cu-promoted $Ni/MgO.Al_2O_3$ catalysts for thermal decomposition of methane and found that the addition of Cu (15 wt%) to $Ni/MgO.Al_2O_3$ dramatically improved catalytic performance with over 80 % CH_4 conversion and H_2 yields.[52,53] Moreover, the introduction of rare earth elements (La, Pr, Nd, Gd, Re and Sm) into Ni–Al catalysts lead to the formation of a hydrotalcite-like structure which greatly changed the activity of Ni particles. Among them, the $Ni/Re/Al_2O_3$ catalysts present the best methane conversion due to the large surface area of Ni particles and the strong interaction between Ni and Re/Al_2O_3.[52,53] Iwasa et al. demonstrated that Pd/ZnO and copper based catalysts show very comparable activities but the Pd containing catalyst is superior in terms of long-term stability.[61] Mayr et al. reported that the partially hydroxylated and fully oxidized Zr^{4+} species in ZrO_xH_y-Cu catalysts exhibiting synergism for selective conversion of methanol.[62] Sun et al. with the help of DFT calculations reported the role of oxidation states of Cu in the methanol reforming process and reported that the activation of the C–H bond is easier than the activation of the C–O bond on the oxygen-pre-covered CuO(111) surface which results in the formation of the CH_3O.[63] Shimizu et al. explored the heterogeneous dehydrogenation of cyclic secondary alcohols

using Co/TiO2 and Ni/ Al2O3 catalyst which led to promising results.51Further palladium based catalytic systems with Ga2O3 (ref. 46) and In2O3 (ref. 47) as support materials were studied by Penner et al. Also metals other than Cu and Pd were investigated and Pt-alloys48 as well as Ni,49 Mo50 based catalysts have been utilized for the hydrogen production from methanol.

As discussed, the industrial basis hydrogen generation is mainly by steam reforming of the natural gases like methane, propane, methanol or other fossil fuels. However, these processes are highly energy demanding and generate low purity of hydrogen with the simultaneous generation of greenhouse gases such as carbon monoxide (CO) and carbon dioxide (CO_2). The generation of this carbonaceous species during this process further shifts the focus to clean source for the generation of pure hydrogen which is water.

1.2.1.3. Hydrogen From Water

Sustainable generation of high quality of hydrogen without the generation of any greenhouse gases is by dissociation water to hydrogen and oxygen:

$$H_2O \rightarrow H_2 + ½\ O_2 \quad (1.4)$$

There are three main ways for the splitting water viz, electrolysis, photolysis and thermolysis.[23-26] Among them the electrolysis of water is the most advanced and studied pathway.

Water electrolysis is the process in which an electrical current is used to induce decomposition of water into hydrogen and oxygen molecules. When electricity is sourced from renewable source, electrolysis produces a net zero greenhouse gas emission. Because of the enormous potential and surplus clean energy produced by solar, wind, or nuclear technologies, water electrolysis is considered as an excellent strategy for the mass production of hydrogen which will also enable greater integration of renewables.[69-71] Currently, only 4 % of the produced H_2 is obtained by

means of water electrolysis.[72,73] There are three types of water electrolysis: alkaline water electrolysis, solid oxide water electrolysis & PEM water electrolysis, Figure 1.2.[74-76]

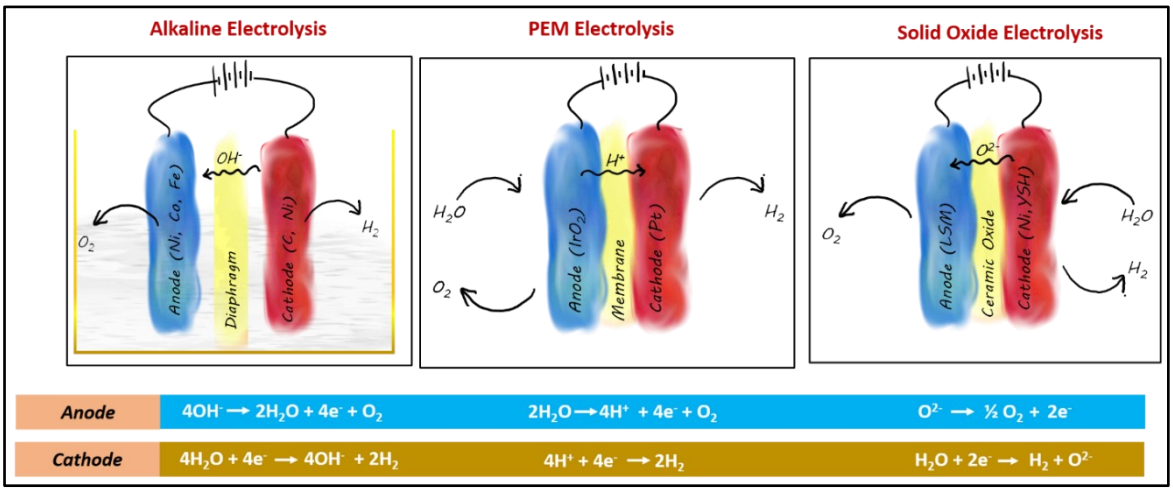

Figure 1.2. Types of water electrolysis and their corresponding half-cell reactions.

Among this, alkaline water electrolysis, which uses KOH/NaOH as electrolyte, is the most matured technology to produce hydrogen with an efficiency 50–70%.[77,79] The reactions and the architectural components are shown in the Figure 1.2. The main disadvantage of the alkaline water electrolysis the corrosive nature of the electrolyte used.[77,79] The other disadvantage is the high ohmic loss across the diaphragm.[77,79]

Proton exchange membrane (PEM) water electrolyzer which consists of a compact cell assembly of anodic and cathodic electrocatalysts separated by the cation exchange membrane.[80,81] Grubb was the first to use the solid sulfonated polystyrene membrane as a polymer electrolyte to exchange the ions from anodic to cathodic side. This membrane acts as an effective barrier to the molecular fuel.[82] The compactness, high hydrogen production rate, absence of corrosive electrolyte along with less ohmic loss and effective separation of the gaseous products make PEM water electrolyzers a preferable option over other electrolyzers.[83,84] The PEM electrolyzers can have an efficacy close to 60-80%.[80-84] However still the

focus is on decreasing the overall cost of the process due to the use of precious metal based electrocatalysts.

Solid oxide electrolyzer (SOE) is promising in hydrogen production; however, issues such as stability and conductivity of ceramic membrane pose challenges.[85,86] SOEs are operated at high temperatures, which results in favourable thermodynamics and kinetics.[88] This leads to higher efficiencies of 85–90 % in comparison to other electrolyzers. Currently, this technology is at the research and development stage and it can use nuclear reactors as the heat source and is thought to be the long-term solution for the hydrogen production.

Photolysis directly utilizes the energy of solar irradiation to split water. Arguably, this method might be considered the most sustainable mode of hydrogen production.[89,90] This could comprise photocatalytic, photoelectrochemical, or photobiological water splitting processes. Photocatalytic water splitting uses particulate semiconductor materials for water splitting, which combines photoelectric conversion and catalyst functions in a single particle.[89,90] On the other hand, photoelectrochemical water splitting uses semiconductor photoelectrodes.[90-92] Combining photovoltaic systems with an external electrocatalyst is an indirect route of photolysis for fuel production. A simple system, inexpensive basic materials, and low-cost processing are the advantages of direct photolysis.[90,92] However, photostability issues and low solar-to-hydrogen (STH) energy conversion efficiency,[91] are the major hurdles towards the commercialization.[89,90] In photobiological water splitting or biophotolysis, microorganisms are used for oxygenic photosynthesis and splitting of water to produce hydrogen.[90] Though, this technology is in its nascent stages, it has the potential to develop into one of the most cost-effective ways to produce hydrogen from renewable energy.

Thermochemical water splitting is a carbon-free high temperature (500–2000°C) hydrogen production technique that uses concentrated solar power or waste heat from nuclear reactors.[93-95] However, direct thermal

splitting of water requires temperatures of at least 2000°C, which leads to technological problems such as the mixing of hydrogen and oxygen.[96,97]. To address this, a number of thermal chemical processes such as S–I, S–Br, Fe–Cl, Hg–Br, and Cu–Cl cycles have been identified; all of these use temperatures below 1000°C and produce H_2 and O_2 in separate steps.[98-101]

1.2.2. Alcohol Fuel Cells

The direct alcohol fuel cells (DAFC) enable the direct conversion of the chemical energy stored in liquid alcohol fuel to electrical energy, with water and carbon dioxide as by-products.[102-104] Compared to the more well-known hydrogen fuelled polymer electrolyte membrane fuel cells (H_2 -O_2), DAFCs present several intriguing advantages as well as a number of challenges.[102-104]

The architecture of DAFCs is similar to that of the H_2-O_2 fuel cells with the membrane electrode assembly (MEA) consisting of anode and cathode catalyst layers in intimate contact on either side of the polymer electrolyte membrane (PEM) (either acid or alkaline based membranes can be used.[103,105] Conventionally, carbon-supported PtRu or (unsupported) PtRu black catalysts are used in the anodic half-cell and carbon-supported Pt or Pt black catalysts are used in the cathodic half-cell. Gas diffusion layers (GDLs) are placed in contact with the catalyst layers to aid reactant distribution, current collection, and catalyst-layer protection. The most studied alcohol fuel cell is the methanol fuel cell (DMFC).

In the DMFC, methanol/water mixture is directly fed to the anode. The methanol is directly oxidized to carbon dioxide with the possible formation of intermediate species such as carbon monoxide, formaldehyde, and/or formic acid which are responsible for the sluggish kinetics of the methanol oxidation reaction (MOR) in the anode.[105-107] The protons produced during the MOR is transported from the anodic to the cathodic half-cell through the Nafion membrane, while the produced electrons flow through an external circuit as shown in Figure 1.3a. The electrons and protons react

with oxygen molecules at the cathode and produce water.[104,105] In the case of an alkaline DMFC, the methanol is oxidized in presence of OH^- ions which are conducted from the cathodic to the anodic half-cell through the alkaline membrane and water is therefore produced at the anode instead of the cathode, Figure 1.3b.[106,108]

The overall reaction process that occurs in an acid-based DMFC is shown below:

Anode reaction:

$$CH_3OH + H_2O \rightarrow CO_2 + 6H^+ + 6e^-$$

Cathode reaction:

$$3/2\ O_2 + 6H^+ + 6e^- \rightarrow 3H_2O$$

Overall reaction:

$$CH_3OH + 3/2\ O_2 \rightarrow CO_2 + 2H_2O$$

In the case of an alkaline-based DMFC, the reaction process is shown below:

Anode reaction:

$$CH_3OH + 6OH^- \rightarrow 6CO_2 + 2H_2O + 6e^-$$

Cathode reaction:

$$3/2\ O_2 + 3H_2O + 6e^- \rightarrow 6OH^-$$

Overall reaction:

$$CH_3OH + 3/2\ O_2 \rightarrow CO_2 + 2H_2O$$

The free energy change, ΔG, associated with the overall reaction can be directly related to the reversible cell potential via:

$$\Delta G = -nFE$$

where n is the number of electrons involved in the chemical reaction (n = 6 electrons per mole of methanol), F is the Faraday constant (96,487 coulombs per mole), and E is the equilibrium (reversible) cell potential.

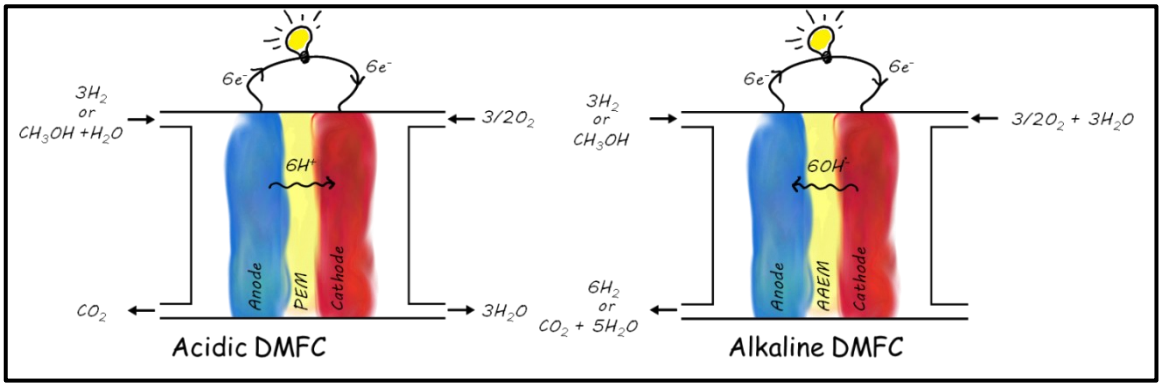

Figure 1.3. Schematics of the acid and alkaline direct methanol fuel cell.

Direct methanol fuel cells (DMFCs) have drawn extensive research attention in recent years because of their high efficiency, high energy density and extremely low emissions and are thought to be the major energy conversion devices in near future. Despite these advantages, the critical issues of methanol crossover and low oxygen reduction kinetics at the cathode are the major hurdles in their path towards commercialization.[104,105,110] Methanol crossover during DMFC operation results in low power output because of chemical oxidation of methanol at the cathode with the help of the cathode catalyst, causing (1) electrode depolarization, (2) mixed potential, resulting in decrease in open-circuit voltage (OCV), (3) chemical consumption of O_2, (4) cathode catalyst poisoning by CO (an intermediate of methanol oxidation), and (5) serious water accumulation on the cathode (water being produced by methanol oxidation), which limits O_2 access to cathode catalyst sites.[104,105,109-112]. Overall, the fuel cell efficiency is greatly affected by the methanol crossover and sluggish ORR kinetics. Because of these issues studies in the DMFC research are directed towards the development of the highly active methanol tolerant ORR catalysts.

1.2.2.1. Oxygen Reduction Reaction Cathode Catalysts

For oxygen reduction reaction, Pt based catalysts are still regarded as the best catalysts but it is difficult to simultaneously achieve desirable methanol tolerance and high ORR activity for most reported Pt based nanomaterials.[104,106,108] Alloy catalysts with resistance to methanol and high activity toward ORR are being considered as the alternative.[108-112] Binary and ternary alloy catalysts based on Pt and Pd different transition metals are reported to improve catalytic activity for ORR in the presence of methanol. Yung-Eun Sung et al., prepared a ternary PtPdCo/C electrocatalysts by borohydride reduction method which demonstrated high methanol tolerance and enhanced ORR activity than the commercial Pt/C electrocatalyst.[123] A. M. Castro Luna et al. investigated PtCo/C and PtCORu/C as cathode catalysts in DMFCs and found that the presence of metal oxide on the surface i.e RuO_2 on their surfaces increases the methanol tolerance.[114] Similarly PtPdCo/C, PtCr/C, PdCo@PdPt/C, PdM(M = Co, Ni, Cr)/C, and PdFe/C catalyst were studied as cathode catalyst in the DMFCs which exhibited improved methanol resistance and ORR activity.[115,116] However, low stability and transition metal dissolution are the major drawback for their application in DMFCs.

The replacement of Pt-based catalysts with Pt-free cathode catalysts is considered a holy grail. The Pt-free materials that have displayed the highest ORR activity when tested are pyrolysed Me-N-C catalysts with the Iron (Fe) and Cobalt (Co) metal centre.[116-119] The first report of M-N-C composites as ORR catalysts was reported way back in 1964 by Jasinski in which Co phthalocyanine was found to exhibit ORR catalytic activity.[116] After that, tremendous efforts have been devoted to the development of M-N-C ORR catalysts by using different precursors and methodologies. Wu et al. prepared nonprecious-metal catalysts with Fe and Co confined in multiple C–N shells by using polyaniline (PANI) as a carbon-nitrogen precursor which exhibited ORR activity closer to that of commercial Pt/C and an enhanced durability in PEMFC tests.[117] Similarly, Dodelet group reported Fe-based catalysts prepared by pyrolyzing ferrous acetate, carbon black, and phenanthroline in argon and ammonia successively with

enhanced ORR activity but with unsatisfying stability.[118,119] Hu et al. prepared Fe_3C nanoparticles encapsulated by graphitic layers through a high-pressure pyrolysis process which showed remarkable stability in both acidic and alkaline electrolyte.[120] The Qiao group developed CNTs with Fe–N decoration from hierarchically porous carbon which posesses high activity by Fe–N species, facile transportation from large pores, and adequate active-site exposure from large surface area.[121] Similarly, Serov et al. synthesized non-precious group metal catalysts based on M–tetraphenylporphyrin (TPP) (M: Fe, Co, Ni, Cu, Mn, and Zn) and iron phthalocyanine (PC).[122] Kong et al. prepared Co–N–C catalysts by mixing etched graphene oxide (GO) sheets with abundant in-plane pores and a porphyrin containing both Co and N elements as the doping precursor.[123] Kwak et al. used different ratios of cysteine (S and N source) and iron (III) tetramethoxyphenylporphyrin (FeTMPP) to achieve a porous material, after a thermochemical decomposition at 900°C in N_2 atmosphere.[124] Overall, it is found that among these M-N-C based catalytic systems with Fe based electrocatalysts outperform the other metals.

Apart from these several nonprecious-metal oxides have also been found to be catalytically active for ORR. Jaramillo et al. and Cheng et al. synthesized Mn oxide electrocatalysts for ORR and later found that the activity can be improved by introducing oxygen deficiency generated by high-temperature treatment in air or argon.[125,126] Dong et al. reported free-standing tubular monolayer super lattices of hollow Mn_3O_4 nanocrystal (h-Mn_3O_4-TMSLs) with outstanding ORR performance in alkaline solution with an onset potential close to 0.91 V.[127] The Dai group grew Co_3O_4 nanocrystals on reduced graphene oxide (RGO) and found such a hybrid material can serve as an efficient ORR catalyst in alkaline solution and reported enhanced ORR performance due to the synergetic chemical coupling effects between graphene oxide and Co_3O_4.[128] Other nonprecious compounds such as MnOOH, TiO_2, NbO_2, ZrO_xN_y, TaO_xN_y, and $CoSe_2$ have also been widely investigated.[129,130] In addition, metal-free catalysts, especially N-doped carbon materials, have been reported for ORR.

In spite of all these efforts much of issues with the cathodic interface of the DMFCs still remains unresolved.

1.3. Aim and Scope

Differing from the previous strategies, the primary aim of this thesis is to develop unconventional fuel cells by employing pH dependent/independent redox couples. In this thesis, by employing a pH independent outer sphere redox couple, issues related to the cathodic interface of the state of art DAFCs is addressed. By employing a pH dependent redox couple, additional functionalities such as alcohol reformation could be integrated to a DAFC reaction pathway during electricity production. Thermodynamic calculations showed the participation of electrochemical neutralization in alcohol reformation and hence attempts were dedicated to harvest it directly using pH dependent hydrogen redox. Electrochemical neutralization without a net redox reaction, offered a unique pathway for desalination of saline water in a process that involves only gases, water, H^+ and OH^- with minimal chances of water contamination. The thesis is divided into following Chapters.

Chapter 1 discusses the state-of-the-art hydrogen and alcohol fuel cells. The architectural components and principle are thoroughly discussed. This chapter also discusses the issues related to hydrogen fuel cell like hydrogen production and how it is being addressed in the literature. Similarly, the problems with the cathodic interface of alcohol fuel cell are also highlighted.

Chapter 2 discusses the implications of modifying the cathodic interface of a direct methanol fuel cell (DMFC) with a pH independent outer sphere redox couple. This chapter discusses in detail how the modification with an outer sphere redox couple can address the parasitic chemistry associated with methanol crossover. This interfacial modification arrests the parasitic chemistry at the cathodic interface and improves the performance metrics nearly by 8 times compared to state of the art DFMC-O_2 fuel cells.

Chapter 3 demonstrates the design and performance of an alcohol reforming fuel cell (ARFC) wherein alcohol reformation is coupled with the electricity production. The thermodynamic calculation showed that alcohol reformation which is otherwise a high temperature/pressure catalytic process can be driven at room temperature and pressure during electricity production with the simultaneous generation of pure hydrogen by utilizing the electrochemical neutralization reaction as the driving force. Since the hydrogen fuel produced is free from carbon containing impurities, ARFC can be directly utilized as a fuel reservoir for a H_2-O_2 fuel cell in a tandem configuration.

Chapter 4 demonstrates a strategy for the direct harvesting of energy of neutralization as electrical driving force which is otherwise impossible as acid base neutralization is not a redox reaction. In this Chapter, by utilizing a pH dependent hydrogen redox reaction, it is shown that energy of neutralization can be directly harvested as electrical driving force without a net redox reaction. This electrochemical neutralization cell employs H^+/H_2 redox couple to perform the neutralization reaction in an electrochemical pathway and the positive entropy change of the reaction allows nearly 30% of electrical energy to be harvested from the surroundings.

Chapter 5 discusses the applications of direct harvesting of neutralization energy as electrical driving force for spontaneous water desalination. The chapter discusses the design, principle and performance of a 3-compartment electrochemical cell for simultaneous water desalination during electricity production. The electrochemical desalination cell driven by the electrochemical neutralization demonstrates performance metrics comparable to the state-of-the-art desalination processes reported in the literature.

Chapter 6 gives a brief summary and future outlook of the work reported in the thesis.

1.4. References

[1] Höök, M.; Tang, X., Depletion of fossil fuels and anthropogenic climate change—A review. *Energy Policy* **2013,** *52*, 797-809.

[2] Badwal, S. P. S.; Giddey, S. S.; Munnings, C.; Bhatt, A. I.; Hollenkamp, A. F., Emerging electrochemical energy conversion and storage technologies. *Front Chem* **2014,** *2*, 79-79.

[3] Gevorkyan, A., Renewable versus nonrenewable resources: an analysis of volatility in futures prices. *Australian Journal of Agricultural and Resource Economics* **2017,** *61* (1), 19-35.

[4] Islam, M. A.; Hasanuzzaman, M.; Rahim, N. A.; Nahar, A.; Hosenuzzaman, M., Global Renewable Energy-Based Electricity Generation and Smart Grid System for Energy Security. *The Scientific World Journal* **2014,** *2014*, 197136.

[5] Baños, R.; Manzano-Agugliaro, F.; Montoya, F. G.; Gil, C.; Alcayde, A.; Gómez, J., Optimization methods applied to renewable and sustainable energy: A review. *Renewable and Sustainable Energy Reviews* **2011,** *15* (4), 1753-1766.

[6] Winter, M.; Brodd, R. J., What Are Batteries, Fuel Cells, and Supercapacitors? *Chem. Rev.* **2004,** *104* (10), 4245-4270.

[7] Eftekhari, A.; Fang, B., Electrochemical hydrogen storage: Opportunities for fuel storage, batteries, fuel cells, and supercapacitors. *Int. J. Hydrogen Energy* **2017,** *42* (40), 25143-25165.

[8] Taner, T., Energy and exergy analyze of PEM fuel cell: A case study of modeling and simulations. *Energy* **2018,** *143*, 284-294.

[9] Wang, Y.; Ruiz Diaz, D. F.; Chen, K. S.; Wang, Z.; Adroher, X. C., Materials, technological status, and fundamentals of PEM fuel cells – A review. *Mater. Today* **2020,** *32*, 178-203.

[10] Wang, L.; Advani, S. G.; Prasad, A. K., Membrane Electrode Assembly with Enhanced Membrane/Electrode Interface for Proton Exchange Membrane Fuel Cells. *The Journal of Physical Chemistry C* **2013,** *117* (2), 945-948.

[11] Sarkar, J.; Bhattacharyya, S. Application of Graphene and Graphene-Based Materials in Clean Energy-Related Devices Minghui. *Arch. Thermodyn.* **2012**, *33* (4), 23–40.

[12] Sharaf, O. Z.; Orhan, M. F. An Overview of Fuel Cell Technology: Fundamentals and Applications. *Renew. Sustain. Energy Rev.* **2014**, *32*, 810–853.

[13] Singla, M. K.; Nijhawan, P.; Oberoi, A. S. Hydrogen Fuel and Fuel Cell Technology for Cleaner Future: A Review. *Environ. Sci. Pollut. Res.* **2021**, *28* (13), 15607–15626.

[14] Grove, W.R. On Voltaic Series and the Combination of Gases by Platinum. Lond. Edinb. Philos. Mag. J. Sci. **1839,** *14,* 127–130.

[15] Grove, W.R. On a Gaseius Voltaic Battery. *Lond. Edinb. Philos. Mag. J. Sci.* **1842,** *21,* 417–420.

[16] Bockris, J.O.M. Review: The hydrogen economy: Its history. *Int. J. Hydrogen Energy* **2013,** *38,* 2579–2588.

[17] Bacon, F. T. a. T. M. F., Series A, Mathematical and Physical Sciences. *Proc. R. Soc. London, Ser. A 334*, 1599.

[18] Ormerod, R. M., Solid oxide fuel cells. *Chem. Soc. Rev.* **2003,** *32* (1), 17-28.

[19] Taner, T., Energy and exergy analyze of PEM fuel cell: A case study of modeling and simulations. *Energy* **2018,** *143*, 284-294.

[20] Wang, Y.; Ruiz Diaz, D. F.; Chen, K. S.; Wang, Z.; Adroher, X. C., Materials, technological status, and fundamentals of PEM fuel cells – A review. *Mater. Today* **2020,** *32*, 178-203.

[21] Wang, L.; Advani, S. G.; Prasad, A. K., Membrane Electrode Assembly with Enhanced Membrane/Electrode Interface for Proton Exchange Membrane Fuel Cells. *The Journal of Physical Chemistry C* **2013,** *117* (2), 945-948.

[22] Felseghi, R. A.; Carcadea, E.; Raboaca, M. S.; Trufin, C. N.; Filote, C. Hydrogen Fuel Cell Technology for the Sustainable Future of Stationary Applications. *Energies* **2019**, *12* (23), 4593.

[23] Pinsky, R.; Sabharwall, P.; Hartvigsen, J.; O'Brien, J. Comparative Review of Hydrogen Production Technologies for Nuclear Hybrid Energy Systems. *Prog. Nucl. Energy* **2020**, *123* (February), 103317.

[24] Kalamaras, C. M.; Efstathiou, A. M. Hydrogen Production Technologies: Current State and Future Developments. *Conf. Pap. Energy* **2013**, *2013*, 1–9.

[25] El-Shafie, M.; Kambara, S.; Hayakawa, Y. Hydrogen Production Technologies Overview. *J. Power Energy Eng.* **2019**, *07* (01), 107–154.

[26] Chen, J.; Sun, J.; Wang, Y. Catalysts for Steam Reforming of Bio-Oil: A Review. *Ind. Eng. Chem. Res.* **2017**, *56* (16), 4627–4637.

[27] Meloni, E.; Martino, M.; Palma, V. A Short Review on Ni Based Catalysts and Related Engineering Issues for Methane Steam Reforming. *Catalysts* **2020**, *10* (3), 352.

[28] J. R. Rostrup-Nielsen, Conversion of hydrocarbons and alco- hols for fuel cells, *Phys. Chem. Chem. Phys.* **2001,** *3 (3)*, 283–288.

[29] Song, L. Zhang, R. B. Watson,D.Braden, and U.S.Ozkan, Investigation of bio-ethanol steam reforming over cobalt-based catalysts, *Catal. Today,* **2007,** *129,* 346–354.

[30] K. L. Hohn and L. D. Schmidt, Partial oxidation ofmethane to syngas at high space velocities over Rh-coated spheres, *App. Catal. A*, **2001,** *211(1),* 53–68.

[31] J. J. Krummenacher, K. N. West, and L. D. Schmidt, Catalytic partial oxidation ofhigher hydrocarbons at millisecond contact times: decane, hexadecane, and diesel fuel, *J. Catal.* **2003,** *215(2),* 332–343.

[32] J.M.Ogden, M.M.Steinbugler,and T. G. Kreutz, Comparison of hydrogen, methanol and gasoline as fuels for fuel cell vehicles: implications for vehicle design and infrastructure development, *J. Power Sources* **1999,** *79(2),*143– 168.

[33] M. Onozaki, K. Watanabe, T. Hashimoto, H. Saegusa, and Y. Katayama, Hydrogen production by the partial oxidation and steam reforming oftar fromhot coke oven gas, *Fuel* **2006,** *85(2),* 143–149.

[34] J. R. Rostrup-Nielsen, Conversion of hydrocarbons and alco- hols for fuel cells, *Phy. Chem. Chem. Phy.* **2001,** *3(3),* 283–288.

[35] L. Bromberg, D. R. Cohn, and A. Rabinovich, Plasma reformer-fuel cell system for decentralized power applications, *Int. J. Hydrog. Energy,* **1997,** *22(1),* 83– 94.

[36] L. Bromberg, D. R. Cohn, A. Rabinovich, and N. Alexeev, Plasma catalytic reforming ofmethane, *Int. J. Hydrog. Energy,* **1999,** *24(12),* 1131–1137.

[37] T. Hammer, T.Kappes, M. Baldauf, Plasma catalytichybrid processes: gas discharge initiation and plasma activation of catalytic processes, *Catal. Today* **2004,** *89(1-2),* 5–14.

[38] T. Paulmier and L. Fulcheri, Use of non-thermal plasma for hydrocarbon reforming, *Chem. Eng. J.,* **2005,** *106(1),* 59–71.

[39] Zhou, L.; Martirez, J.M.P.; Finzel, J.; Zhang, C.; Swearer, D.F.; Tian, S.; Robatjazi, H.; Lou, M.; Dong, L.; Henderson, L.; et al. Light-driven methane dry reforming with single atomic site antenna-reactor plasmonic photocatalysts. *Nat. Energy*, **2020,** *5,* 61–70.

[40] Tang, Y.; Wei, Y.; Wang, Z.; Zhang, S.; Li, Y.; Nguyen, L.; Li, Y.; Zhou, Y.; Shen, W.; Tao, F.F.; et al. Synergy of single-atom Ni and Ru sites on CeO_2 for dry reforming of CH_4. *J. Am. Chem. Soc.* **2019,** *141,* 7283–7293.

[41] Jones, G.; Jakobsen, J.G.; Shim, S.S.; Kleis, J.; Andersson, M.P.; Rossmeisl, J.; Abild-Pedersen, F.; Bligaard, T.; Helveg, S.; Hinnemann, B.; et al. First principles calculations and experimental insight into methane steam reforming over transition metal catalysts. *J. Catal.* **2008,** *259,* 147–160.

[42] Wei, J.; Iglesia, E. Isotopic and kinetic assessment of the mechanism of reactions of CH4 with CO_2 or H_2O to form synthesis gas and carbon on nickel catalysts. *J. Catal.* **2004,** *224,* 370–383.

[43] Theofanidis, S.A.; Galvita, V.V.; Poelman, H.; Marin, G.B. Enhanced carbon-resistant dry reforming Fe-Ni catalyst: Role of Fe. *ACS Catal.* **2015,** *5,* 3028–3039.

[44] Abelló, S.; Bolshak, E.; Montane, D. Ni–Fe catalysts derived from hydrotalcite-like precursors for hydrogen production by ethanol steam reforming. *Appl. Catal. A* **2013,** *450,* 261–274.

[45] Profeti, L.P.; Ticianelli, E.A.; Assaf, E.M. Co/Al_2O_3 catalysts promoted with noble metals for production of hydrogen by methane steam reforming. *Fuel* **2008,** *87,* 2076–2081.

[46] Laosiripojana, N.; Assabumrungrat, S. Methane steam reforming over $Ni/Ce–ZrO_2$ catalyst: Influences of $Ce–ZrO_2$ support on reactivity, resistance toward carbon formation, and intrinsic reaction kinetics. *Appl. Catal. A* **2005,** *290,* 200–211.

[47] Zhang, S.; Muratsugu, S.; Ishiguro, N.; Tada, M. Ceria-doped Ni/SBA-16 catalysts for dry reforming of methane. *ACS Catal.* **2013,** *3,* 1855–1864.

[48] Palmer, C.; Upham, D.C.; Smart, S.; Gordon, M.J.; Metiu, H.; McFarland, E.W. Dry reforming of methane catalysed by molten metal alloys. *Nat. Catal.* **2020,** *3,* 83–89.

[49] Nieva, M.A.; Villaverde, M.M.; Monzón, A.; Garetto, T.F.; Marchi, A.J. Steam-methane reforming at low temperature on nickel-based catalysts. *Chem. Eng. J.* **2014,** *235,* 158–166.

[50] Ermakova, M.A.; Ermakov, D.Y.; Kuvshinov, G.G.; Plyasova, L.M. New nickel catalysts for the formation of filamentous carbon in the reaction of methane decomposition. *J. Catal.* **1999,** *187,* 77–84.

[51] Chen, L.; Li, H.; Zhan, W.; Cao, Z.; Chen, J.; Jiang, Q.; Jiang, Y.; Xie, Z.; Kuang, Q.; Zheng, L. Controlled encapsulation of flower-like Rh–Ni alloys with MOFs via tunable template Dealloying for enhanced selective hydrogenation of alkyne. *ACS Appl. Mater. Interfaces* **2016,** *8,* 31059–31066.

[52] Rastegarpanah, A.; Meshkani, F.; Rezaei, M. Thermocatalytic decomposition of methane over mesoporous nanocrystalline promoted $Ni/MgO{\cdot}Al_2O_3$ catalysts. *Int. J. Hydrogen Energy.* **2017,** *42,* 16476–16488.

[53] Anjaneyulu, C.; Naresh, G.; Kumar, V.V.; Tardio, J.; Rao, T.V.; Venugopal, A. Influence of rare earth (La, Pr, Nd, Gd, and Sm) metals on the methane decomposition activity of Ni–Al catalysts. *ACS Sustain. Chem. Eng.* **2015,** *3,* 1298–1305.

[54] Balaraman, E.; Khaskin, E.; Leitus, G.; Milstein, D. Catalytic Transformation of Alcohols to Carboxylic Acid Salts and H 2 Using Water as the Oxygen Atom Source. *Nat. Chem.* **2013**, *5* (2), 122–125.

[55] Cai, F.; Lu, P.; Ibrahim, J. J.; Fu, Y.; Zhang, J.; Sun, Y. Investigation of the Role of Nb on Pd−Zr−Zn Catalyst in Methanol Steam Reforming for Hydrogen Production. *Int. J. Hydrogen Energy* **2019**, *44* (23), 11717–11733.

[56] Choi, J.; MacArthur, A. H. R.; Brookhart, M.; Goldman, A. S. Dehydrogenation and Related Reactions Catalyzed by Iridium Pincer Complexes. *Chem. Rev.* **2011**, *111* (3), 1761–1779.

[57] Iulianelli, A.; Ribeirinha, P.; Mendes, A.; Basile, A. Methanol Steam Reforming for Hydrogen Generation via Conventional and Membrane Reactors: A Review. *Renew. Sustain. Energy Rev.* **2014**, *29*, 355–368.

[58] Palo, D. R.; Dagle, R. A.; Holladay, J. D. Methanol Steam Reforming for Hydrogen Production. *Chem. Rev.* **2007**, *107* (10), 3992–4021.

[59] Trincado, M.; Banerjee, D.; Grützmacher, H. Molecular Catalysts for Hydrogen Production from Alcohols. *Energy Environ. Sci.* **2014**, *7* (8), 2464–2503.

[60] Xu, X.; Shuai, K.; Xu, B. Review on Copper and Palladium Based Catalysts for Methanol Steam Reforming to Produce Hydrogen. *Catalysts* **2017**, *7* (6), 1–15.

[61] Iwasa, N.; Yoshikawa, M.; Nomura, W.; Arai, M. Transformation of Methanol in the Presence of Steam and Oxygen over ZnO-Supported Transition Metal Catalysts under Stream Reforming Conditions. *Appl. Catal. A Gen.* **2005**, *292* (1–2), 215–222.

[62] Mayr, L.; Klötzer, B.; Zemlyanov, D.; Penner, S. Steering of Methanol Reforming Selectivity by Zirconia-Copper Interaction. *J. Catal.* **2015**, *321*, 123–132.

[63] Sakong, S.; Gross, A. Total Oxidation of Methanol on Cu(110): A Density Functional Theory Study. *J. Phys. Chem. A* **2007**, *111* (36), 8814–8822.

[64] Lorenz, H.; Penner, S.; Jochum, W.; Rameshan, C.; Klötzer, B. Pd/Ga2O3 Methanol Steam Reforming Catalysts: Part II. Catalytic Selectivity. *Appl. Catal. A Gen.* **2009**, *358 (2),* 203–210.

[65] Lorenz, H.; Turner, S.; Lebedev, O. I.; Van Tendeloo, G.; Klötzer, B.; Rameshan, C.; Pfaller, K.; Penner, S. Pd-In2O3 Interaction Due to Reduction in Hydrogen: Consequences for Methanol Steam Reforming. *Appl. Catal. A Gen.* **2010**, *374 (1–2),* 180–188.

[66] Park, J. H.; Kim, Y. T.; Park, E. D.; Lee, H. C.; Kim, J.; Lee, D. Markedly High Catalytic Activity of Supported Pt-MoOx Nanoclusters for Methanol Reforming to Hydrogen at Low Temperatures. *ChemCatChem* **2013**, *5 (3),* 806–814.

[67] Matsumura, Y.; Tanaka, K.; Tode, N.; Yazawa, T.; Haruta, M. Catalytic Methanol Decomposition to Carbon Monoxide and Hydrogen over Nickel Supported on Silica. *J. Mol. Catal. A Chem.* **2000**, *152 (1–2),* 157–165.

[68] Gao, Q.; Zhang, C.; Wang, S.; Shen, W.; Zhang, Y.; Xu, H.; Tang, Y. Preparation of Supported Mo_2C-Based Catalysts from Organic-Inorganic Hybrid Precursor for Hydrogen Production from Methanol Decomposition. *Chem. Commun.* **2010**, *46* (*35),* 6494–6496.

[69] Staffell, I.; Scamman, D.; Velazquez Abad, A.; Balcombe, P.; Dodds, P. E.; Ekins, P.; Shah, N.; Ward, K. R. The Role of Hydrogen and Fuel Cells in the Global Energy System. *Energy Environ. Sci.* **2019**, *12 (2),* 463–491.

[70] Howard, A. S. The Future of Nuclear Energy in the U.S. *Glob. Warm. Energy Policy* **2001**, 213–217.

[71] Sartbaeva, A.; Kuznetsov, V. L.; Wells, S. A.; Edwards, P. P. Hydrogen Nexus in a Sustainable Energy Future. *Energy Environ. Sci.* **2008**, *1 (1),* 79–85.

[72] S. Shiva Kumar, V. H. Hydrogen Production by PEM Water Electrolysis – A Review. *Mater. Sci. Energy Technol.* **2019**, *2 (3),* 442–454.

[73] Antar, Y. N. and A. *Hydrogen Generation by Water Electrolysis, Advances In Hydrogen Generation Technologies, Murat Eyvaz, IntechOpen*; 2018.

[74] Browne, M. P.; Sofer, Z.; Pumera, M. Layered and Two Dimensional Metal Oxides for Electrochemical Energy Conversion. *Energy Environ. Sci.* **2019**, *12 (1),* 41–58.

[75] Khan, M. A.; Zhao, H.; Zou, W.; Chen, Z.; Cao, W.; Fang, J.; Xu, J.; Zhang, L.; Zhang, J. *Electrochem. Energ. Rev.* **2018,** *1,* 483–530.

[76] Sapountzi, F. M.; Gracia, J. M.; Weststrate, C. J.; Fredriksson, H. O. A.; Niemantsverdriet, J. W., Electrocatalysts for the generation of hydrogen, oxygen and synthesis gas. *Prog. Energy Combust. Sci.* **2017,** *58*, 1-35.

[77] Rashid, M. M.; Mesfer, M. K. Al; Naseem, H.; Danish, M. Hydrogen Production by Water Electrolysis: A Review of Alkaline Water Electrolysis, PEM Water Electrolysis and High Temperature Water Electrolysis. *Int. J. Eng. Adv. Technol.* **2015**, *3,* 2249–8958.

[78] Scott, K. Chapter 1: Introduction to Electrolysis, Electrolysers and Hydrogen Production. *RSC Energy Environ. Ser.* **2020**, 1–27.

[79] Brauns, J.; Turek, T. Alkaline Water Electrolysis Powered by Renewable Energy: A Review. *Processes* **2020**, *8 (2),* 248.

[80] Xiang, C.; Papadantonakis, K. M.; Lewis, N. S. Principles and Implementations of Electrolysis Systems for Water Splitting. *Mater. Horizons* **2016**, *3 (3),* 169–173.

[81] Schalenbach, M.; Tjarks, G.; Carmo, M.; Lueke, W.; Mueller, M.; Stolten, D. Acidic or Alkaline? Towards a New Perspective on the Efficiency of Water Electrolysis. *J. Electrochem. Soc.* **2016**, *163 (11),* F3197–F3208.

[82] Aricò, A. S.; Siracusano, S.; Briguglio, N.; Baglio, V.; Di Blasi, A.; Antonucci, V. Polymer Electrolyte Membrane Water Electrolysis:

Status of Technologies and Potential Applications in Combination with Renewable Power Sources. *J. Appl. Electrochem.* **2013**, *43 (2),* 107–118.

[83] Leng, Y.; Chen, G.; Mendoza, A. J.; Tighe, T. B.; Hickner, M. A.; Wang, C. Y. Solid-State Water Electrolysis with an Alkaline Membrane. *J. Am. Chem. Soc.* **2012**, *134* (22), 9054–9057.

[84] Grubb, W. T., Ionic Migration in Ion-exchange Membranes. *The Journal of Physical Chemistry* **1959,** *63 (1),* 55-58.

[85] Miller, H. A.; Bouzek, K.; Hnat, J.; Loos, S.; Bernäcker, C. I.; Weißgärber, T.; Röntzsch, L.; Meier-Haack, J. Green Hydrogen from Anion Exchange Membrane Water Electrolysis: A Review of Recent Developments in Critical Materials and Operating Conditions. *Sustain. Energy Fuels* **2020**, *4 (5),* 2114–2133.

[86] Vincent, I.; Bessarabov, D. Low Cost Hydrogen Production by Anion Exchange Membrane Electrolysis: A Review. *Renewable and Sustainable Energy Reviews*. **2018,** 1690–1704.

[87] Ursua, A.; Sanchis, P.; Gandia, L. M. Hydrogen Production from Water Electrolysis : Current Status and Future Trends. *Proc. IEEE* **2012**, *100 (2),* 410–426.

[88] Antar, Y. N. and A. Hydrogen Generation by Water Electrolysis, Advances In Hydrogen Generation Technologies, Murat Eyvaz, IntechOpen. *2018*.

[89] Takata, T.; Jiang, J.; Sakata, Y.; Nakabayashi, M.; Shibata, N.; Nandal, V.; Seki, K.; Hisatomi, T.; Domen, K. Photocatalytic Water Splitting with a Quantum Efficiency of Almost Unity. *Nature* **2020**, *581 (7809),* 411–414.

[90] Wang, Z.; Li, C.; Domen, K. Recent Developments in Heterogeneous Photocatalysts for Solar-Driven Overall Water Splitting. *Chem. Soc. Rev.* **2019**, *48 (7),* 2109–2125.

[91] Yamada, T.; Domen, K. Development of Sunlight Driven Water Splitting Devices towards Future Artificial Photosynthetic Industry. *Chem. Engineering* **2018**, *2 (3),* 1–18.

[92] Tee, S. Y.; Win, K. Y.; Teo, W. S.; Koh, L. D.; Liu, S.; Teng, C. P.; Han, M. Y. Recent Progress in Energy-Driven Water Splitting. *Adv. Sci.* **2017**, *4 (5),* 1600337

[93] Rao, C. N. R.; Lingampalli, S. R.; Dey, S.; Roy, A. Solar Photochemical and Thermochemical Splitting of Water. *Philos. Trans. R. Soc. A Math. Phys. Eng. Sci.* **2016**, *374.*

[94] Muhich, C. L.; Ehrhart, B. D.; Witte, V. A.; Miller, S. L.; Coker, E. N.; Musgrave, C. B.; Weimer, A. W. Predicting the Solar Thermochemical Water Splitting Ability and Reaction Mechanism of Metal Oxides: A Case Study of the Hercynite Family of Water Splitting Cycles. *Energy Environ. Sci.* **2015**, *8 (12),* 3687–3699.

[95] Safari, F.; Dincer, I. A Review and Comparative Evaluation of Thermochemical Water Splitting Cycles for Hydrogen Production. *Energy Conversion and Management.* **2020,** *205,* 112182,

[96] Rao, C. N. R.; Dey, S. Solar Thermochemical Splitting of Water to Generate Hydrogen. *Proc. Natl. Acad. Sci. U. S. A.* **2017**, *114 (51),* 13385–13393.

[97] Safari, F.; Dincer, I. A Study on the Fe–Cl Thermochemical Water Splitting Cycle for Hydrogen Production. *Int. J. Hydrogen Energy* **2020,** *38 (45),* 18867–18875.

[98] Naterer, G. F.; Gabriel, K.; Wang, Z. L.; Daggupati, V. N.; Gravelsins, R. Thermochemical Hydrogen Production with a Copper-Chlorine Cycle. I: Oxygen Release from Copper Oxychloride Decomposition. *Int. J. Hydrogen Energy* **2008,** *33(20),* 5439–5450.

[99] Onuki, K.; Kubo, S.; Terada, A.; Sakaba, N.; Hino, R. Thermochemical Water-Splitting Cycle Using Iodine and Sulfur. *Energy Environ. Sci.* **2009**, *2 (5),* 491–497.

[100] Zhang, Y.; Peng, P.; Ying, Z.; Zhu, Q.; Zhou, J.; Wang, Z.; Liu, J.; Cen, K. Experimental Investigation on Multiphase Bunsen Reaction in the Thermochemical Sulfur-Iodine Cycle. *Ind. Eng. Chem. Res.* **2014**, *53 (8),* 3021–3028.

[101] Dehghani, S.; Sayyaadi, H.; Pourali, O. Equilibrium Conversion and Reaction Analysis in Sulfur-Iodine Thermochemical Hydrogen Production Cycle. *Can. J. Chem. Eng.* **2015**, *93 (4),* 708–726.

[102] Fadzillah, D. M.; Kamarudin, S. K.; Zainoodin, M. A.; Masdar, M. S. Critical Challenges in the System Development of Direct Alcohol Fuel Cells as Portable Power Supplies: An Overview. *Int. J. Hydrogen Energy* **2019**, *44 (5),* 3031–3054.

[103] Lamy, C.; Lima, A.; LeRhun, V.; Delime, F.; Coutanceau, C.; Léger, J. M. Recent Advances in the Development of Direct Alcohol Fuel Cells (DAFC). *J. Power Sources* **2002**, *105 (2),* 283–296.

[104] Song, S.; Wang, Y.; Tsiakaras, P.; Shen, P. K. Direct Alcohol Fuel Cells: A Novel Non-Platinum and Alcohol Inert ORR Electrocatalyst. *Appl. Catal. B Environ.* **2008**, *78 (3–4),* 381–387.

[105] Aricò, A.S., Baglio, V., and Antonucci, V.: Direct methanol fuel Cells: History, status and perspectives. In *Electrocatalysis of Direct Methanol Fuel Cells: From Fundamentals to Applications*, Wiley-VCH Verlag GmbH & Co. KGaA: Weinheim, Germany, **2009;** pp. 1.

[106] Varcoe, J. R.; Beillard, M.; Halepoto, D. M.; Kizewski, J. P.; Poynton, S.; Slade, R. C. T. Membrane and Electrode Materials for Alkaline Membrane Fuel Cells. *ECS Trans.* **2019**, *16 (2),* 1819–1834.

[107] Neburchilov, V.; Martin, J.; Wang, H.; Zhang, J. A Review of Polymer Electrolyte Membranes for Direct Methanol Fuel Cells. *J. Power Sources* **2007**, *169 (2),* 221–238.

[108] Sarapuu, A.; Kibena-Põldsepp, E.; Borghei, M.; Tammeveski, K. Electrocatalysis of Oxygen Reduction on Heteroatom-Doped Nanocarbons and Transition Metal-Nitrogen-Carbon Catalysts for Alkaline Membrane Fuel Cells. *J. Mater. Chem. A* **2018**, *6 (3),* 776–804.

[109] Zhang, Y.; Huang, B.; Luo, G.; Sun, T.; Feng, Y.; Wang, Y.; Ma, Y.; Shao, Q.; Li, Y.; Zhou, Z.; et al. Atomically Deviated Pd-Te Nanoplates Boost Methanol-Tolerant Fuel Cells. *Sci. Adv.* **2020**, *6 (31),* 1–10.

[110] Fadzillah, D. M.; Kamarudin, S. K.; Zainoodin, M. A.; Masdar, M. S. Critical Challenges in the System Development of Direct Alcohol Fuel Cells as Portable Power Supplies: An Overview. *Int. J. Hydrogen Energy* **2019**, *44 (5),* 3031–3054.

[111] Asteazaran, M.; Bengió, S.; Triaca, W. E.; Castro Luna, A. M. Methanol Tolerant Electrocatalysts for the Oxygen Reduction Reaction. *J. Appl. Electrochem.* **2014**, *44 (12),* 1271–1278.

[112] Wang, X.; Li, Z.; Qu, Y.; Yuan, T.; Wang, W.; Wu, Y.; Li, Y. Review of Metal Catalysts for Oxygen Reduction Reaction: From Nanoscale Engineering to Atomic Design. *Chem* **2019**, *5 (6),* 1486–1511.

[113] Cho, Y. H.; Kim, O. H.; Chung, D. Y.; Choe, H.; Cho, Y. H.; Sung, Y. E. PtPdCo Ternary Electrocatalyst for Methanol Tolerant Oxygen Reduction Reaction in Direct Methanol Fuel Cell. *Appl. Catal. B Environ.* **2014**, *154–155*, 309–315.

[114] Asteazaran, M.; Bengió, S.; Triaca, W. E.; Castro Luna, A. M. Methanol Tolerant Electrocatalysts for the Oxygen Reduction Reaction. *J. Appl. Electrochem.* **2014**, *44 (12),* 1271–1278.

[115] Gewirth, A.A., Varnell, J.A., and DiAscro, A.M. Nonprecious metal catalysts for oxygen reduction in heterogeneous aqueous systems. *Chem. Rev.* **2018,** *118,* 2313–2339.

[116] Jasinski, R. A new fuel cell cathode catalyst. *Nature,* **1964,** *201,* 1212–1213.

[117] Wu, G., More, K.L., Johnston, C.M., and Zelenay, P. High-performance electrocatalysts for oxygen reduction derived from polyaniline, iron, and cobalt. *Science, **2011,** 332,* 443–447.

[118] Lefe` vre, M., Proietti, E., Jaouen, F., and Dodelet, J.P. (2009). Iron-based catalysts with improved oxygen reduction activity in polymer electrolyte fuel cells. *Science* **2009,** *324,* 71–74.

[119] Proietti, E., Jaouen, F., Lefe` vre, M., Larouche, N., Tian, J., Herranz, J., and Dodelet, J.P. Iron-based cathode catalyst with enhanced power density in polymer electrolyte membrane fuel cells. *Nat. Commun.* **2011,** *2,* 416.

[120] Hu, Y., Jensen, J.O., Zhang, W., Cleemann, L.N., Xing, W., Bjerrum, N.J., and Li, Q. Hollow spheres of iron carbide nanoparticles encased in graphitic layers as oxygen reduction catalysts. *Angew. Chem. Int. Ed.* **2014,** *53,* 3675–3679.

[121] Liang, J., Zhou, R.F., Chen, X.M., Tang, Y.H., and Qiao, S.Z. Fe–N decorated hybrids of CNTs grown on hierarchically porous carbon for high-performance oxygen reduction. *Adv. Mater.* **2014,** *26,* 6074–6079.

[122] Serov, A.A.; Min, M.; Chai, G.; Han, S.; Seo, S.J.; Park, Y.; Kim, H.; Kwak, C. Electroreduction of oxygen over iron macrocyclic catalysts for DMFC applications. *J. Appl. Electrochem.* **2009**, *39*, 1509–1516.

[123] Kong, W.; Yao, K.; Duan, X.; Liu, Z.; Hu, J. Holey Co, N-codoped graphene aerogel with in-plane pores and multiple active sites for efficient oxygen reduction. *Electrochim. Acta* **2018**, *269*, 544–552.

[124] Kwak, D.-H.; Han, S.-B.; Kim, D.-H.; Won, J.-E.; Park, K.-W. Amino acid-derived non-precious catalysts with excellent electrocatalytic performance and methanol tolerance in oxygen reduction reaction. *Appl. Catal. B Environ.* **2018**, *238*, 93–103.

[125] Gorlin, Y., and Jaramillo, T.F. A bifunctional nonprecious metal catalyst for oxygen reduction and water oxidation. *J. Am. Chem. Soc.* **2010,** *132,* 13612–13614.

[126] Cheng, F., Zhang, T., Zhang, Y., Du, J., Han, X., and Chen, J. Enhancing electrocatalytic oxygen reduction on MnO_2 with vacancies. *Angew. Chem.* **2013,** *125,* 2534– 2537.

[127] Li, T., Xue, B., Wang, B., Guo, G., Han, D., Yan, Y., and Dong, A. Tubular monolayer superlattices of hollow Mn3O4 nanocrystals and their oxygen reduction activity. *J. Am. Chem. Soc.* **2017,** *139,* 12133–12136.

[128] Liang, Y., Li, Y., Wang, H., Zhou, J., Wang, J., Regier, T., and Dai, H. Co_3O_4 nanocrystals on graphene as a synergistic catalyst for oxygen reduction reaction. *Nat. Mater.* **2011,** *10,* 780–786.

[129] Liang, Y., Wang, H., Diao, P., Chang, W., Hong, G., Li, Y., Gong, M., Xie, L., Zhou, J., Wang, J., et al. Oxygen reduction electrocatalyst based on strongly coupled cobalt oxide nanocrystals and carbon nanotubes. *J. Am. Chem. Soc.* **2012,** *134,* 15849– 15857.

[130] Suntivich, J., Gasteiger, H.A., Yabuuchi, N., Nakanishi, H., Goodenough, J.B., and Shao- Horn, Y. (2011). Design principles for oxygen- reduction activity on perovskite oxide catalysts for fuel cells and metal–air batteries. *Nature Chem* **2011,** *3,* 546–550.

Chapter 2

A Direct Alcohol Fuel Cell Driven by a pH Independent Redox Couple

Abstract: Molecular oxygen, the conventional electron acceptor in fuel cells poses challenges specific to direct alcohol fuel cells (DAFCs). Due to the coupling of alcohol dehydrogenation with the scission of oxygen on the positive electrode during the alcohol crossover, the benchmark Pt-based air cathode experiences severe competition and depolarization losses. The necessity of heavy precious metal loading with domains for alcohol tolerance in the state-of-the-art DAFC cathode is a direct consequence of this. Though efforts are dedicated to selectively cleave oxygen, the root of the problem being the inner sphere nature of either half-cell chemistry is often overlooked. Using a pH independent outer sphere electron acceptor which does not form a bond with the cathode during redox energy transformation, we effectively decoupled the interfacial chemistry from parasitic chemistry leading to a DAFC driven by alcohol passive carbon nanoparticles, with performance metrics ~8 times higher than Pt based DAFC-O_2.

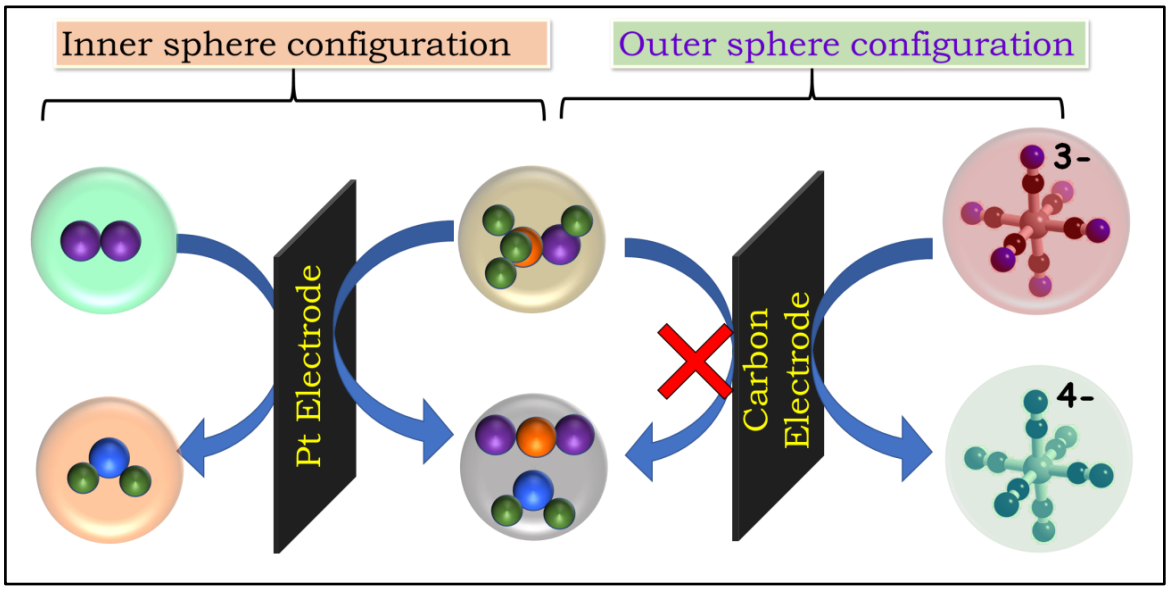

The chapter contains the data taken from my original published work: Zahid Bhat et.al., J. Phys. Chem. Lett. 2017, 8, 3523-3529. Copyright American Chemical Society

2.1. Introduction

Electrochemical energy storage and conversion devices such as H_2-O_2 fuel cells, supercapacitors and batteries are propelled by their potentiality to construct zero emission energy technologies.[1-13] Though H_2-O_2 or proton exchange membrane fuel cell (PEMFC) technology is a promising zero emission technology with high efficiency, the safety and complexities associated with H_2 storage projected small molecule powered direct alcohol fuel cells (DAFCs) encouraging alternative to H_2-O_2 fuel cells.[14-16] However, the multi-electron alcohol oxidation kinetics proceed dominantly through a parallel pathway mechanism on the benchmark Pt based electrocatalysts, strongly blocking its catalytic domains by CO.[17-19] Secondly, alcohol crossover usually encountered in liquid fed fuel cells, becomes a serious issue at higher current densities ultimately poisoning the Pt based cathode catalysts.[20-22] This necessitates heavy loading of precious metal cathode catalysts and engineering its catalytic domains for selective oxygen reduction reaction (ORR).[23-25] All these practically hinder the commercial outreach of DAFC technology. Even though enormous efforts are dedicated to engineer the catalytic domains to favor selective ORR with inherent alcohol inertness, these strategies have so far not addressed the root of the problem, i.e the inner sphere electron transfer nature of either half-cell chemistry. Here we show a direct methanol fuel cell (DMFC) with a precious metal-free cathode containing only carbon nanoparticles with an outer sphere diffusing molecule that can undergo fast redox reaction as electron acceptor. Outer sphere electron acceptors are known in Li-O_2 batteries as mediators and flow batteries as electron acceptors.[26-27] In a significant development Lin *et al.* constructed an all alkaline quinone based flow battery and Gong *et al.* proposed an iron-based flow battery using outer sphere electron acceptors.[28,29]

Apart from being a simple electron acceptor, the introduction of an outer sphere electron acceptor to a fuel cell solves issues specific to DAFC

technology for the following reasons. Firstly, since the inner sphere ORR is replaced by the redox reaction of an outer sphere redox species, intimate contact is not required with the cathode, therefore simple carbon nanoparticles are enough to carry out the reaction at required current density. This turns in to a DAFC with a precious metal-free cathode. Secondly, the carbon cathode is kinetically inert towards alcohol oxidation leading to a DAFC which is free from the complexities of alcohol crossover associated with the cathode. Thirdly, the carbonate accumulation and subsequent clogging of gas diffusion layer (GDL) usually encountered in conventional air breathing DAFC is largely suppressed in the present DAFC configuration as it is a closed architecture. The new DAFC with the outer sphere redox species delivered a power density of ~110 mW/cm^2 at a current density of ~280 mA/cm^2 (at 80°C) which is ~8 times higher than that of the state-of-the-art Pt based DAFC-O_2.

2.2. Materials and Methods

Methanol (99.8%), Potassium ferricyanide (99%), sodium hydroxide (85%) and sulphuric acid (98%) were procured from Sigma Aldrich India and were used as received. Pt/C was procured from Johnson Matthey India. Toray carbon was procured from the fuel cell store, USA.

The electrochemical measurements were recorded with VMP-300 Electrochemical Work Station (Biologic, France). A standard 3 electrode electrochemical cell setup was used to perform the electrochemical measurements with platinum (2 mm diameter) or glassy carbon (3 mm diameter) as working electrode, Ag/AgCl (3.5 M KCl) as reference and platinum mesh as the counter electrode.

Methanol oxidation in acidic and alkaline media was carried out with 0.5 M methanol in 0.5 M H_2SO_4 and 1 M KOH in nitrogen purged solutions at different scan rates ranging from 10 mV/s to 100 mV/s. The cyclic voltammetry was done at a scan rate of 1 mV/s to get the Tafel plots. CO stripping measurements were carried out in 0.5 M H_2SO_4 and 1 M KOH by first purging the solutions with nitrogen, then with carbon

monoxide and finally again with nitrogen before carrying out the measurement. The electrode was held at a potential of 0.2 V vs. RHE. The measurements were done at a scan rate of 1 mV/s.[30,31] pH dependence was carried out by using different pH solutions made with different concentrations of sulphuric acid for acidic pH solutions and potassium hydroxide for alkaline solutions. The ionic strength of the solutions was maintained by using potassium sulphate salt.

Nicholson's method, Klinger and Kochi's method and RDE methods were used to calculate the heterogeneous rate constants and number of electrons. The first two methods are based upon peak potential difference with respect to scan rate.

Nicholson method employs the relation between kinetic parameter (ψ) with the rate constant (k^o) which is given as,

$$\psi = k^0 \left[\frac{\pi D n v F}{RT}\right]^{-1/2}$$

where D is the diffusion coefficient, n is the number of electrons, ν is the scan rate, F is the Faraday constant, R is the universal gas constant and T is the temperature. The kinetic parameter is deduced from the peak potential difference (ΔE). The function which fits the Nicholson data for the practical purpose is given by,

$$\psi = k^0 \left[\frac{-0.6228 + 0.0021\Delta E}{1 - 0.017\Delta E}\right]$$

By plotting ψ against the 1/square root of scan rate the heterogeneous rate constant was calculated from the slope. Nicholson method is valid up to peak potential separation below 150 mV.[32]

Klinger and Kochi method is used when the peak potential difference exceeds 200 mV. According to this method the heterogeneous rate constant is given by the following relation,

$$k^0 = 2.18 \left[\frac{\beta D n v F}{RT}\right]^{-1/2} \exp\left[\frac{-\alpha^2 n F \Delta E}{RT}\right]$$

The value of transfer coefficient is calculated from the slope of the plot of peak potential vs log of scan rate.[33]

Diffusion coefficients were calculated from chronoamperometry using the Cottrell equation.[34]

$$i(t) = \frac{nFACD^{1/2}}{(\pi t)^{1/2}}$$

RDE measurements were done with nitrogen purged solution of 10 mM potassium ferricyanide solution in 0.1 M KOH at a scan rate of 10 mV/s with a three-electrode system containing platinum disc electrode (0.196 cm^2) as working electrode, Ag/AgCl (3.5 M KCl) as reference electrode and platinum wire as counter electrode at different RPM values (100, 400, 900, 1600, 2500, 3600, 4900, 6400). Number of electrons were calculated using the Koutecky-Levich equation,

$$\frac{1}{j} = \frac{1}{j_k} + \frac{1}{j_l}$$

j is the total current density, j_k is kinetic current density and j_l is the limiting current density.

$$j_l = 0.62nFD^{2/3}v^{-1/6}C\ \omega^{1/2}$$

n is the number of electrons, F is the Faraday constant, D (cm^2/s) is the diffusion constant, v is the kinematic viscosity (cm/s), C ($moles/cm^3$) is the bulk concentration and ω is the rotation rate (radians/second).The reciprocal of current density was plotted against reciprocal of rotation rates at different potentials (150 mV, 250 mV, 275 mV, 300 mV, 320 mV). The slope is equal to $1/0.62nFD^{2/3}v^{-1/6}C$ from which the number of electrons was calculated. The intercept of the plot gives the reciprocal of

kinetic current density. The kinetic current is related to overpotential by the following relation,

$$j_k = k^0 CF exp\left[\frac{-\alpha nF}{RT}(E - E^0)\right]$$

The rate constant and transfer coefficient were calculated by plotting overpotential against log of kinetic current density, the slope of which is equal to $2.303\alpha nF/RT$ and the x-intercept gives the exchange cureent density which is equal to FCk^0 from which the value of k^0 was calculated.[35]

In-situ spectroelectrochemistry data of potassium ferro-ferricyanide was collected with 0.2 mM of ferricyanide in 0.1 M KOH at a scan rate of 5 mV/s with a three-electrode system consisting platinum mesh electrode as working electrode, Hg/HgO (1 M NaOH) as reference electrode, platinum wire as counter electrode. The spectrum of potassium ferricyanide was taken as the background.

DMFC-ferricyanide fuel cell was assembled as follows. The anode electrode was fabricated by coating the catalyst i.e., Pt/C (60 wt% Pt) on Toray carbon paper with a loading of 0.2 mg/cm^2. Similarly, for the cathode, Ketjen black carbon nanoparticles were used in place of Pt/C. The respective catalyst inks were prepared by dispersing known amounts of Pt/C (10 wt% of Nafion binder) and Ketjen black (10 wt% of PTFE binder) in isopropanol by sonication for about 30 minutes. A pre-treated Nafion 117 membrane was sandwiched between the two electrodes and the whole setup was placed between the graphite plates with serpentine channels having inlets and outlets for the flowing solutions. Stainless steel endplates were used to tighten the setup. 3 M methanol in 2 M KOH was used as the anolyte (50 mL/minute) and 0.6 M potassium ferricyanide in 2 M KOH was used the catholyte (50 mL/minute). For Pt based DMFC-O_2 fuel cell, the anode was fabricated as in the case of DMFC-ferricyanide. The air cathode ink was fabricated by sonicating Pt/C (1 mg of Pt per cm^2), isopropanol and 10 wt% PTFE binder for 30 minutes. The resulting ink was sprayed on to Toray carbon paper. A pre-treated Nafion 117

membrane was sandwiched between the two electrodes and the whole setup was placed between the graphite plates with serpentine channels. 3 M methanol in 2 M KOH was used as the anolyte (50 mL/minute) and humidified O_2 was continuously supplied to the cathode at a flow rate 0.25 slpm.

2.3. Result and Discussion

The architectural components and potential cathodic reactions due to alcohol crossover in new carbon nanoparticles driven DAFC with an outer sphere electron acceptor is compared with those in a conventional Pt based DAFC-O_2 in Scheme 1. Both fuel cells consist of an anodic and a cathodic chamber separated by a Nafion 117 membrane.

In the new direct methanol fuel cell (DMFC) architecture, anodic compartment is filled with 3 M methanol (in 2 M KOH) and it contains Pt supported on carbon (Pt/C) as the anode electrocatalyst at a loading of 0.5 mg/cm^2 and the cathodic compartment is filled with 0.6 M potassium ferricyanide (in 2 M KOH) as the electron acceptor. Ferricyanide is a known outer sphere redox species that can undergo fast electron transfer even on carbon-based materials,[36] therefore the cathodic reaction required only high surface area carbon nanoparticles to drive the reaction. This configuration is chosen for the following reasons. Methanol oxidation is a pH dependent process and therefore the Nernstian electromotive force vs. pH plot (Pourbaix diagram) for methanol oxidation should demonstrate a slope of -59 mV/pH. Based on this at pH 14 methanol oxidation should have a Nernstian voltage of -826 mV vs. SHE.[37] On the other hand, ferricyanide redox reaction is pH independent thereby providing a constant formal potential of ~0.45 V irrespective of the pH.[38] Therefore if both reactions are coupled in a DMFC architecture one can expect a fuel cell with a voltage of ~1.3 V in which methanol can get oxidized on Pt/C anode and the ferricyanide can function the role of a powerful electron acceptor simply on carbon based cathodes. Experimental Pourbaix

diagram for methanol oxidation is shown in Figure 2.1a and it demonstrates a slope of -66 mV/pH which in turn is close to that of theoretical Nernstian shift. Slight deviation from theoretical value could be due to poisoning of Pt/C catalyst during methanol oxidation which is widely recognized in the fuel cell literature.[39]

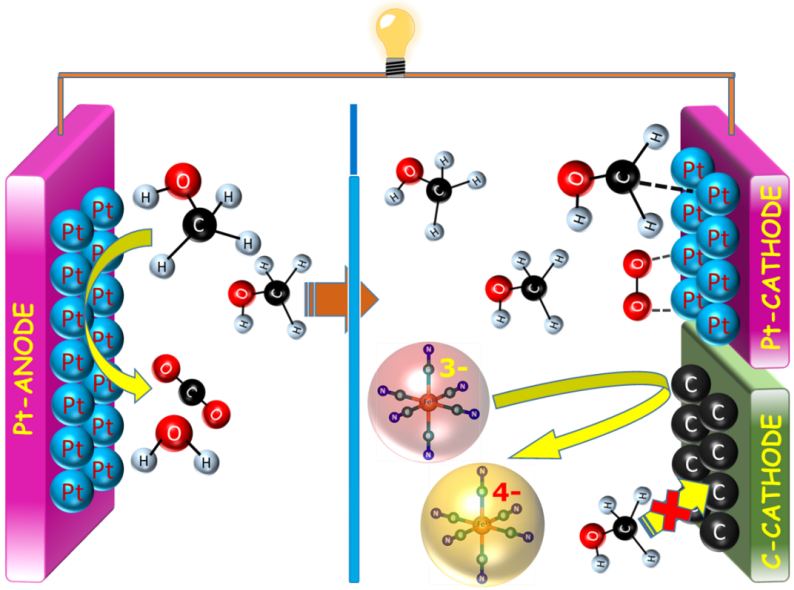

Scheme 1. Schematic representation of architectural components and potential cathodic reactions due to alcohol crossover in conventional Pt based DAFC-O_2 and carbon nanoparticles driven DAFC with an outer sphere electron acceptor.

Experimental Pourbaix diagram for methanol oxidation is shown in Figure 2.1a and it demonstrates a slope of -66 mV/pH which in turn is close to that of theoretical Nernstian shift. Slight deviation from theoretical value could be due to poisoning of Pt/C catalyst during methanol oxidation which is widely recognized in the fuel cell literature.[39] An alkaline pH for methanol oxidation is further justified by the increased kinetics for methanol oxidation on Pt/C in basic pH compared to acidic pH, Figure 2.1b. The current at the peak potential at the same concentration of methanol is found to be amplified by ~20 times in alkaline medium on the same Pt/C catalyst, demonstrating the clear advantages of an alkaline pH for methanol oxidation. This is further

supported by amplified value of electron transfer rate constants for methanol oxidation on Pt/C electrode (at the peak potential) in alkaline pH compared to acidic pH, calculated using Klinger and Kochi method, [40] Figure 2.1b and Table 2.1 and is found to be ~9 times higher in favor of alkaline medium (see experimental section for more details). The Tafel plots, Figure 2.1c further demonstrate the factors controlling the true rate of the reactions such as Tafel slopes and exchange current densities are noticeably improved in favor of alkaline medium compared to the acidic medium, Figure 2.1c and Table 2.1. It should be noted that the electrochemically active area (ECASA) of Pt/C catalysts is higher in acidic medium, owing to the proximity of OH^- adsorption and oxygen adsorption in alkaline medium. For these reasons, the true area normalized parameters are obtained using ECASA in acidic medium, in line with the literature.[41,42] The supremacy of alkaline pH for methanol oxidation is attributed to reduced poisoning of Pt/C catalytic domains, CO stripping voltammograms, Figure 2.1d, wherein CO accumulation is found to be minor in alkaline medium compared to acidic medium. This is due to the abundance of -OH groups in basic pH that can chemically oxidize CO to CO_2 which is widely reported in the literature.[43-45]

Table 2.1. Comparison of methanol oxidation in acidic and alkaline media on a Pt/C electrode.

Medium	**Area (cm^2/g)**	**Exchange current density ($\mu A/cm^2$)**	**Tafel slope (mV/decade)**	**$K^0 \times 10^2$ (cm/s)**
H_2SO_4	57.1	1.0	142	1.45
KOH	28.5	7.9	124	9.64

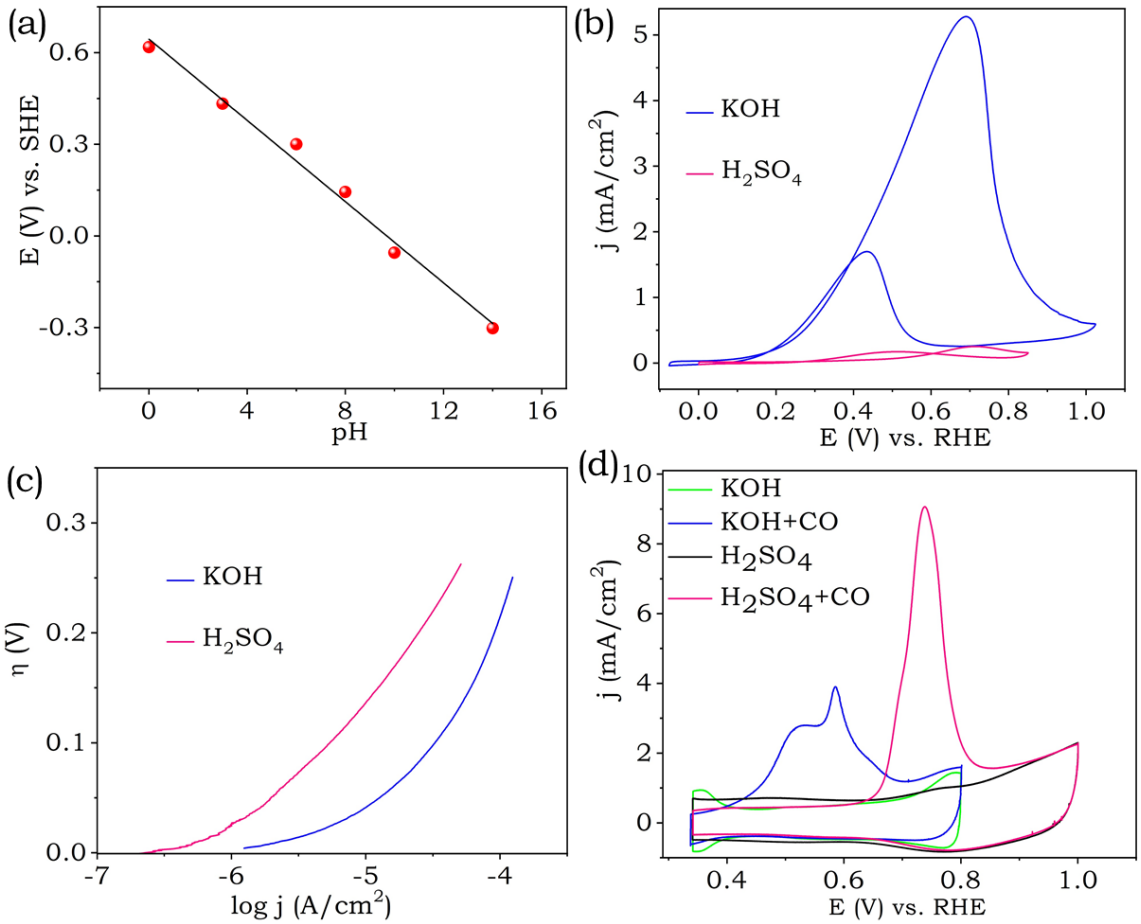

Figure 2.1. (a) Experimental Pourbaix diagram for methanol oxidation, (b) cyclic voltammograms of methanol (0.5 M) oxidation on a Pt/C electrode at a scan rate of 20 mV/s in 0.5 M H_2SO_4 and 1 M KOH, (c) Tafel plots for methanol (0.5 M) oxidation on a Pt/C electrode in 0.5 M H_2SO_4 and 1 M KOH and (d) CO stripping voltammograms of Pt/C electrode in 0.5 M H_2SO_4 and 1 M KOH.

On the other hand, the CV of ferricyanide on carbon based glassy carbon electrode is found to be almost independent of the pH, Figure 2.2a. The formal potentials vs. pH, Figure 2.2b, shows a near zero slope (~1.5 mV/pH) affirming this point. The electron transfer rate constant of ferricyanide on carbon electrode is estimated by Klinger and Kochi method and Nicholson's method independently (see experimental section for more details), Figure 2.2c-d and Table 2.2, and is found to be in the range of 6-9×10^{-2} cm/s suggesting it is a fast and reversible redox reaction.[46]

Therefore simple carbon-based materials will be able to drive the reaction at required current density.

The number of electrons during ferricyanide/ferrocyanide redox reaction estimated by Rotating Disk Electrode (RDE) measurements and the Koutecky-Levich plot (K-L plot) is found to be ~1.06 which is very close to the theoretical value of 1.[47] The electron transfer rate constant extracted from the K-L plot is found to be 7.25×10^{-2} cm/s, Figure 2.3a, and Table 2.3, which is in agreement with the Nicholson's method and Klinger and Kochi method, Figure 2.2 & Table 2.2. Therefore, as noted above the high reaction rate constant makes it possible to employ simple carbon electrode to drive the reaction at required current density which is further demonstrated in the fuel cell polarization studies given below.

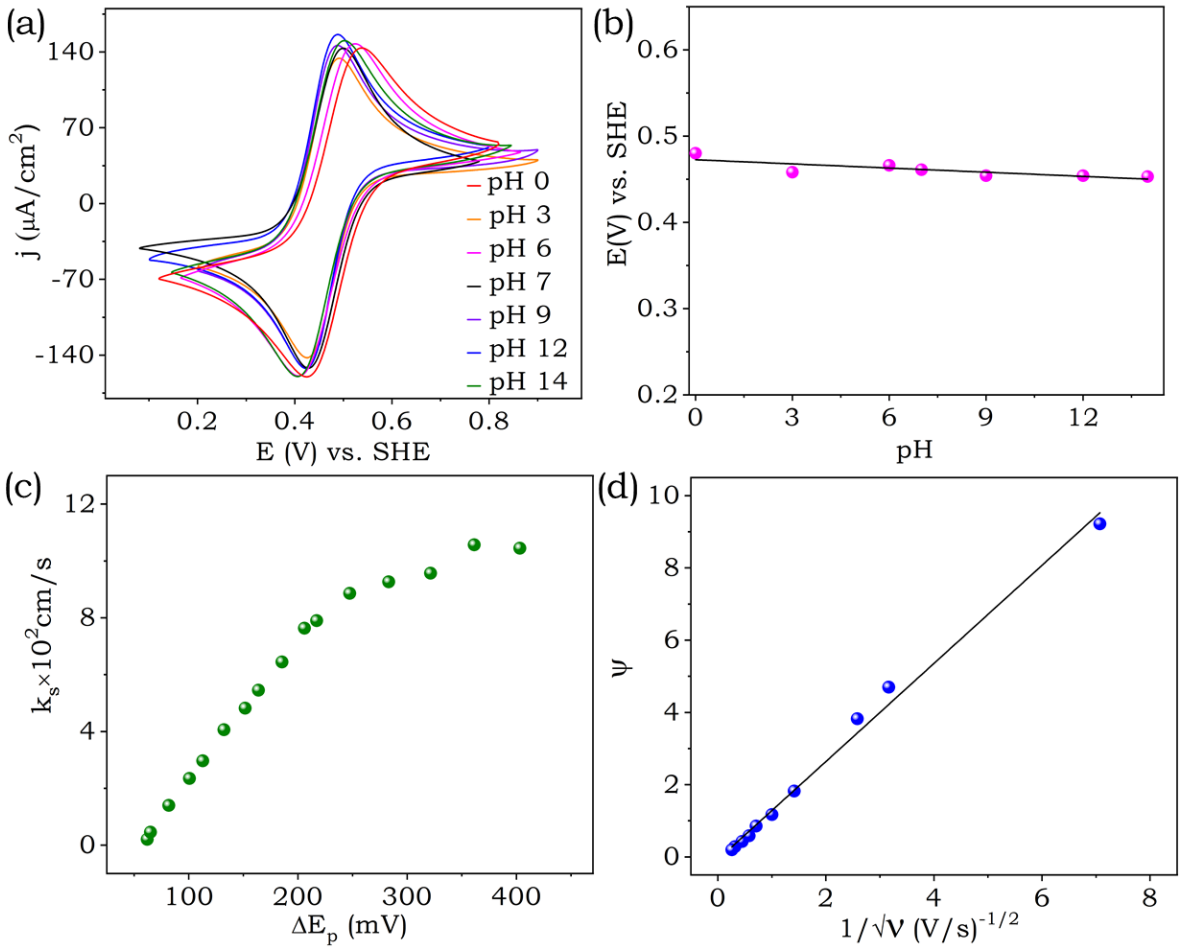

Figure 2.2. (a) Cyclic voltammograms of ferricyanide (10 mM) on a glassy carbon electrode with respect to the pH, and (b) the corresponding

Pourbaix diagram. (c) Variation of heterogeneous rate constant with peak potential separation as per Klinger and Kochi method and (d) the plot for the Nicholson function vs. inverse square root of scan rate.

Table 2.2. Comparison of heterogeneous rate constants for ferricyanide using different methods.

Methods	$K^0 \times 10^2$ (cm/s)
Nicholson	6.17
Klinger and Kochi	9.00

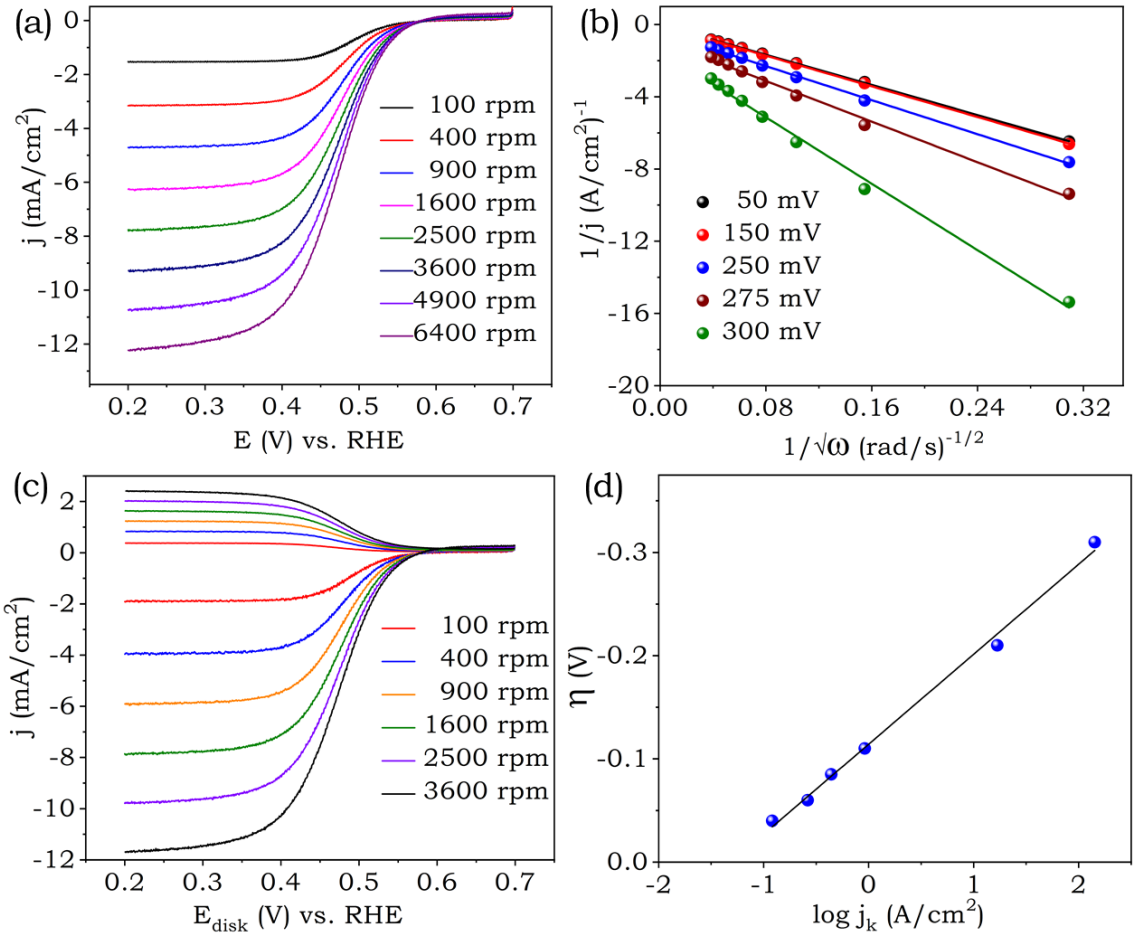

Figure 2.3 (a) Rotating disk electrode measurements obtained on a glassy carbon disk electrode for potassium ferricyanide (10 mM) in 1 M KOH at different rotation rates, and (b) Koutecky–Levich plots at different potentials. (c) Rotating ring disk electrode measurements for potassium

ferricyanide (10 mM) with glassy carbon ring and glassy carbon disk electrodes. (d) Plot of overpotential vs. log of kinetic current for the calculation of intrinsic rate constant.

Table 2.3. Parameters extracted from the RDE experiments during ferricyanide redox reaction.

Parameters	Values
Number of electrons	**1.06**
Symmetry factor (β)	**0.24**
Rate constant ($K^0 \times 10^2$) (cm/s)	**7.25**

The concentrations of methanol, alkali and ferricyanide are optimized in proposed DMFC to maximize the performance, Figure 2.4a-c, and better performance is obtained with 3 M methanol in 2 M KOH as anolyte and 0.6 M ferricyanide in 2 M KOH as the catholyte. It should be noted that 0.6 M ferricyanide is the solubility limit of ferricyanide in 2 M KOH and ferricyanide solubility decreased with increase in alkali concentration. For this reason, even though higher alkali concentration (> 2 M KOH) slightly increased the fuel cell performance as shown in, Figure 2.4a, 2 M KOH was chosen for fuel cell studies. Further the increase in fuel cell performance with increase in methanol concentration was only marginal, Figure 2.4c, therefore 3 M methanol was chosen as the optimum concentration. The fuel cell polarization curve for DMFC containing 3 M methanol (in 2 M KOH) and 0.6 M ferricyanide (in 2 M KOH) separated by a Nafion-117 membrane is shown in Figure 2.5a and it demonstrates an OCV of ~1.1 V analogues to conventional Pt based DMFC-O_2 fuel cell, Figure 2.5b. The peak power density of Pt free DMFC is found to be ~115 mW/cm^2 at a current density of 280 mA/cm^2 (at 80°C) which is ~8 times higher than Pt based DMFC-O_2 fuel cell Figure 2.5a, b and Table 2.4. The

steady state voltage during long time polarization at a higher current density (100 mA/cm^2) with the same concentration of alcohol is found to be at least ~300 mV higher in the present DMFC configuration than Pt based DMFC-O_2 fuel cells at a lower current density (50 mA/cm^2), Figure 2.5c. This corresponds to an energy density of ~3.4 Wh/kg of methanol which is ~3 times higher than Pt based DMFC-O_2 fuel cell, Figure 2.5c and Table 2.4

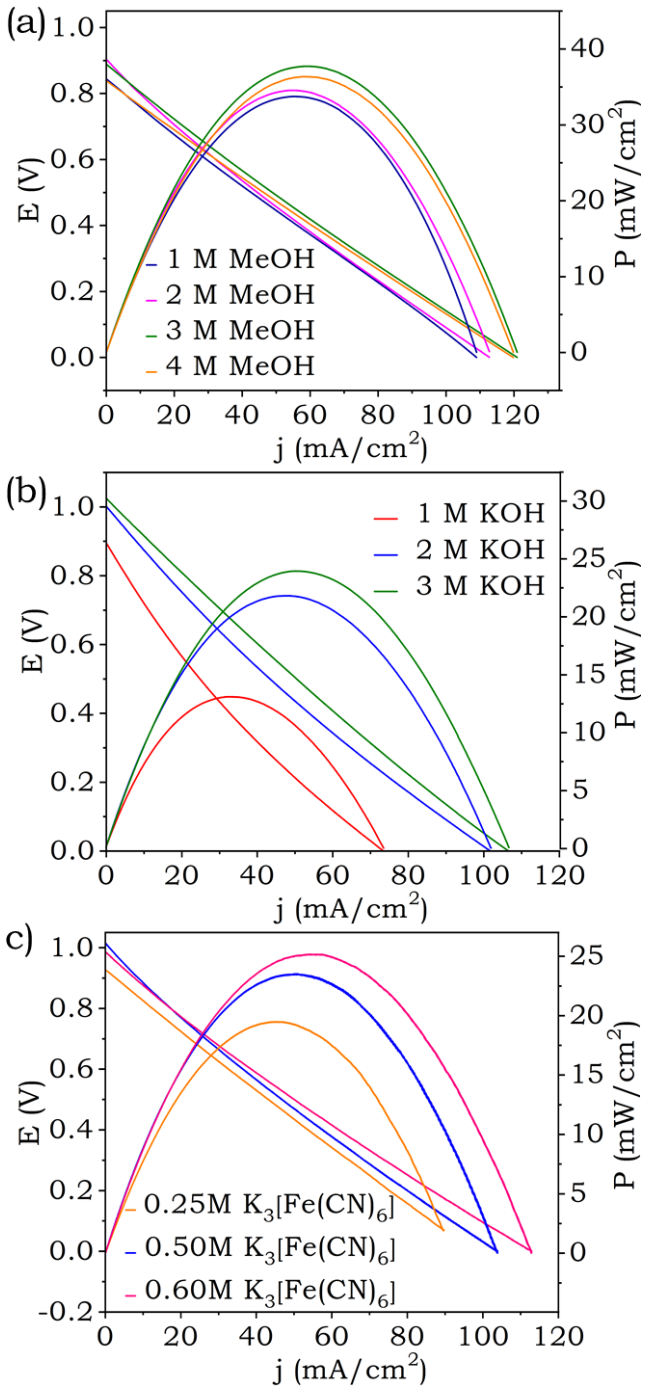

Figure 2.4. Optimization of performance in DMFC-ferricyanide fuel cell. (a) potassium hydroxide, (b) potassium ferricyanide and (c) methanol.

The Tafel plot extracted from the polarization data at 25°C, Figure 2.5d, suggests the factors controlling the true rate of the reactions are amplified with a lower Tafel slope and higher exchange current density in the present DMFC configuration compared to Pt based DMFC-O_2, Table 2.4.

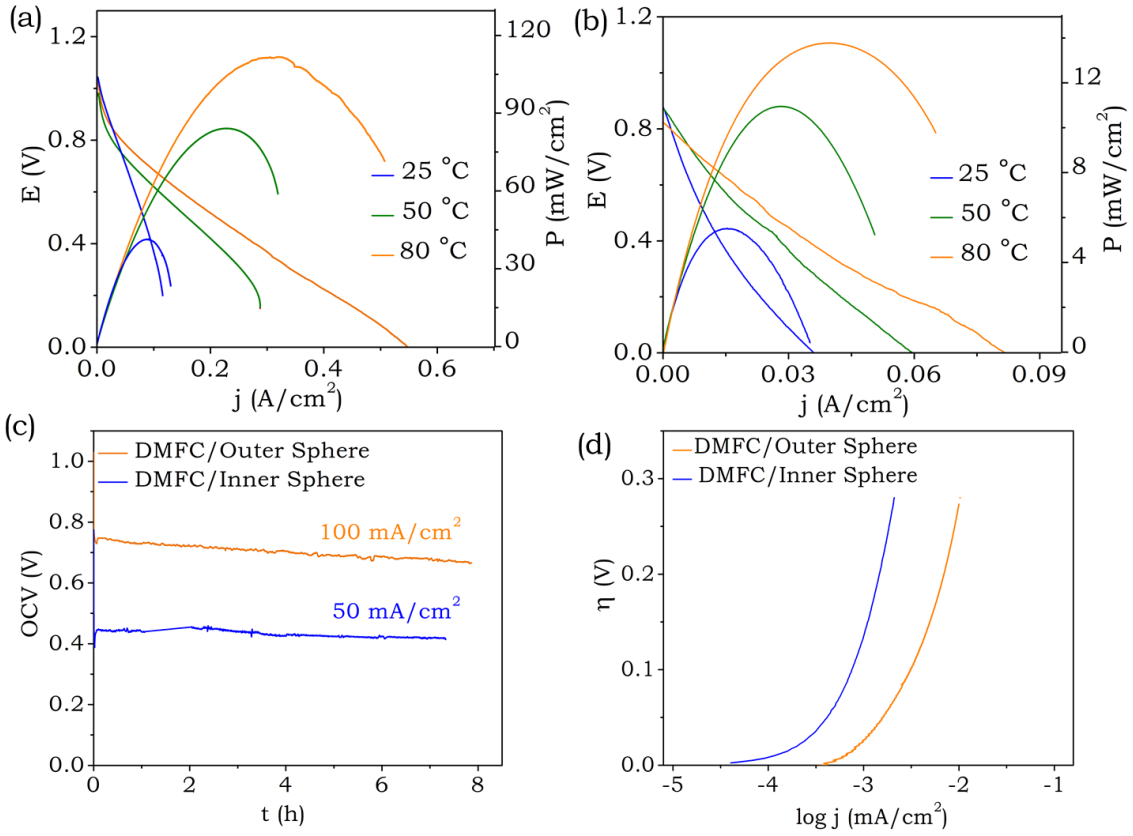

Figure 2.5. (a) Polarization curves of DMFC-ferricyanide (3 M Methanol in 2 M KOH as anolyte and 0.6 M potassium ferricyanide in 2 M KOH as catholyte) fuel cell at different temperatures. Anode Pt loading is 0.2 mg/cm² and cathode carbon loading is 3 mg/cm² and (b) the corresponding performance of Pt based DMFC-O_2 fuel cell at different temperatures. Anode Pt loading is 0.2 mg/cm² and cathode Pt loading is 1 mg/cm². (c) Galvanostatic polarization curves for the DMFC-ferricyanide (at 100 mA/cm²) and Pt based DMFC-O_2 (at 50 mA/cm²) at 80°C and (d) Tafel plots extracted from the polarization data at 25°C.

Table 2.4. Comparison of fuel cell relevant parameters extracted from Figure 2.5.

Fuel cell	Peak current density (mA/cm^2)	Power density (mW/cm^2)	Energy density (Wh/kg)	Exchange current density ($\mu A/cm^2$)	Tafel slope (mV/decade)
DMFC-ferricyanide	280 (80°C)	115 (80°C)	3.4 (80°C)	2.0 (25°C)	350 (25°C)
DMFC-O_2	42 (80°C)	13 (80°C)	1.1 (80°C)	0.46 (25°C)	422 (25°C)

In this Chapter, we do not claim the comparisons are straightforward, because the performance of Pt based DMFC-O_2 can be further improved by increasing the partial pressure of O_2 and Pt loading, however it should be noted that these will have significant cost implications. The performance of DMFC-ferricyanide should be looked at from the aspect of simple carbon-based cathode without the complexities associated with methanol crossover, carbon corrosion and numerous other advantages as noted below.

The stability of carbon cathode is analyzed by FTIR data before and after long time polarization indicating the absence of carbon corrosion which is usually encountered in Pt based DMFC, Figure 2.6a. Pt in presence of O_2 oxidant is known to accelerate carbon corrosion which is evidently present in the FTIR spectral patterns after long term polarization in Pt based DMFC-O_2 fuel cells, Figure 2.6a.[48,49] Methanol crossover and subsequent competition at the cathode is monitored by following the OCV vs. time and cyclic voltammetry with the cathode as working electrode. As shown the OCV vs. time profile demonstrates a self-discharge rate of 100 mV/hr for Pt based DMFC-O_2 fuel cell which is ~2.5 times higher than that for DMFC-ferricyanide fuel cell, Figure 2.6b. The cyclic voltammograms in a diffusion cell with the cathode as working

electrode demonstrate the growing signals due to methanol oxidation with respect to time in DMFC-O_2 fuel cell suggesting alcohol diffusivity and subsequent competition at the cathode, Figure 2.6c. The corresponding voltammograms in DMFC-ferricyanide did not reveal a signal due to methanol clearly demonstrating carbon cathode is kinetically inert towards methanol, Figure 2.6d. Therefore, the present DMFC configuration with an outer sphere redox species demonstrates significant advancement compared to the state-of-the-art Pt based DMFC-O_2, fueling its commercial outreach.

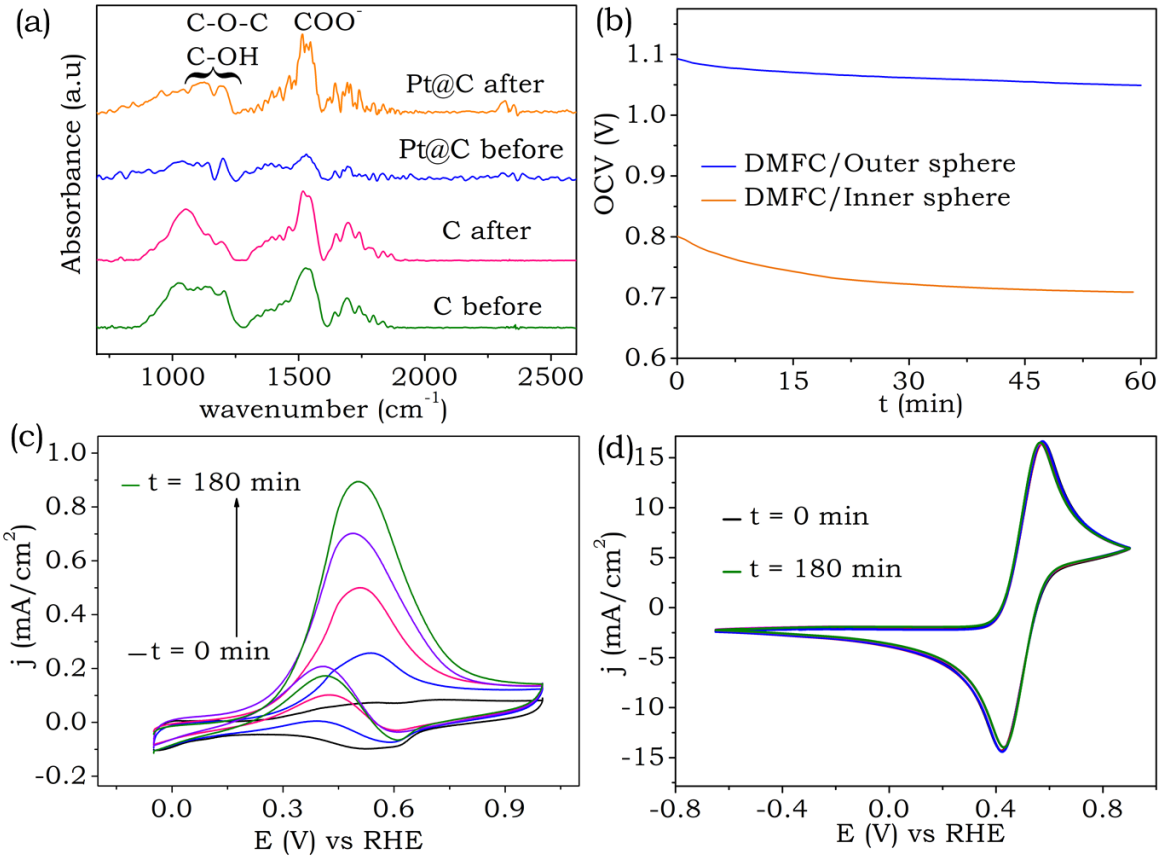

Figure 2.6. (a) FTIR spectra of Pt/C cathode in DMFC-O_2 fuel cell and carbon cathode in DMFC-ferricyanide fuel cell before and after long time stability tests, (b) open circuit voltage vs. time for DMFC-O_2 and DMFC-ferricyanide fuel cell. (c) and (d) are the methanol oxidation profiles at different time intervals at a scan rate of 20 mV/s with the cathode as working electrode in (c) DMFC-O_2 fuel cell and (d) DMFC-ferricyanide fuel cell.

During the operation of the DMFC, it is known that the complete oxidation of methanol generates CO_2.[50,51] The ex-situ FTIR spectral data collected indicate the accumulation of formate species in the electrolyte, Figure 2.7, suggesting the dominance of a parallel pathway mechanism. Further, the limiting half-cell reaction in proposed DMFC-ferricyanide fuel cell is investigated by collecting individual half-cell voltage profiles during the fuel cell polarization studies. As shown in Figure 2.7b, the cathode is found to limit the overall fuel cell performance and it could be due to the lower concentration of ferricyanide (0.6 M) compared to methanol (3 M).

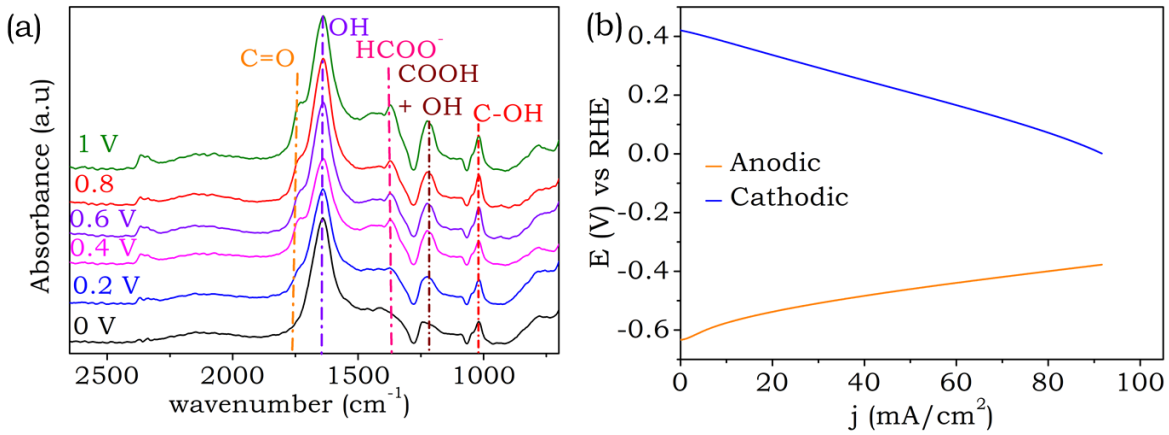

Figure 2.7. (a) Ex-situ FTIR spectra of the electrolyte during methanol oxidation on a Pt/C electrode after holding the potential for a minute at mentioned potentials and (b) Individual half-cell polarization data of anode and cathode in DMFC-ferricyanide fuel cell.

$$K_3[Fe(CN)_6] + K^+ + e^- \longrightarrow K_4[Fe(CN)_6] \qquad (2.1)$$

$$CH_3OH + 6\ OH^- \longrightarrow CO_2 + 5\ H_2O + 6\ e^- \qquad (2.2)$$

$$CH_3OH + 6\ K_3[Fe(CN)_6] + 6\ KOH \longrightarrow 6\ K_4[Fe(CN)_6] + CO_2 + 5\ H_2O \qquad (2.3)$$

Based on the above studies the following anodic and cathodic half-cell reactions (Eq. 2.1and 2.2) are suggested and the complete cell reaction (Eq. 2.3) involves oxidation of methanol to CO_2 and the reduction of

ferricyanide to ferrocyanide with the electron flow through the external circuit.

Taken together, DMFC fuel cell driven by an outer-sphere electron acceptor has numerous advantages with significant reduction in cost of electricity per kW over its Pt based DMFC with inner sphere electron acceptor.

2.4. Conclusions

In this Chapter, we have successfully demonstrated a new DAFC configuration containing a pH independent outer sphere electron acceptor that can be driven by simple and alcohol passive carbon electrode exhibiting performance metrics ~8 times higher than Pt based DAFC-O_2. This configuration leads to a DAFC with a Pt free cathode and a closed architecture. Proposed DAFC addresses alcohol crossover, carbonate clogging and cost issues associated with the state-of-the-art Pt based DMFC-O_2 fuel cells. Even though the performance metrics are improved significantly upon the interfacial modification of the cathode with a pH independent redox couple, we note that this strategy could not introduce any additional functionality to the DAFC architecture. In the Chapter to follow (Chapter 3), we could integrate additional functionality to a DAFC architecture by modifying the cathodic interface by a pH dependent redox species.

2.5. References

[1] Mahne, N.; Schafzahl, B.; Leypold, C.; Leypold, M.; Grumm, S.; Leitgeb, A.; Strohmeier, G. A.; Wilkening, M.; Fontaine, O.; Kramer, D.; Slugovc, C.; Borisov, S. M.; Freunberger, S. A. Singlet Oxygen Generation as a Major Cause for Parasitic Reactions during Cycling of Aprotic Lithium–oxygen Batteries. *Nat. Energy* **2017**, *2*, 17036.

[2] Mourad, E.; Coustan, L.; Lannelongue, P.; Zigah, D.; Mehdi, A.; Vioux, A.; Freunberger, S. A.; Favier, F.; Fontaine, O. Biredox Ionic

Liquids with Solid-like Redox Density in the Liquid State for High-Energy Supercapacitors. *Nat. Mater.* **2016**, *1*, 456-452.

[3] Elia, G. A.; Hassoun, J. A Polymer Lithium-Oxygen Battery. *Sci. Rep.* **2015**, *5*, 12307.

[4] Tintula, K. K.; Jalajakshi, A.; Sahu, A. K.; Pitchumani, S.; Sridhar, P.; Shukla, A. K. Durability of Pt/C and Pt/MC-PEDOT Catalysts under Simulated Start-Stop Cycles in Polymer Electrolyte Fuel Cells. *Fuel Cells* **2013**, *13* (2), 158–166.

[5] Larcher, D.; Tarascon, J.-M. Towards Greener and More Sustainable Batteries for Electrical Energy Storage. *Nat. Chem.* **2015**, *7* (1), 19–29.

[6] Gao, P.-C.; Tsai, W.-Y.; Daffos, B.; Taberna, P.-L.; Pérez, C. R.; Gogotsi, Y.; Simon, P.; Favier, F. Graphene-like Carbide Derived Carbon for High-Power Supercapacitors. *Nano Energy* **2015**, *12*, 197–206.

[7] Reddy, A. L. M.; Nagarajan, S.; Chumyim, P.; Gowda, S. R.; Pradhan, P.; Jadhav, S. R.; Dubey, M.; John, G.; Ajayan, P. M. Lithium Storage Mechanisms in Purpurin Based Organic Lithium-Ion Battery Electrodes. *Sci. Rep.* **2012**, *2*, 960.

[8] Reddy, M. V; Subba Rao, G. V; Chowdari, B. V. R. Metal Oxides and Oxysalts as Anode Materials for Li Ion Batteries. **2013**, *113* (7), 5364–5457.

[9] Gao, J.; Li, L.; Tan, J.; Sun, H.; Li, B.; Idrobo, J. C.; Singh, C. V.; Lu, T. M.; Koratkar, N. Vertically Oriented Arrays of ReS2 Nanosheets for Electrochemical Energy Storage and Electrocatalysis. *Nano Lett.* **2016**, *16* (6), 3780–3787.

[10] Peng, Z.; Freunberger, S. a.; Chen, Y.; Bruce, P. G. A Reversible and Higher-Rate Li-O2 Battery. *Science (80),* **2012**, *337* (6094), 563–566.

[11] Kannan, R.; Kakade, B. A.; Pillai, V. K. Polymer Electrolyte Fuel Cells Using Nafion-Based Composite Membranes with Functionalized Carbon Nanotubes. *Angew. Chem. Int. Ed. Engl.* **2008**, *47*, 2693–2696.

[12] Eshetu, G. G.; Armand, M.; Scrosati, B.; Passerini, S. Energy Storage Materials Synthesized from Ionic Liquids. *Angewandte.* **2014**, 13342–13359.

[13] Gonzalez-Pedro, V.; Juarez-Perez, E. J.; Arsyad, W. S.; Barea, E. M.; Fabregat-Santiago, F.; Mora-Sero, I.; Bisquert, J. General Working Principles of CH3NH3PbX3 Perovskite Solar Cells. *Nano Lett.* **2014**, *14* (2), 888–893.

[14] Kreuer, K. D. On the Development of Proton Conducting Polymer Membranes for Hydrogen and Methanol Fuel Cells. *J. Memb. Sci.* **2001**, *185* (1), 29–39.

[15] Borup, R.; Meyers, J.; Pivovar, B.; Kim, Y. S.; Mukundan, R.; Garland, N.; Myers, D.; Wilson, M.; Garzon, F.; Wood, D.; et al. Scientific Aspects of Polymer Electrolyte Fuel Cell Durability and Degradation. *Chem. Rev.* **2007**, *107* (10), 3904–3951.

[16] Ross, D. K. Hydrogen Storage: The Major Technological Barrier to the Development of Hydrogen Fuel Cell Cars. *Vacuum* **2006**, *80* (10), 1084–1089.

[17] Parrondo, J.; Hou, G.; Parrondo, J.; Ramani, V.; Prakash, J.; Kinetic and Mechanistic Investigation of Methanol Oxidation on a Smooth Polycrystalline Pt Surface. *J. Electrochem. Soc.* **2013**, *161*, F252–F258.

[18] Yu, E. H.; Scott, K.; Reeve, R. W. A Study of the Anodic Oxidation of Methanol on Pt in Alkaline Solutions. *J. Electroanal. Chem.* **2003**, *547* (1), 17–24.

[19] Zhao, X.; Yin, M.; Ma, L.; Liang, L.; Liu, C.; Liao, J.; Lu, T.; Xing, W. Recent Advances in Catalysts for Direct Methanol Fuel Cells. *Energy Environ. Sci.* **2011**, *4* (8), 2736.

[20] Paik, Y.; Kim, S.-S.; Han, O. H. Methanol Behavior in Direct Methanol Fuel Cells. *Angew. Chem. Int. Ed.* **2008**, *47* (1), 94–96.

[21] Gurau, B.; Smotkin, E. S. Methanol Crossover in Direct Methanol Fuel Cells: A Link between Power and Energy Density. *J. Power Sources* **2002**, *112* (2), 339–352.

[22] Eccarius, S.; Garcia, B. L.; Hebling, C.; Weidner, J. W. Experimental Validation of a Methanol Crossover Model in DMFC Applications. *J. Power Sources* **2008**, *179* (2), 723–733.

[23] Gewirth, A. A.; Thorum, M. S. Electroreduction of Dioxygen for Fuel-Cell Applications: Materials and Challenges. *Inorg. Chem.* **2010**, *49* (8), 3557–3566

[24] Anju, V. G.; Manjunatha, R.; Austeria, P. M.; Sampath, S. Primary and Rechargeable Zinc – Air Batteries Using Ceramic and Highly Stable TiCN as an Oxygen Reduction Reaction Electrocatalyst †. *J. Mater. Chem. A Mater. Energy Sustain.* **2016**, *4*, 5258–5264.

[25] Malko, D.; Lopes, T.; Symianakis, E.; Kucernak, A. R. The Intriguing Poison Tolerance of Non-Precious Metal Oxygen Reduction Reaction (ORR) Catalysts. *J. Mater. Chem. A* **2016**, *4* (1), 142–152.

[26] Knudsen, K. B.; Luntz, A. C.; Jensen, S. H.; Vegge, T.; Hjelm, J. Redox Probing Study of the Potential Dependence of Charge Transport Through Li2O2. *J. Phys. Chem. C* **2015**, *119* (51), 28292–28299.

[27] Winsberg, J.; Janoschka, T.; Morgenstern, S.; Hagemann, T.; Muench, S.; Hauffman, G.; Gohy, J. F.; Hager, M. D.; Schubert, U. S. Poly(TEMPO)/Zinc Hybrid-Flow Battery: A Novel, "green," High Voltage, and Safe Energy Storage System. *Adv. Mater.* **2016**, *28* (11), 2238–2243.

[28] Lin, K.; Chen, Q.; Gerhardt, M. R.; Tong, L.; Kim, S. B.; Eisenach, L.; Valle, A. W.; Hardee, D.; Gordon, R. G.; Aziz, M. J.; et al. Alkaline Quinone Flow Battery. *Science* **2015**, *349,* 1529-1532.

[29] Gong, K.; Xu, F.; Grunewald, J. B.; Zhao, Y.; Gu, S.; Yan, Y. All-Soluble All-Iron Aqueous Redox-Flow Battery. *ACS Energy Lett.* **2016**, 1–5.

[30] Roca-Ayats, M.; García, G.; Galante, J. L.; Peña, M. A.; Martínez-Huerta, M. V. TiC, TiCN, and TiN Supported Pt Electrocatalysts for CO and Methanol Oxidation in Acidic and Alkaline Media. J. Phys. Chem. C 2013, 117 (40), 20769–20777.

[31] Spendelow, J. S.; Lu, G. Q.; Kenis, P. J. A.; Wieckowski, A. Electrooxidation of Adsorbed CO on Pt(1 1 1) and Pt(1 1 1)/Ru in Alkaline Media and Comparison with Results from Acidic Media. J. Electroanal. Chem. 2004, 568 (1–2), 215–224.

[32] Nicholson, R. S. Theory and Application of Cyclic Voltammetry F M Measurement of Electrode Reaction Kinetics. *Anal. Chem.* **1965,** 37 (11), 1351–1355.

[33] Rowley-Neale, S. J.; Brownson, D. A. C.; Banks, C. E. Defining the Origins of Electron Transfer at Screen-Printed Graphene-like and Graphite Electrodes: MoO2 Nanowire Fabrication on Edge Plane Sites Reveals Electrochemical Insights. *Nanoscale* **2016,** 8 (33), 15241–15251.

[34] Wang, D.; Chen, S.; Liu, J.; Xu, C. Determination of Diffusion Coefficient of Isopropanol in Alkaline Medium Using Electrochemical Methods on Pd Electrode. *Open Electrochem. J.* **2010,** No. 2, 11–14.

[35] Huskinson, B.; Marshak, M. P.; Suh, C.; Er, S.; Gerhardt, M. R.; Galvin, C. J.; Chen, X.; Aspuru-Guzik, A.; Gordon, R. G.; Aziz, M. J. A Metal-Free Organic–inorganic Aqueous Flow Battery. *Nature* **2014,** 505 (7482), 195–198.

[36] Nugent, J. M.; Santhanam, K. S. V; Rubio, A.; Ajayan, P. M. Fast Electron Transfer Kinetics on Multiwalled Carbon Nanotube Microbundle Electrodes. *Nano Lett.* **2001**, *1* (2), 87–91.

[37] Jing, M.; Jiang, L.; Yi, B.; Sun, G. Comparative Study of Methanol Adsorption and Electro-Oxidation on Carbon-Supported Platinum in Acidic and Alkaline Electrolytes. *J. Electroanal. Chem.* **2013**, *688*, 172–179.

[38] Lin, K.; Gómez-Bombarelli, R.; Beh, E. S.; Tong, L.; Chen, Q.; Valle, A.; Aspuru-Guzik, A.; Aziz, M. J.; Gordon, R. G. A Redox-Flow Battery with an Alloxazine-Based Organic Electrolyte. *Nat. Energy* **2016**, *1*, 16102.

[39] Chung, D. Y.; Kim, H.; Chung, Y.-H.; Lee, M. J.; Yoo, S. J.; Bokare, A. D.; Choi, W.; Sung, Y.-E. Inhibition of CO Poisoning on Pt Catalyst

Coupled with the Reduction of Toxic Hexavalent Chromium in a Dual-Functional Fuel Cell. *Sci. Rep.* **2014**, *4* (ii), 7450.

[40] Klinger, R. J.; Kochi, J. K. Electron-Transfer Kinetics from Cyclic Voltammetry. Quantitative Description of Electrochemical Reversibility. *J. Phys. Chem.* **1981**, *85* (Scheme I), 1731–1741.

[41] Krishnamurthy, B.; Deepalochani, S. Performance of Platinum Black and Supported Platinum Catalysts in a Direct Methanol Fuel Cell. *Int. J. Electrochem. Sci* **2009**, *4*, 386–395.

[42] Zadick, A.; Dubau, L.; Sergent, N.; Berthomé, G.; Chatenet, M. Huge Instability of Pt/C Catalysts in Alkaline Medium. *ACS Catal.* **2015**, *5* (8), 4819–4824.

[43] Jiang, J.; Kucernak, A. Electrooxidation of Small Organic Molecules on Mesoporous Precious Metal Catalysts I: CO and Methanol on Platinum. *J. Electroanal. Chem.* **2002**, *533* (1–2), 153–165.

[44] Jiang, J.; Kucernak, A. Electrooxidation of Small Organic Molecules on Mesoporous Precious Metal Catalysts II: CO and Methanol on Platinum-Ruthenium Alloy. *J. Electroanal. Chem.* **2003**, *543* (2), 187–199.

[45] Russel, A. E. Electrocatalysis: Theory and Experiment at the Interface. *Phys. Chem. Chem. Phys.* **2008**, *10* (25), 3607.

[46] Muhammad, H.; Tahiri, I. A.; Muhammad, M.; Masood, Z.; Versiani, M. A.; Khaliq, O.; Latif, M.; Hanif, M. A Comprehensive Heterogeneous Electron Transfer Rate Constant Evaluation of Dissolved Oxygen in DMSO at Glassy Carbon Electrode Measured by Different Electrochemical Methods. *J. Electroanal. Chem.* **2016**, *775*, 157–162.

[47] Tucceri, R. The Charge Transport Process at Gold Electrodes Modified by Thick Nickel Hydroxide Films. A Study Employing Rotating Disc Electrode Voltammetry in the Presence of the Fe(CN)63−/4− Redox Couple. *J. Electroanal. Chem.* **2016**, *782*, 125–132.

[48] Yu, X.; Ye, S. Recent Advances in Activity and Durability Enhancement of Pt/C Catalytic Cathode in PEMFC. Part I. Physico-

Chemical and Electronic Interaction between Pt and Carbon Support, and Activity Enhancement of Pt/C Catalyst. *J. Power Sources* **2007**, *172* (1), 133–144.

[49] Yu, X.; Ye, S. Recent Advances in Activity and Durability Enhancement of Pt/C Catalytic Cathode in PEMFC. Part II: Degradation Mechanism and Durability Enhancement of Carbon Supported Platinum Catalyst. *J. Power Sources* **2007**, *172* (1), 145–154.

[50] Liu, H.; Song, C.; Zhang, L.; Zhang, J.; Wang, H.; Wilkinson, D. P. A Review of Anode Catalysis in the Direct Methanol Fuel Cell. *J. Power Sources* **2006**, *155* (2), 95–110.

[51] Huang, T.; Mao, S.; Zhou, G.; Zhang, Z.; Wen, Z.; Huang, X.; Ci, S.; Chen, J. A High-Performance Catalyst Support for Methanol Oxidation with Graphene and Vanadium Carbonitride. *Nanoscale* **2015**, *7* (4), 1301–1307.

Chapter 3

A Direct Alcohol Fuel Cell Driven by a pH Dependent Redox Couple

Abstract: In this Chapter, additional functionality of hydrogen production is integrated to a direct alcohol fuel cell during electricity production by interfacial modification of the cathodic interface by utilizing a pH dependent redox couple. 'Hydrogen economy' could enable a carbon-neutral sustainable energy chain. However, issues with safety, storage, and transport of molecular hydrogen impede its realization. Alcohols as liquid H_2 carriers could be enablers, but state-of-the-art reforming is difficult, requiring high temperatures >200°C and pressures >25 bar, and the resulting H_2 is carbonized beyond tolerance levels for direct use in fuel cells. Here, we demonstrate ambient temperature and pressure alcohol reforming in a fuel cell (ARFC) with simultaneous electrical power output. The alcohol is oxidized at the alkaline anode, where the resulting CO_2 is sequestrated as carbonate. Carbon-free H_2 is liberated at the acidic cathode. The neutralization energy between alkaline anode and acidic cathode drives the process, particularly the unusually high entropy gain (1.27-fold ΔH). The significantly positive temperature coefficient of the resulting electromotive force allows to harvest a large fraction of the output energy from the surrounding, achieving a thermodynamic efficiency as high as 2.27. MoS_2 as the cathode catalyst allows alcohol reforming even under open-air conditions; a challenge that state-of-the-art alcohol reforming failed to overcome. We further show reforming of a wide range of alcohols. The ARFC offers an unprecedented route towards hydrogen economy as CO_2 is simultaneously captured and pure H_2 produced at mild conditions.

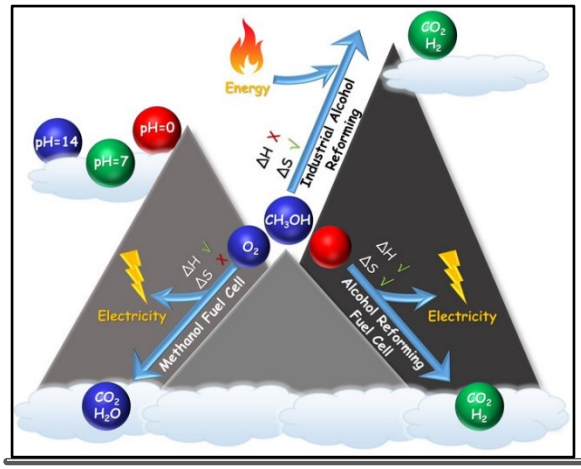

The chapter contains the data taken from my original published work: Zahid Bhat et.al., ACS Sustain. Chem. Eng. 2021, 9, 8, 3104–3111. Copyright American Chemical Society

3.1. Introduction

The variability of renewable energy resources due to characteristic weather fluctuations increase the mismatch between energy generation and demand, and bridging this gap requires the development of efficient energy storage and conversion strategies. [1-13] "Hydrogen economy" or sustainable hydrogen fuel production and its subsequent utilization for energy conversion, can accommodate renewable energy fluctuations since hydrogen is a non-polluting energy carrier molecule.[14-16] 'Hydrogen economy' in principle provides a pathway towards a carbon neutral economy because hydrogen is an environmentally friendly alternative to fossil fuels and the utilization of the former for energy conversion with the help of a proton exchange membrane fuel cell (PEMFC) is a potential zero-emission energy pathway.[14-19] However, the prime challenges in realizing a mighty 'hydrogen economy' are storage, safety and transportation issues associated with molecular hydrogen, which in turn projected lower aliphatic alcohols which are liquids at room temperature as efficient hydrogen carrier molecules.[20-23] Even though this has rekindled hope in hydrogen economy, hydrogen extraction by state of the art alcohol reforming process is prohibitively expensive, invariably requiring high precious metal catalyst loading, high temperatures >200ºC and high pressures >25 bar.[24-31] Even with such a large energy input, the generated H_2 fuel streams are often carbonized (primarily with CO and CO_2) with levels well exceeding the tolerance level for directly utilizing in a PEMFC thereby requiring energy intensive fuel purification modules. [24-28] It should be noted that there were laudable developments in catalysis for lowering the temperature and pressure requirements for alcohol reforming, [29-33] however, the production of carbon free molecular hydrogen from alcohols at room temperature and pressure remain as an elusive challenge even today. Recently some of us have formulated a 'fuel exhaling fuel cell' wherein the hydrogen fuel consumed in the anodic half-cell is exhaled as molecular hydrogen at the cathodic half-cell by

interconverting the energy of neutralization as electromotive force.[34] These results and our thermodynamic calculations (Calculation 3.1) motivated us to employ the energy of neutralization for alcohol reforming at room temperature and pressure as a combination of the two predicted an overall negative free energy change of 476.1 kJ/mol.

Based on this, we have developed a room temperature alcohol reforming fuel cell (ARFC) chemistry where electric power generation is integrated with spontaneous hydrogen fuel production via the inter-conversion of neutralization energy as electrical driving force, which transforms fuel cells from simple fuel utilization devices to fuel reservoirs. The formulated chemistry is very unusual compared to state of the art energy conversion pathways as the former is driven primarily by its distinctly high positive entropic heat (~127% of ΔH) which is often insignificant for the latter (<~10%), Thermodynamic Calculation 3.1.[35-37] Since temperature coefficient of electromotive force (dE/dT) is directly related to entropy change, a positive dE/dT of ~ 2.39 mV/K for ARFC, (as discussed below) enable the device to obtain ~0.46 V (at 298 K) of electrical driving force by harvesting heat from the surroundings leading to a thermodynamic efficiency as high as 2.27. Since the decarbonization and fuel generation half cells are delinked by a cation selective membrane in proposed ARFC, generated hydrogen fuel is inherently pure enabling its direct utilization in a PEMFC without any purification module. The dependency of decarbonization half-cell on the hydroxide ion concentration allow CO_2 capture which in turn offers opportunities for hydrogen generation with CO_2 capture. The ability of the proposed ARFC for on-demand fuel generation can be utilized to address storage issues associated with molecular hydrogen by linking the ARFC with a PEMFC in a tandem configuration. ARFC based hydrogen economy offers a feasible solution for reviving hydrogen economy from its twilight as CO_2 is captured and electric power is harnessed simultaneously during hydrogen fuel production as well as its utilization.

3.2. Materials and Methods

Methanol (99.8%), ethanol (99.9%), sulphuric acid (99.99%), potassium hydroxide (85%), acetic acid (99.7%), sodium acetate (99%), potassium phosphate (99%), potassium hydrogen phosphate (99%) and potassium dihydrogen phosphate (99%), ammonium molybdate tetrahydrate (99.98%), thiourea (99.8%) and chloroplatinic acid hexahydrate (99.9%) were from Sigma Aldrich India. Platinum supported on carbon (Pt/C) with 60 wt% Pt and PtRu supported on carbon (PtRu/C) with Pt (40 wt%), Ru (40 wt%) and C (20 wt %)) were from Johnson Matthey India.

Electrochemical measurements were carried out using Biologic potentiostat (VMP-300), ATR-FTIR spectra were measured using a Bruker Alpha instrument. NMR (^{1}H and ^{13}C) were measured with a Bruker 400 MHz instrument. Gas chromatograms were measured with Intuvo 9000 GC System (Agilent Technologies) and in-situ electrochemical mass-spectrometry was carried out with HPR-20 R&D (Hiden analytical) Quadrupole mass analyzer. Scanning electron microscopy with energy dispersive X-ray spectrum (Zeiss Ultra plus-4095) were used to study morphology and elemental analysis of MoS_2. XRD measurements were performed using Bruker D_8 advance diffractometer.

In acidic media, $Hg/HgSO_4$ (K_2SO_4) was used as reference electrode and platinum mesh as the counter electrode. In alkaline media, Hg/HgO (1 M KOH) was used as the reference electrode and platinum mesh as the counter electrode. For the RHE scale conversion of the reference electrodes, a Pt disk was used as the working electrode and Pt foil as the counter electrode in H_2 saturated solutions and the potential was scanned in the H_2 evolution/oxidation regions. The average of the two potentials at which the current crossed zero was taken as the equilibrium potential for the H_2 electrode. Alcohol oxidation was carried out using a Pt/C or Pt-Ru/C coated glassy carbon electrode as the working electrode. The catalyst slurry was prepared by dispersing the Pt/C or PtRu/C in

isopropyl alcohol (5 μg/μl) by sonication for 30 minutes. From the slurry, 5 μl was drop casted on a glassy carbon disc electrode with an area of 0.071 cm^2. Before each measurement, the electrodes were cycled in the solutions to obtain a reproducible cyclic voltammogram. For the Tafel plots, linear sweep voltammetry was performed at 1 mV/s. Before each experiment, the solutions were purged with high purity N_2 for 15 minutes. To construct the Pourbaix diagram for the methanol oxidation reaction, the open circuit voltage of methanol containing electrolyte was measured on a Pt electrode as a function of pH. The different pH solutions were prepared by making different buffer solutions; HSO_4^-/ SO_4^{2-} (pH 1 to 2), acetate buffer (pH 3–5), and phosphate buffer (pH 5 to 12) were used to prepare the respective solutions. For pH = 0 and pH = 14 solutions, 0.5 M H_2SO_4 and 1 M KOH solutions, respectively, were used. The pH of each solution was adjusted using 1 M H_2SO_4 or 1 M KOH solutions.

CO stripping measurements were carried out in 0.5 M H_2SO_4 and 1 M KOH by first purging the solutions with N_2 for 15 minutes. The electrode was then held at a potential of 0.2 V vs. RHE and the solution was purged with CO for 1 hour followed by N_2 purging for 15 minutes before carrying out the stripping. The CO stripping measurements were done at a scan rate of 1 mV/s with Pt/C in acidic (0.5 M H_2SO_4) and alkaline media (1 M KOH) and with Pt/C and Pt-Ru/C in alkaline medium (1 M KOH).The hydrogen evolution reaction (HER) in acidic (0.5 M H_2SO_4) and alkaline (1 M KOH) media were carried out with polycrystalline platinum electrode (area= 0.0314 cm^2) as the working electrode at a scan rate of 50 mV/s. Prior to each measurement, the solutions were first saturated with hydrogen by continuous purging. To construct the Pourbaix diagram for the HER, cyclic voltammograms were measured in different pH solutions. The corresponding Pourbaix diagrams show the potential at 10 mA/cm^2 versus pH.

A two-compartment cell separated by a pre-treated Nafion 117 membrane was used for the fuel cell experiments. The anode was prepared by coating PtRu/C (40:40 wt% Pt:Ru) on a Toray carbon paper with a

loading of 1 mg/cm^2. The PtRu/C was dispersed with 10 wt% Nafion binder in isopropanol by sonication for about 30 minutes to prepare the catalyst ink, which was brush coated onto the carbon electrode. The cathode was made by electrodepositing platinum from chloroplatinic acid onto a titanium mesh at a current density of 5 mA/cm^2 for 7 minutes, which corresponds to a Pt loading of ~1 mg/cm^2. The anolyte contained 2 M methanol in 6 M KOH and the catholyte 3 M H_2SO_4. The anolyte and the catholyte volumes employed were 20 ml. H_2 generated at the cathode was collected by water displacement technique using graduated burette for quantification. The hydrogen fuel was collected in the calibrated cylinder by connecting the cathodic outlet of the device to the graduated burette. During the combined galvanostatic polarization of the ARFC and the air-breathing PEMFC, the H_2 from the ARFC was pumped directly into the PEMFC. The purity of the H_2 was confirmed by the GC and in-situ electrochemical mass spectroscopy. The mass analyzer was calibrated for Ar, H_2, CO_2, N_2, and H_2O.

MoS_2 was synthesized according to the literature.[35-37] 1 mM $(NH_4)_6Mo_7O_{24}{\cdot}4H_2O$ and 30 mM thiourea were dissolved in 35 mL distilled water under vigorous stirring to form a homogeneous solution. After stirring for 30 minutes, the solution was transferred into a 100 mL Teflon lined stainless steel autoclave and maintained at 180 °C for 24 h. Then the reaction mixture was allowed to cool down to room temperature naturally. The product was washed with distilled water and the resulting powder was dried in a vacuum oven and characterized by various techniques.

3.3. Results and Discussion

Alcohol oxidation reaction (AOR) is a pH dependent process, and therefore, the Nernstian electromotive force (EMF) for AOR (for e.g., methanol oxidation) shifts negatively with respect to the pH (please refer to Figure 2.1, Chapter 2 for further details). Comparative cyclic

voltammograms and Tafel plots suggest amplified kinetics for methanol oxidation on Pt based electrodes in alkaline medium compared to acidic medium, justifying the choice of an alkaline medium for housing methanol in the ARFC. This is due to the hydroxide assisted removal of accumulated CO on Pt in alkaline medium as reported by others. [38-41]. Removal of accumulated CO on Pt can be further accelerated by alloying Pt with Ru due to the operation of a bi-functional mechanism in CO oxidation. [42-45]

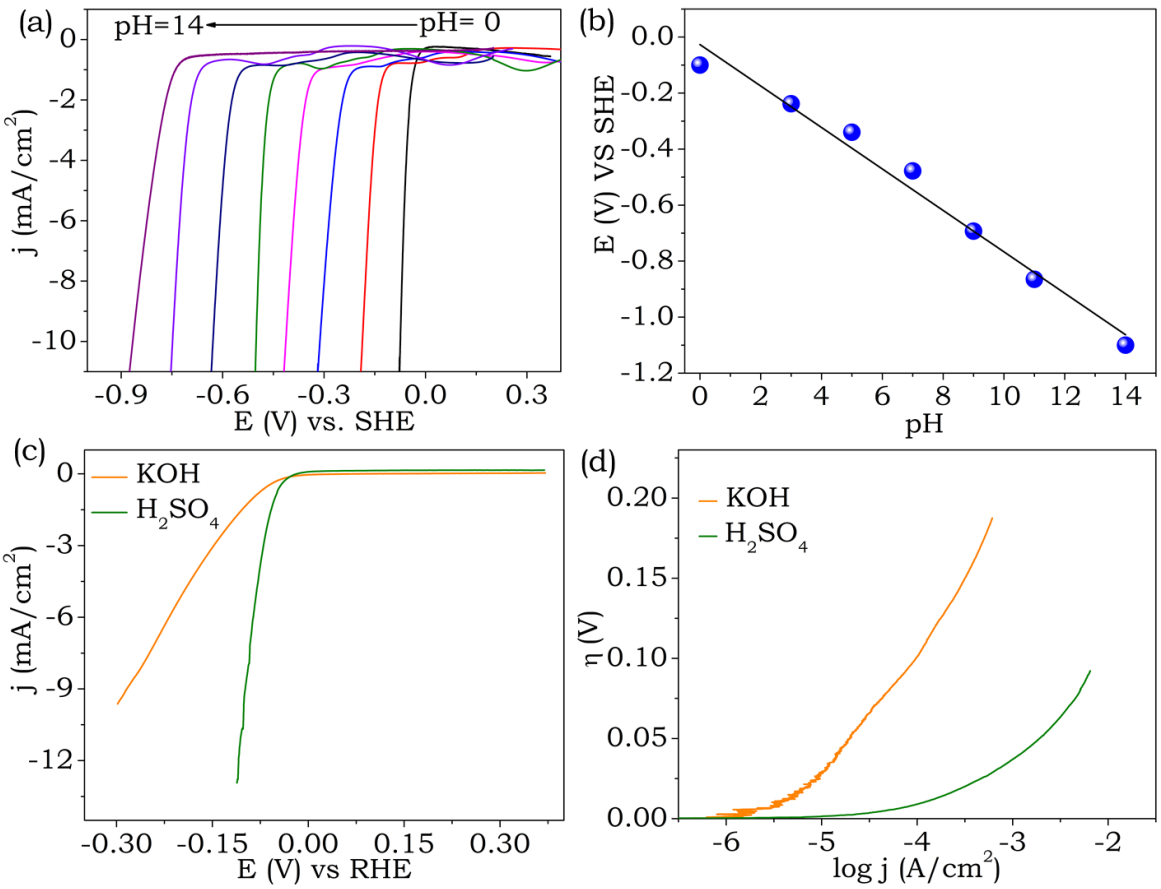

Figure 3.1: (a) Linear sweep voltammograms for hydrogen evolution reaction (HER) in different pH solutions at 20 mV/s. and (b) corresponding pourbaix diagram for hydrogen evolution reaction. (c) comparative linear sweep voltammograms for hydrogen evolution reaction (HER) in pH=14 solution (orange trace) and in pH=0 solution (green trace) on a Pt electrode at a scan rate of 20 mV/s and (d) Tafel plot for the HER in pH=0 and pH =14. (The corresponding LSVs for the Tafel plot were done at 1mV/s scan rate).

Table 3.1. Comparison of hydrogen evolution reactions in acidic (0.5 M H_2SO_4) and alkaline (1 M KOH) media on polycrystalline Pt electrode. Exchange current densities are normalized with respect to geometric electrode area.

Medium	Tafel Slope (mV/dec)	Exchange Current Density (mA/cm²)
H_2SO_4	36	0.104
KOH	74	0.005

Nevertheless, pH dependent electromotive force for AOR and HER as shown in Figure 3.2a highlights that when alkaline solution of methanol at pH=14 is coupled to an acidic medium at pH=0 through an ion exchange membrane, alcohol reformation (alcohol oxidation to H_2 and CO_2) at room temperature (25°C) and pressure (1 atm) should be spontaneous, equations 3.1-3.3. This configuration should make AOR half-cell negative with respect to the acidic half-cell, which is indeed the case as shown in Figure 3.2b. The overall cell reaction for alcohol reformation (equation 3.3) involves acid-base recombination in an electrochemical pathway and consequently, the inter-conversion of energy of neutralization as electromotive force should play a crucial role for making this possible. As discussed below, our thermodynamic calculation very well supports this claim, Calculation 3.1.

$$6\ H^{+}_{(aq)} + 6\ e^{-} \longrightarrow 3\ H_{2(g)} \quad E^0 = 0\ \text{V vs SHE} \quad (3.1)$$

$$CH_3OH_{(l)} + 6\ OH^{-} \longrightarrow CO_{2(g)} + 5\ H_2O_{(l)} + 6\ e^{-} \quad E^0 = -0.81\ \text{V vs SHE} \quad (3.2)$$

$$CH_3OH_{(l)} + 6\ H^{+}_{(aq)} + 6\ OH^{-}_{(aq)} \longrightarrow CO_{2(g)} + 5\ H_2O_{(l)} + 3\ H_{2(g)} \quad E^0 = -0.81\ \text{V} \quad (3.3)$$

Like the AOR, hydrogen evolution reaction (HER) is also a pH dependent electrochemical reaction, linear sweep voltammetry (LSV) and Pourbaix diagram, Figure 3.1a and Figure 3.1b. An acidic medium for performing the HER in ARFC is justified by the amplified exchange current density and electron transfer kinetics of HER on Pt electrodes in acidic

solution compared to alkaline solution, comparative LSV and Tafel plots, Figure3.1c-Figure 3.1d and Table 3.1. The lower Tafel slope for HER on the Pt electrode in acidic medium compared to alkaline medium reflects that the parameters governing the rate of the reactions are amplified in acidic medium which is attributed mainly to the nature of the reactant, in the former it being hydronium ion compared to H_2O in the latter. [46-52]

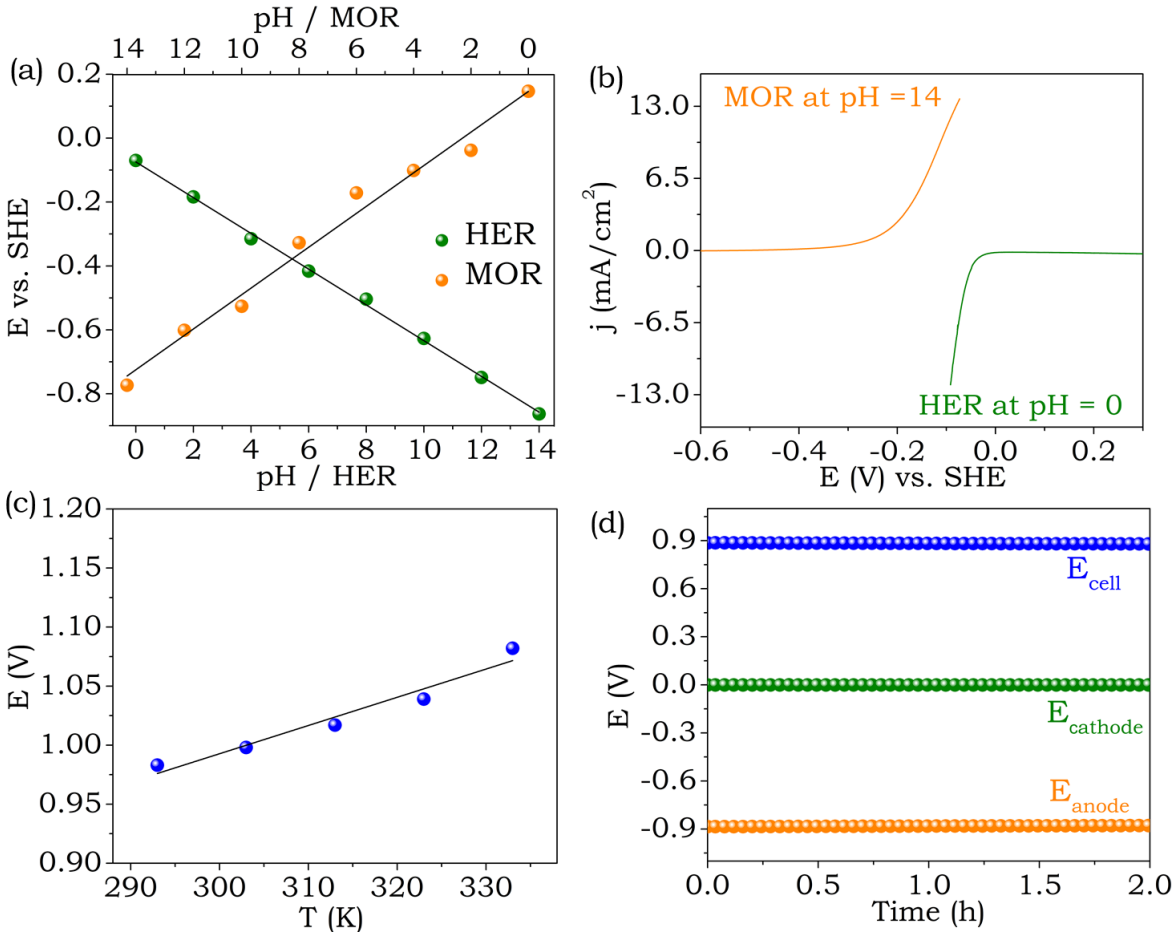

Figure 3.2: (a) Pourbaix diagrams for methanol oxidation reaction (MOR) and hydrogen evolution reaction (HER) (b) Linear sweep voltammograms for methanol (0.5 M) oxidation reaction in pH=14 solution and hydrogen evolution reaction (HER) in pH=0 solution on a Pt electrode at a scan rate of 50 mV/s. (c) EMF versus cell temperature for the alcohol reforming fuel cell with 2 M methanol in 6 M KOH as the anolyte and 2 M H_2SO_4 as the catholyte. Anodic and cathodic electrocatalysts were PtRu/C (at a loading of 1 mg/cm^2) and Pt supported on Ti mesh (at a loading of 1 mg/cm^2) respectively and (d) single electrode potentials (two electrode configuration)

of alkaline methanol half-cell relative to the acidic half-cell along with the total cell potential.

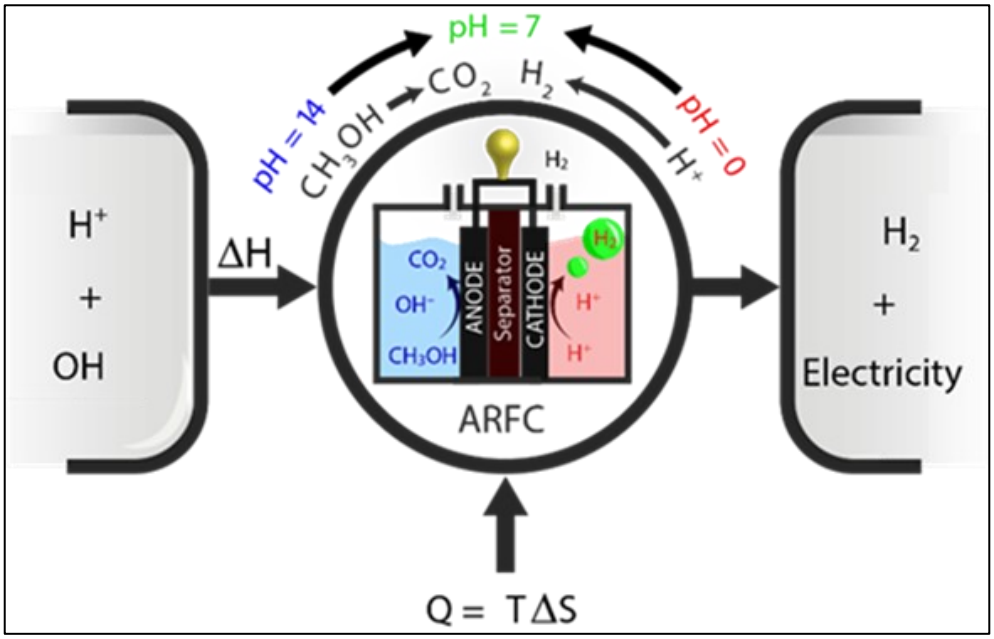

Scheme 3.1. Scheme of alcohol reforming fuel cell (ARFC) chemistry driven by neutralization energy.

ARFC chemistry driven by neutralization energy (Scheme 3.1) is quite unique compared to the state-of-the-art direct methanol fuel cell (DMFC) pathway as the former is driven by its distinctly high and positive entropic heat (~127 % of ΔH at 298 K) which is negative and insignificant for the latter (<4 % of ΔH at 298 K), thermodynamic calculation 3.1. Since it is known that the direction of entropic heat is decided by the sign of temperature coefficient of EMF (dE/dT) because of their direct relation, we have estimated the dE/dT for the ARFC pathway driven by the neutralization energy. As shown, in Figure 3.2c, this pathway has a positive dE/dT of ~2.39 mV/K which enables the device to harvest ~0.46 V out of 0.82 V from the surroundings (at 298 K) leveraging a thermodynamic efficiency as high as ~2.27. As shown in our thermodynamic calculation (Calculation 3.1) for the DMFC pathway the thermodynamic efficiency is ~0.97 because of its negligible (and negative) entropic heat, indicating that the ARFC chemistry aided by neutralization energy is very unique as it is primarily driven by its highly positive

entropic heat. As shown in the calculation, the chemical reformation (CAR) pathway is an uphill thermodynamic route because of its significantly positive enthalpy change which explains the reasons for its high temperature and high-pressure requirements, calculations 3.1.[24-31] The overall negative free energy change of ~-476 kJ/mol for the ARFC chemistry predicts that alcohol reformation driven by the neutralization energy eventually enable spontaneous aqueous phase alcohol reformation at room temperature and pressure with simultaneous electric power generation or an alcohol reforming fuel cell (ARFC). This demonstrates that coupling of alcohol oxidation in the alkaline half-cell and hydrogen evolution in the acidic half-cell (Figure 3.1b) make spontaneous alcohol reformation feasible or alcohol reformation during electric power generation because of the pH dependence of the respective half-cell reactions as discussed below.

Calculation 3.1: Thermodynamics of the cell reactions

Calculation of the thermodynamics of the cell reactions for the ARFC and the competing chemistries, i.e., chemical MeOH dehydrogenation and the direct methanol fuel cell. All thermodynamic parameters are taken from Atkins, Physical Chemistry, 11th Edition.

(a) Alcohol reforming fuel cell driven by neutralization energy

The net cell reaction is

$$CH_3OH_{(l)} + 6\ H^+_{(aq)} + 6\ OH^-_{(aq)} \longrightarrow CO_{2(g)} + 5\ H_2O_{(l)} + 3\ H_{2(g)} \qquad (3.3)$$

Using Hess's law, combining the following reactions yields the overall heat of reaction in Eq. 3.3:

Reaction 1: combustion of methanol:

$$CH_3OH_{(l)} + 3/2\ O_{2(g)} \longrightarrow CO_{2(g)} + 2\ H_2O_{(l)} \quad \Delta H_1 = -726\ \text{kJ mol}^{-1} \qquad (3.4)$$

Reaction 2: Splitting of water into molecular hydrogen and oxygen:

$$3\ H_2O_{(l)} \longrightarrow 3\ H_{2(g)} + 3/2\ O_{2(g)} \qquad \Delta H_2 = 286\ \text{kJ mol}^{-1} \qquad (3.5)$$

Reaction 3: Acid-base neutralization:

$$6\ H^{+}_{(aq)} + 6\ OH^{-}_{(aq)} \longrightarrow 6\ H_2O_{(l)} \qquad H_3 = -57.1\ \text{kJ mol}^{-1} \qquad (3.6)$$

Adding reactions 1 to 3 yields Eq. 3.3. Its heat of reaction is

$$\Delta H_{\text{total}} = \Delta H_1 + 3\,\Delta H_2 + 6\,\Delta H_3 = -726 + 3 \cdot 286 + (6 \cdot -57.1)$$

$$= -210\ \text{kJ mol}^{-1} \quad (3.7)$$

The entropy change of the reaction is

$$\Delta S_{\text{total}} = S_{(\text{products})} - S_{(\text{reactants})}$$

$$= \left(S_{CO_2} + 5\,S_{H_2O} + 3\,S_{H_2}\right) - \left(S_{CH_3OH} + 6\,S_{H^+} + 6\,S_{OH^-}\right)$$

$$= (213.74 + 5 \cdot 69.91 + 3 \cdot 130.68) - \left(126.8 + 6 \cdot 0 + 6 \cdot (-10.75)\right)$$

$$= 893.03\ \text{J K}^{-1}\ \text{mol}^{-1} \qquad (3.8)$$

The free energy change of the reaction is

$$\Delta G = \Delta H - T\Delta S = -210\ \text{kJ mol}^{-1} - \left(298\ \text{K} \cdot 893.03\ \text{J K}^{-1}\ \text{mol}^{-1}\right)$$

$$= -476.12\ \text{kJ mol}^{-1} \qquad (3.9)$$

The corresponding electromotive force is

$$E = -\frac{\Delta G}{nF} = \frac{-476{,}120}{6 \cdot 96485} = 0.82\ \text{V} \qquad (3.10)$$

With the thermodynamic efficiency being

$$\eta = \frac{\Delta G}{\Delta H} = \frac{-476.12}{-210} = 2.27 \qquad (3.11)$$

(b) Chemical dehydrogenation of methanol

The net cell reaction is

$$CH_3OH_{(l)} + H_2O_{(l)} \longrightarrow CO_{2(g)} + 3\ H_{2(g)} \qquad (3.12)$$

Again, combining the following reactions yields the overall heat of reaction in Eq. 3.12:

Reaction 1: combustion of methanol:

$$CH_3OH_{(l)} + 3/2\ O_{2(g)} \longrightarrow CO_{2(g)} + 2\ H_2O_{(l)} \quad \Delta H_1 = -726\ \text{kJ mol}^{-1} \qquad (3.4)$$

Reaction 2: Splitting of water into molecular hydrogen and oxygen:

$$3\ H_2O_{(l)} \longrightarrow 3\ H_{2(g)} + 3/2\ O_{2(g)} \qquad \Delta H_2 = 286\ \text{kJ mol}^{-1} \qquad (3.13)$$

Adding reactions 1 and 2 yields Eq. 3.12. Its heat of reaction is

$$\Delta H_{\text{total}} = \Delta H_1 + 3\,\Delta H_2 = -726 + 3 \cdot 286 = 132\ \text{kJ mol}^{-1} \qquad (3.14)$$

The entropy change of the reaction is

$\Delta S_{\text{total}} = S_{(\text{products})} - S_{(\text{reactants})}$

$= \left(S_{CO_2} + 3\, S_{H_2}\right) - \left(S_{CH_3OH} + 3\, S_{H_2O}\right)$

$= (213.74 + 3 \cdot 130.68) - (126.8 + 5 \cdot 69.91)$

$= 129.48\ \text{J K}^{-1}\ \text{mol}^{-1}$ (3.15)

The free energy change of the reaction is

$\Delta G = \Delta H - T\Delta S = 132\ \text{kJ mol}^{-1} - \left(298\ \text{K} \cdot 129.48\ \text{J K}^{-1}\ \text{mol}^{-1}\right)$

$= 93.41\ \text{kJ mol}^{-1}$ (3.16)

This formally corresponds to a negative electromotive force

$E = -\frac{\Delta G}{nF} = -\frac{93{,}410}{6 \cdot 96485} = -0.16\ \text{V}$ (3.17)

(c) Direct methanol-O_2 fuel cell

The net cell reaction is

$CH_3OH_{(l)} + 3/2\ O_{2(g)} \longrightarrow CO_{2(g)} + 2\ H_2O_{(l)}\ \ \Delta H_1 = -726\ \text{kJ mol}^{-1}$ (3.18)

The entropy change of the reaction is

$\Delta S_{\text{total}} = S_{(\text{products})} - S_{(\text{reactants})}$

$= \left(S_{CO_2} + 2\, S_{H_2O}\right) - \left(S_{CH_3OH} + 3/2\, S_{O_2}\right)$

$= (213.74 + 2 \cdot 69.91) - (126.8 + 3/2 \cdot 205.14)$

$= -80.95\ \text{J K}^{-1}\ \text{mol}^{-1}$ (3.19)

The free energy change of the reaction is

$\Delta G = \Delta H - T\Delta S = -726\ \text{kJ mol}^{-1} - \left(298\ \text{K} \cdot 80.95\ \text{J K}^{-1}\ \text{mol}^{-1}\right)$

$= 701.9\ \text{kJ mol}^{-1}$ (3.20)

The corresponding electromotive force is

$E = -\frac{\Delta G}{nF} = \frac{-701{,}900}{6 \cdot 96485} = 1.21\ \text{V}$ (3.21)

With the thermodynamic efficiency being

$\eta = \frac{\Delta G}{\Delta H} = \frac{-701.9}{-726} = 0.96$ (3.22)

The polarization curves for the ARFC, Figure 3.3a, demonstrates an open circuit voltage (OCV) of ~0.9 V and a peak power density of ~42 mW/cm^2 at a current density of ~75 mA/cm^2 (orange trace). The polarization curve without methanol in the anodic half-cell even though

showing similar OCV yielded negligible performance, confirming methanol to be the electron donor and the pH gradient to provide the driving force for the reaction, Figure 3.3a (blue trace). The galvanostatic discharge of the ARFC at a current density of 70 mA/cm^2, Figure 3.3b, demonstrates close to theoretical H_2 yield according to Eq. 3.1 and hence near absence of parasitic chemistry at the cathodic half-cell. This purity of gas is confirmed by in-situ electrochemical mass spectrometry during galvanostatic operation in which the cathodic half-cell evolved exclusively H_2, Figure 3.3c, and confirming Eq 3.1 as the cathodic half-cell reaction. Contrary to state-of-the-art chemical reforming techniques, the H_2 produced by the ARFC is inherently separated from the carbonaceous product stream which remains at the anode side (Scheme 3.1, Figure 3.3c). This enables its direct use in a PEMFC without any further purification. This direct link of an ARFC and an air breathing PEMFC in a tandem configuration is shown in Figure 3.3d,e. The latter achieved a peak power density of ~50 mW/cm^2 at ~220 mA/cm^2, Figure 3.3d. In the tandem configuration, the galvanostatic discharge of the PEMFC at 20 mA/cm^2 demonstrated a discharge plateau close to 0.7 V (Figure 3.3e, orange trace) lasting for ~17 hours corresponding to the life of the ARFC, Figure 3.3f (green trace). Therefore, the ARFC enable spontaneous production of pure hydrogen with electric power generation via alcohol reforming at room temperature and pressure.

The ARFC can reform even longer chain aliphatic alcohols such as ethanol to pure molecular hydrogen with concurrent electric power production, Figure 3.4, demonstrating a wider scope of fuels which will be promising for a sustainable energy landscape. Similar results were obtained with a range of alcohols viz., longer chain aliphatic alcohols like pentanol, secondary alcohols like isopropyl alcohol, aromatic alcohols like benzyl alcohol, and diols like ethylene glycol making this strategy a universal one, Figure 3.4. This introduces an ARFC based hydrogen economy which is unprecedented in the aspect that electric power is

harnessed during hydrogen fuel production as well as its utilization, Figure 3.3a and Figure 3.3e.

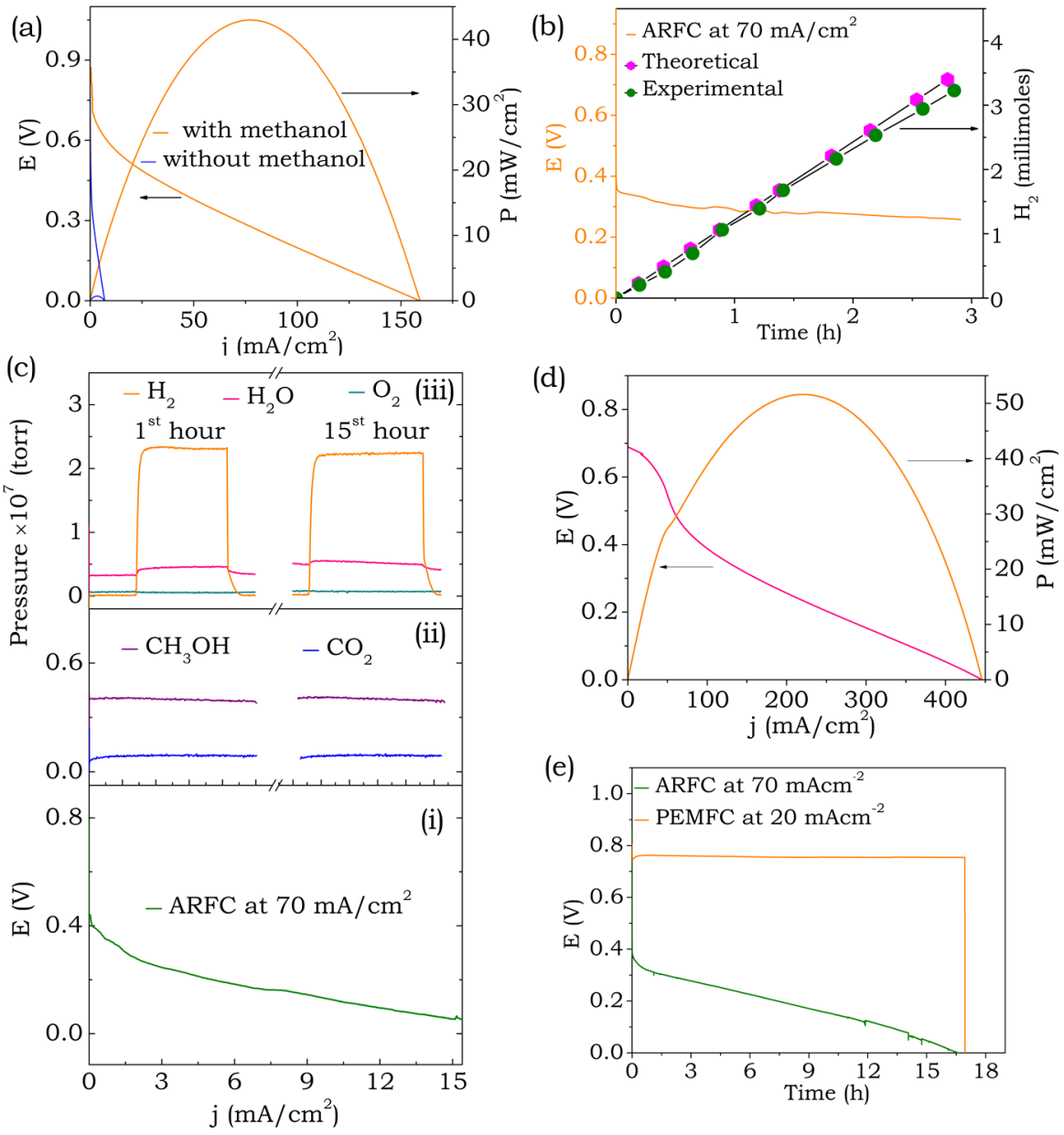

Figure 3.3: (a) Polarization curve for alcohol reforming fuel cell (ARFC) with methanol as the fuel (2 M methanol in 6 M KOH as the anolyte and 3 M H_2SO_4 as the catholyte). (b) Measured versus expected H_2 evolution at the cathode of the ARFC at 70 mA/cm^2. (c) In-situ electrochemical mass spectrometry of the gas phase in the cathodic (iii) and anodic (ii) half-cells of the ARFC during intermittent operation (1 h off/on) at 70 mA/cm^2 with the voltage evolution shown in (i). (d) Polarization curve for PEMFC

cathodic exhaust of ARFC as the fuel. (e) Voltage versus time upon feeding an air breathing PEMFC at 20 mA/cm^2 with the cathodic exhaust of an ARFC at 70 mA/cm^2. This demonstrates electric power generation from methanol-to-H_2 reforming as well as H_2 use. For the ARFC, electrocatalysts were 1 mg/cm^2 PtRu/C at anode and 1 mg/cm^2 of Pt on Ti mesh at cathode, respectively. For the air breathing PEMFC, electrocatalysts were 1 mg/cm^2 Pt/C at anode as well as cathode.

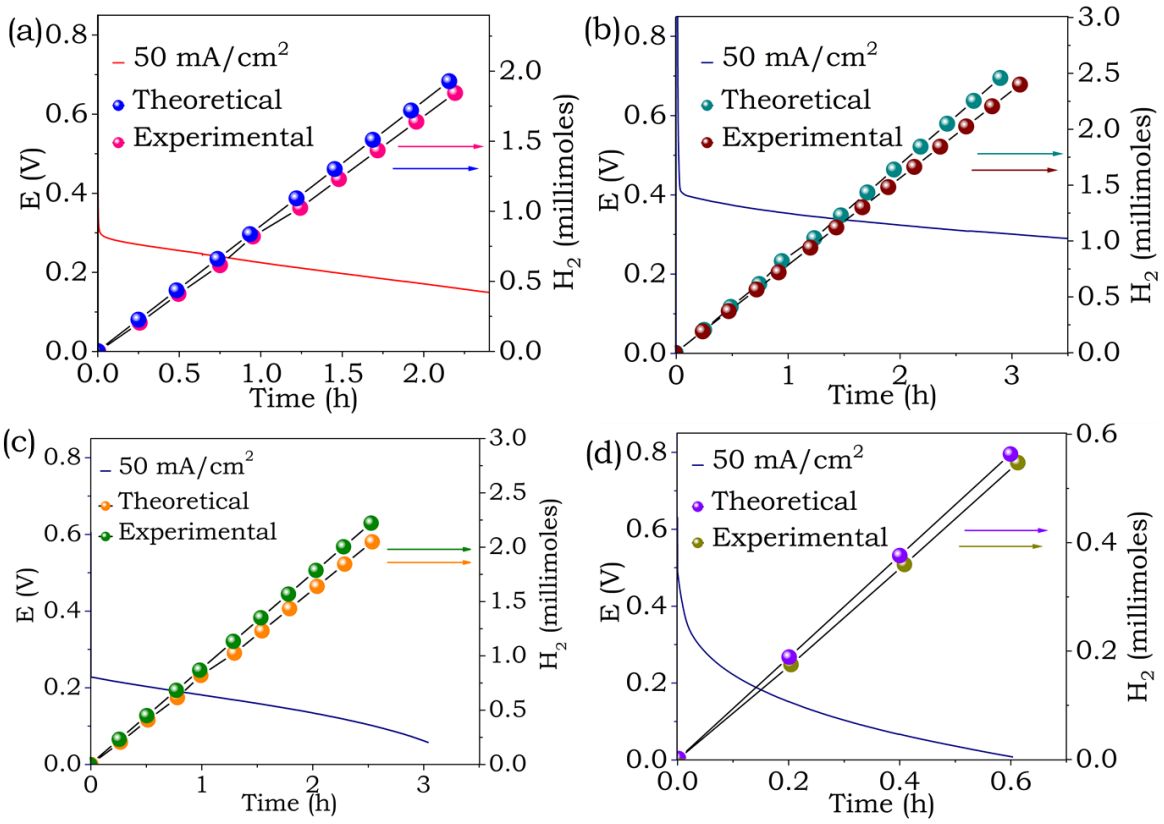

Figure 3.4: Galvanostatic polarization of ARFC at 50 mA/cm^2 with H_2 quantification at the cathode with (a) Ethanol, (b) Ethylene glycol, (c) Benzyl alcohol and (d) Pentanol as fuel in the anodic half-cell.

The emanated gaseous species from the alkaline half-cell of the ARFC should be primarily carbon dioxide (Eq. 3.2), however, in-situ electrochemical mass spectrometry did not detect any CO_2 evolution throughout the polarization, Figure 3.3c (ii). Ex-situ FTIR and ^{13}C NMR spectroscopic analysis of the anolyte after the long-term discharge, Figure 3.5a and Figure 3.5b, show vibrations at ~1610 cm^{-1} and a peak at ~168

ppm respectively, indicating the accumulation of carbonate species in the anodic half-cell. FTIR bands at ~ 1380 cm^{-1}, Figure 3.5a, and ^{13}C / ^{1}H NMR peaks at ~171 ppm / 8.5 ppm, Figure 3.4b / Figure 3.4c) suggest incompletely oxidized aldehydic and carboxylic species to form next to CO_2, which is possible given the well-known parallel pathway mechanism in methanol oxidation reaction where methanol can be simultaneously ox-oxidized to CO_2 with and without the intermediacy of CO.[34,38] Therefore, CO_2 evolved during alcohol reformation is accumulated as carbonate (CO_3^{2-}) in alkaline medium providing opportunities for its sequestration which eventually leads to exclusive hydrogen fuel production during alcohol reforming.

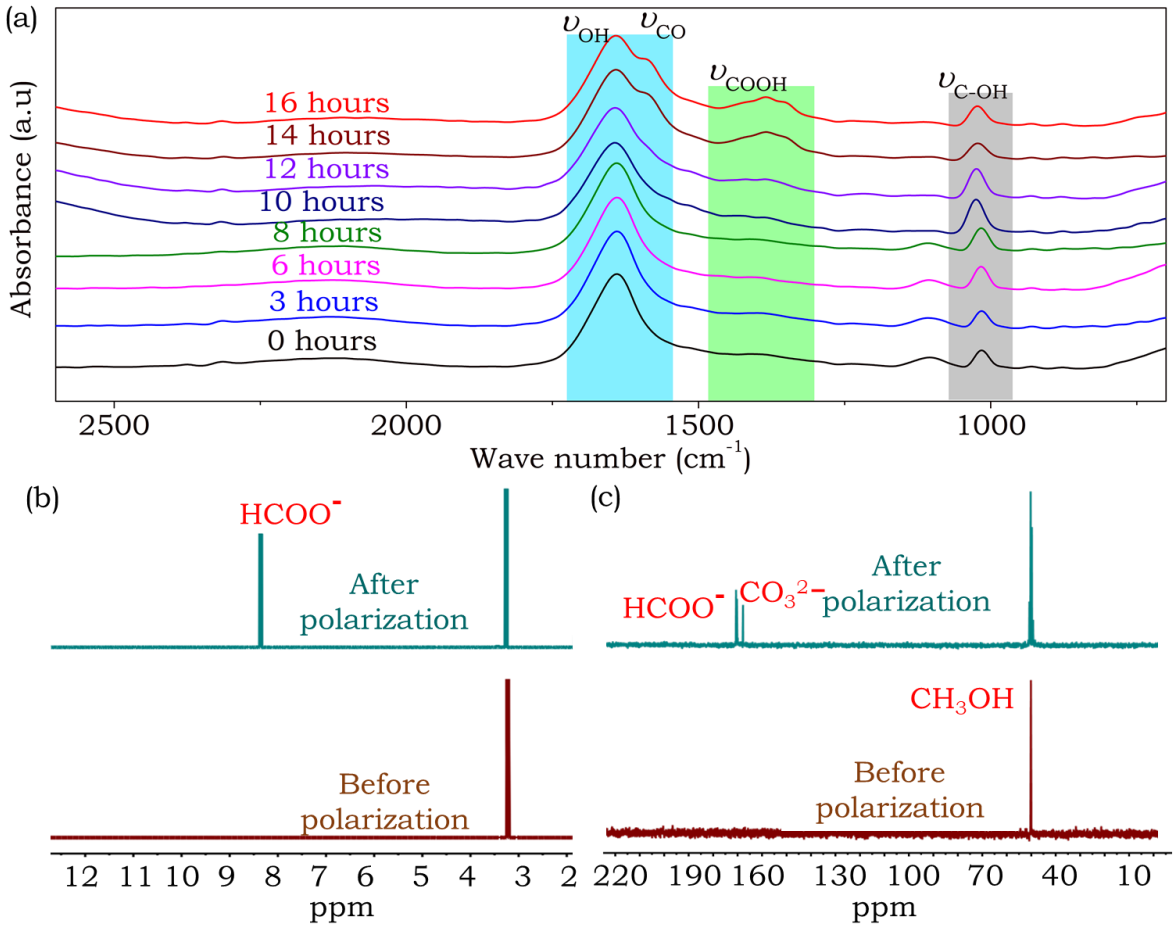

Figure 3.5: (a) Ex-situ FTIR spectra of the anolyte (2 M methanol in 6 M KOH) after different times during galvanostatic polarization at 70 mA/cm^2 current density. (b) ^{13}C NMR spectra of the anolyte before and after long term galvanostatic polarization at 70 mA/cm^2 with 2 M methanol in 6 M

KOH as the anolyte and 3 M H_2SO_4 as the catholyte. (c) ^1H NMR spectra of the anolyte before and after long term galvanostatic polarization at 70 mA/cm^2.

The emanated gaseous species from the alkaline half-cell of the ARFC should be primarily carbon dioxide (Eq. 3.2), however, in-situ electrochemical mass spectrometry did not detect any CO_2 evolution throughout the polarization, Figure 3.3c (ii). Ex-situ FTIR and ^{13}C NMR spectroscopic analysis of the anolyte after the long-term discharge, Figure 3.5a and Figure 3.5b, show vibrations at ~1610 cm^{-1} and a peak at ~168 ppm respectively, indicating the accumulation of carbonate species in the anodic half-cell. FTIR bands at ~ 1380 cm^{-1}, Figure 3.5a, and ^{13}C / ^1H NMR peaks at ~171 ppm / 8.5 ppm, Figure 3.4b / Figure 3.4c) suggest incompletely oxidized aldehydic and carboxylic species to form next to CO_2, which is possible given the well-known parallel pathway mechanism in methanol oxidation reaction where methanol can be simultaneously oxidized to CO_2 with and without the intermediacy of CO.[34,38] Therefore, CO_2 evolved during alcohol reformation is accumulated as carbonate (CO_3^{2-}) in alkaline medium providing opportunities for its sequestration which eventually leads to exclusive hydrogen fuel production during alcohol reforming. We do not rule out the possibility of bicarbonate accumulation as the pH in the anodic half-cell tend to converge towards neutral pH during long term polarization (as explained below). These corroborates equation 2 as the anodic half-cell reaction.

Relying on neutralization, OH^- and H^+ are consumed at anode and cathode (Eqs. 3.1 and 3.2) and K^+ is transported from one to the other to balance charges. Accordingly, the pH of anolyte and catholyte converged to neutral pH during simultaneous electricity and H_2 generation, Figure 3.6a. It is pertinent to mention here that the formation of carbonates and bicarbonates in the cathodic half-cell results in higher pH change in the anolyte (ΔpH = 6.2) than in the catholyte (ΔpH = 5.3) due to the CO_2/CO_3^{2-} equilibrium as depicted by the equations (Eq. 3.23 and 3.24),

$$CO_2 + OH^- \rightleftharpoons HCO_3^- \qquad (3.23)$$

$$HCO_3^- + OH^- \rightleftharpoons CO_3^{2-} + H_2O \qquad (3.24)$$

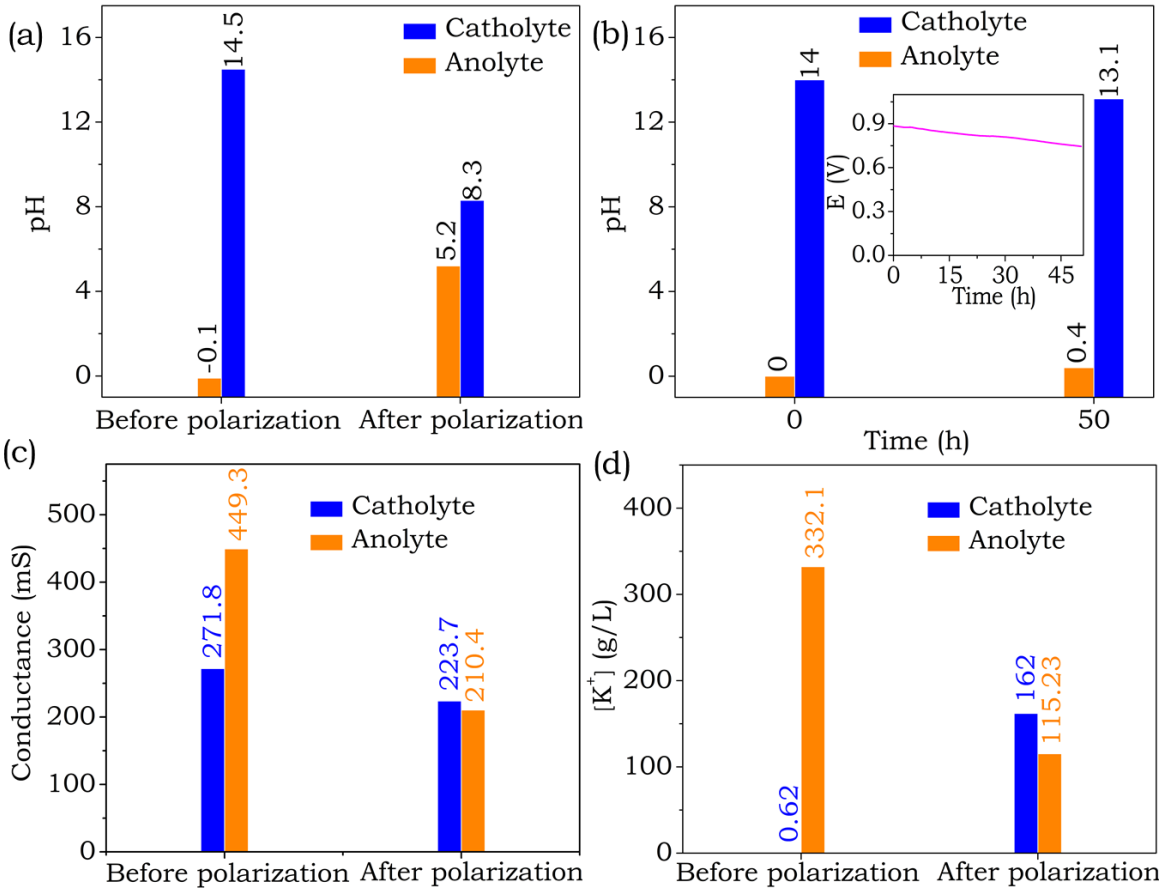

Figure 3.6: (a) pH measurements of anodic and cathodic half-cells of the ARFC before and after long term galvanostatic polarization at 50 mA/cm^2, (b) (c) pH of the ARFC as a function of time of the ARFC with 2 M methanol in 6 M KOH as the anolyte and 3 M H_2SO_4 as the catholyte., the inset shows the corresponding open circuit voltage. (c) Inductively coupled plasma-mass spectrometry (ICP-MS) measurement of the K^+ concentration in the ARFC before and after long term galvanostatic polarization at 50 mA/cm^2, (c) electrolyte conductance of the anodic and cathodic half-cells of the ARFC before and after long term galvanostatic polarization at 50 mA/cm^2. The Anodic and cathodic electrocatalysts were Pt-Ru/C at a loading of 1 mg/cm^2 and Pt at a loading of 1 mg/cm^2 on Ti mesh, respectively.

The pH of the electrolytes did not change noticeably at the open circuit voltage even after 50 hours, Figure 3.6b, confirming the pH convergence in Figure 3.6a not to result from diffusion driven neutralization. Inductively coupled plasma-mass spectrometry (ICP-MS) and electrolytic conductance measurements, Figure 3.6c and Figure 3.6d, further indicate there is accumulation and depletion of K^+ ions in the cat-

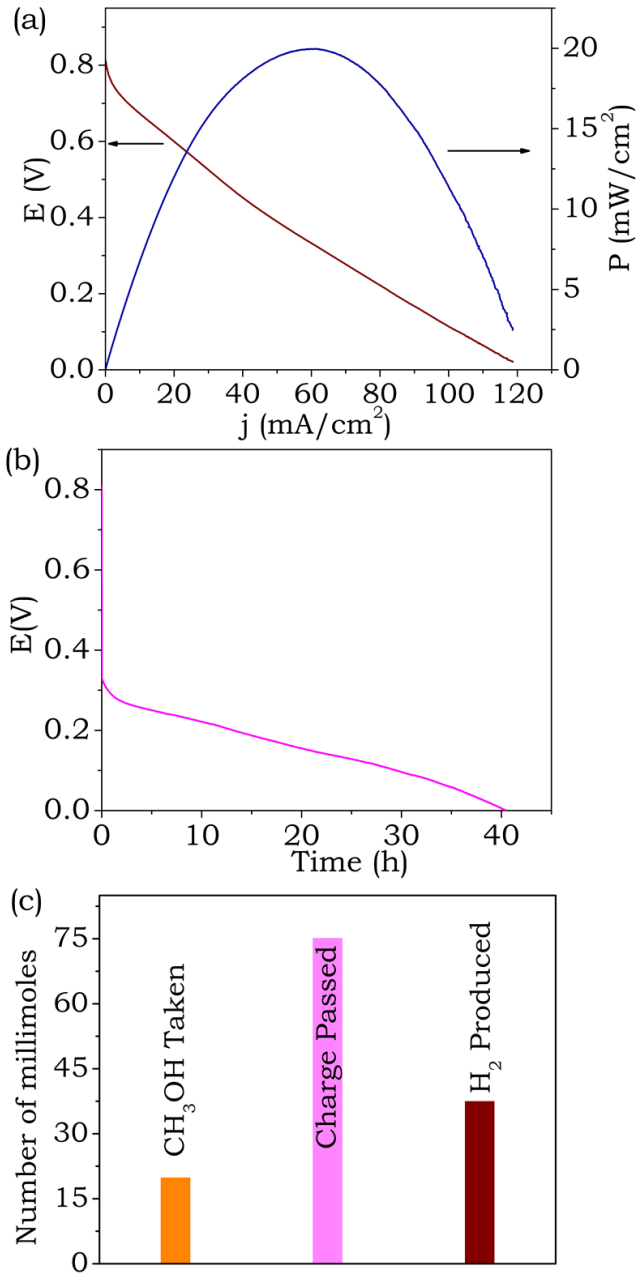

Figure 3.7: (a) Polarization curve of the ARFC with 1 M methanol in 6 M KOH as the anolyte and 3 M H_2SO_4 as the catholyte, (b) corresponding galvanostatic discharge profile at 50 mA/cm^2 and (c) charge passed and

H_2 produced versus methanol consumed for efficiency calculations. Anodic and cathodic electrocatalysts were Pt-Ru/C at a loading of 1 mg/cm^2 and Pt at a loading of 1 mg/cm^2 on Ti mesh, respectively.

-hodic and anodic half-cells respectively during long term polarization. These indicate the migration of potassium ions from the anodic half-cell to the cathodic half-cell for the charge balance during the discharge chemistry. Therefore, the pH changes in respective half-cells (Figure 3.6a) when current is drawn from the ARFC (Figure 3.3c (i)) is mainly due to neutralization reaction occurring electrochemically at the half-cells.

To determine the methanol to hydrogen fuel conversion efficiency, the galvanostatic discharge of the ARFC was carried out with stoichiometric ratio of methanol (1 M), alkali (6 M KOH) and acids (3 M H_2SO_4). This ratio was chosen based on Eq 3.3 which translates into 6 M KOH and 3 M H_2SO_4 for the complete oxidation of 1 M methanol. The ARFC with this stoichiometry yielded a power density of ~20 mW/cm^2 at ~60 mA/cm^2 peak current density, Figure 3.7a and the lower performance compared to Figure 3.3a is due to low methanol concentration. This ARFC was discharged fully at 50 mA/cm^2 till the electromotive force dropped to zero, Figure 3.7b. The cumulative charge from the galvanostatic polarization Figure 3.7b corresponds to an energy density of ~253 Wh/kg which corresponds ~62 % of methanol to hydrogen conversion, Figure 3.7c. The relatively lower conversion could be due to the well-known parallel pathway mechanism of methanol oxidation on Pt based electrodes as explained earlier.[29,31,32,41]

Calculation 3.2: H_2 yield and conversion efficiency

The theoretical calculations were done based on Faraday's law. Considering that the HER is a two-electron reaction, the moles of H_2 hydrogen n produced in a given time t by applying a current i is given by

$$n_{H_2} = \frac{i \cdot t}{2 \cdot F} \qquad (3.25)$$

The conversion factor of 24.78 L/mol was used to interconvert the number of moles and the volume.

The net chemical equation for the ARFC (Eq 3.3) shows that 3 moles of hydrogen are produced per mole of methanol. Hence, the conversion efficiency was calculated according to

$$\text{Conversion efficiency} = \frac{\text{moles of hydrogen produced}}{3 \cdot \text{moles of methanol consumed}} \qquad (3.26)$$

with an anolyte volume of 20 ml and a methanol concentration of 1 M, the total amount of methanol consumed was 20 mmol. The discharge current used was 50 mA for the time of a full discharge of 40 h 21 min = 2421 min

$$n_{H_2} = \frac{50\ \text{mA} \cdot 2421 \cdot 60\ \text{s}}{2 \cdot F} = 37.64\ \text{mmol} \qquad (3.27)$$

$$\text{Conversion efficiency} = \frac{37.64}{3 \cdot 20} = 0.62 \qquad (3.28)$$

One of the major issues with direct alcohol fuel cell is alcohol cross-over through the membrane to the cathodic half-cell which triggers parasitic chemistry such as competitive adsorption/oxidation at the cathode in the long run. This is investigated at the open circuit voltage in a diffusion type ARFC containing 2 M methanol in 6 M KOH as the anolyte and 3 M H_2SO_4 as the catholyte separated by a Nafion 117 membrane. Cathodic CVs of the HER after various times up to 50 hours at OCV do indicate blocking of HER activity of Pt/C electrode, Figure 3.8a. We investigated methanol cross-over using CVs of the methanol oxidation reaction after various times at OCV. Signatures of methanol in the acidic half-cell became visible after ~10 hours, Figure 3.8b and calibration plots suggest that the anolyte to contain ~100 mM methanol after 50 hours, Figure 3.8c and Figure 3.8d. This can lead to competitive adsorption of methanol on Pt domains, nevertheless, this can be addressed by modifying the membrane properties and by employing alcohol tolerant HER electrocatalysts like MoS_2, Ni_3S_2 instead of Pt [52-57] in the cathodic half-

cell as demonstrated with MoS_2 in Figure 3.8e. Such alcohol tolerant electrocatalysts can also prevent proton consuming parasitic oxygen reduction (if oxygen is present) reaction which is possible with Pt electrodes, Figure 3.8f.

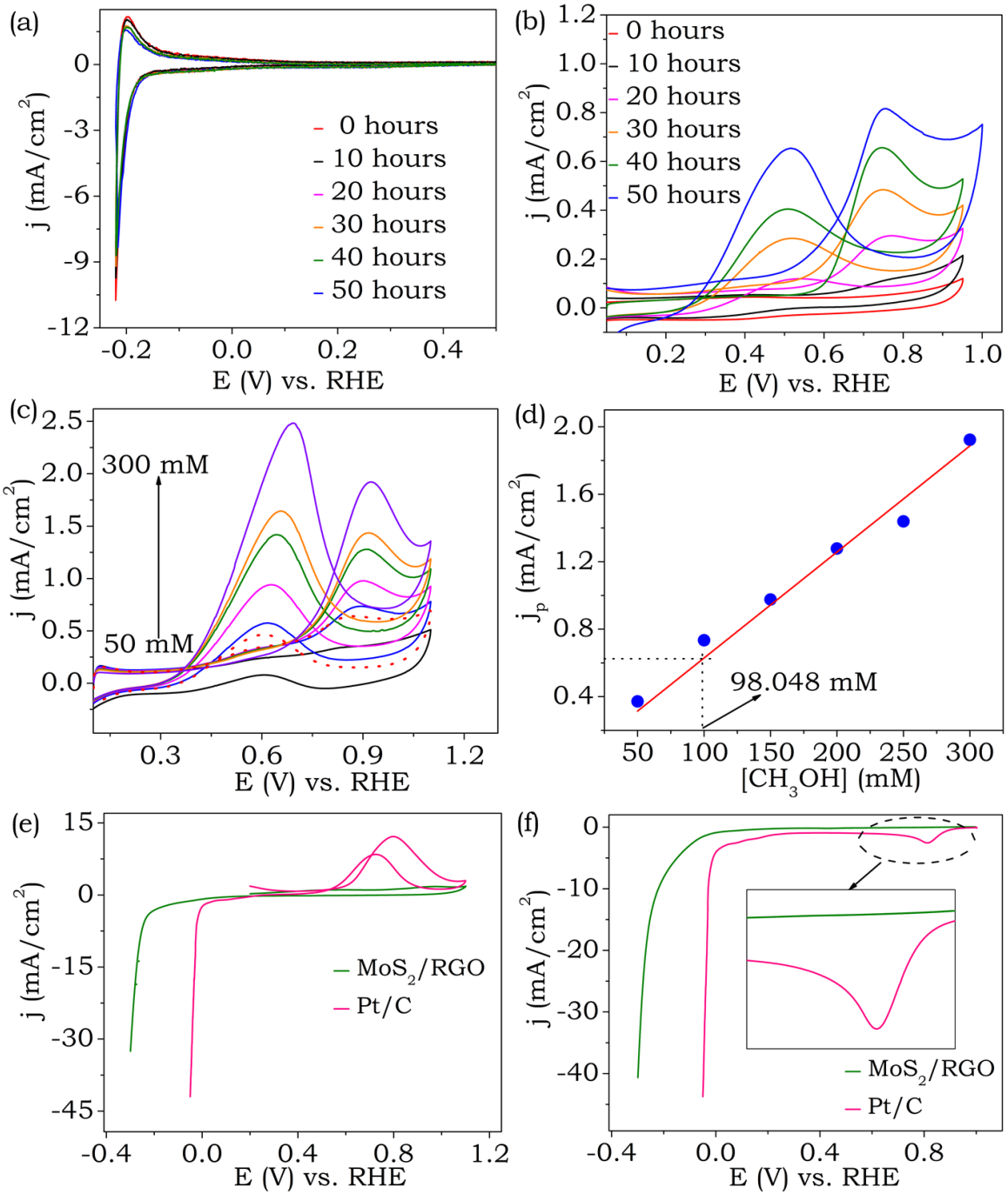

Figure 3.8: Cyclic voltammograms with a Pt/C electrode at a scan rate of 50 mV/s in the cathodic compartment of the ARFC for (a) hydrogen evolution reaction and (b) methanol oxidation reaction in the cathodic

compartment when the cell was kept at OCV up to 50 hours. The ARFC initially contained 2 M methanol in 6 M KOH as the anolyte and 3 M H_2SO_4 as the catholyte. (c) Cyclic voltammograms on a Pt/C electrode at a scan rate of 50 mV/s for different methanol concentrations in 3 M H_2SO_4 and (d) the corresponding calibration curve. The dotted line in Figure 3.7b approximately corresponds to methanol concentration in the cathode of ARFC after 50 hours. (e) Simultaneous methanol oxidation reaction and hydrogen evolution reaction and (f) simultaneous oxygen reduction reaction and hydrogen evolution reaction on MoS_2 and Pt/C.

In order to validate this, we have also carried out the ARFC performance by using MoS_2 as the cathode catalyst. MoS_2 catalyst was synthesized and characterized as per the literature (See Experimental section for synthetic procedure). The polarization curves for the ARFC/MoS_2, Figure 3.9a, demonstrates an open circuit voltage (OCV) of ~0.9 V and a peak power density of ~25 mW/cm^2 at ~80 mA/cm^2 peak current density. The galvanostatic discharge of the ARFC/MoS_2 at a current density of 50 mA/cm^2, Figure 3.9b, shows a H_2 generation which is close to theoretically expected rate. In order to see the effect of O_2 on the cathodic half-cell we characterized the gaseous species exhaled from the cathodic half-cell by DEMS, Figure 3.9c. As it is evident from the Figure 3.9c, the presence of O_2 does not noticeably affect the performance of the MoS_2 based ARFC (ARFC/MoS_2), however, HER rate significantly dropped in case of Pt/C based ARFC. The amount of hydrogen generated at the Pt/C cathode decreased significantly in presence of O_2 due to the dominance of proton consuming oxygen reduction reaction (ORR) over HER, Figure 3.9d. This suggests that by interfacial modification of the cathode electrocatalysts, alcohol reformation can be accomplished even in the presence of oxygen.

Taken together, the proposed ARFC uses the energy of neutralization to drive alcohol reforming with simultaneous electric power generation. The ARFC based hydrogen economy is distinct because it harnesses

electric power during hydrogen fuel production as well as its utilization and CO_2 is captured, which in turn offers a feasible solution for reviving hydrogen economy from its twilight. Note that the direct harvesting of neutralization energy as electrical energy via H_2 redox is one type of neutralization cell reported in the literature[34] where the solubility of H_2 species in the electrolyte can greatly limit the energy density of the overall the device. Secondly, this issue of limited solubility of electron donor (H_2) and its insufficient availability near the electrocatalyst may lead to fuel st-

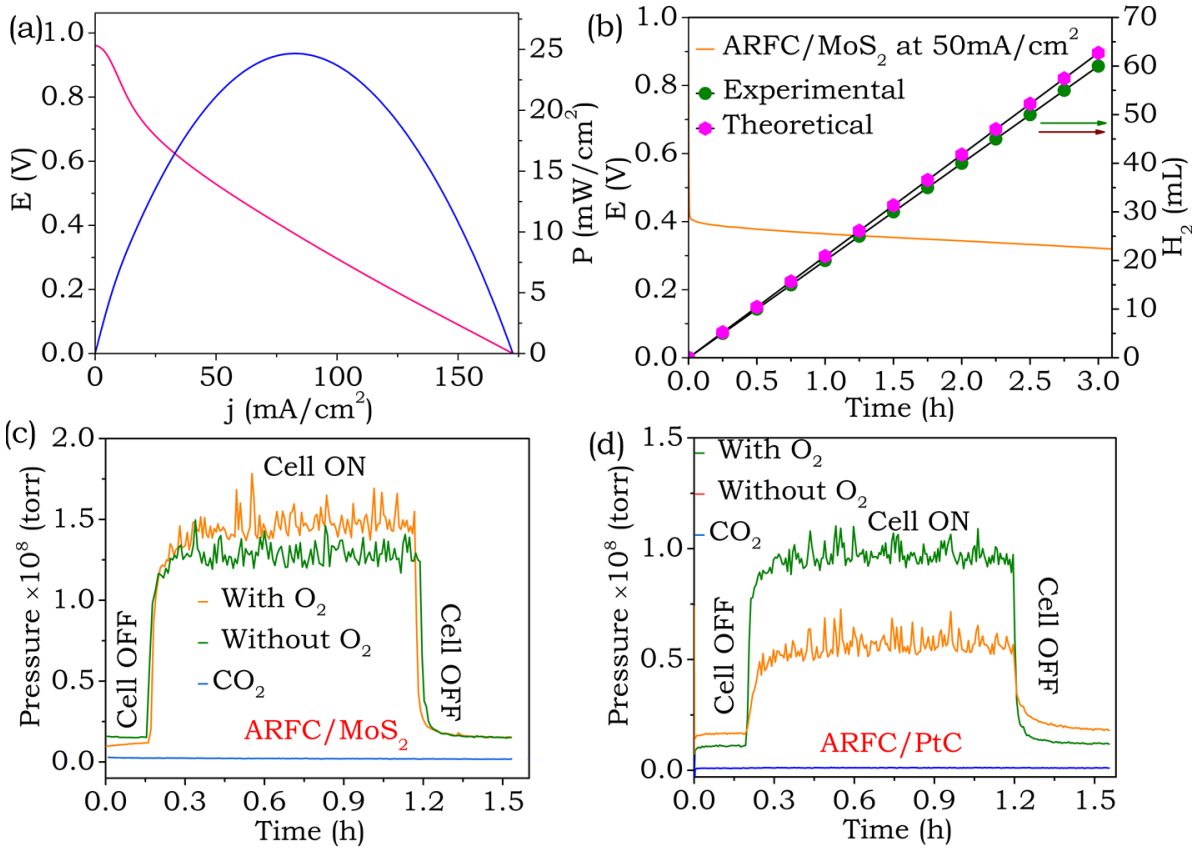

Figure 3.9: MoS_2 based Alcohol reforming fuel cell (ARFC/MoS_2) performance. (a) Polarization curve for ARFC/MoS_2 with methanol as the fuel (2 M methanol in 6 M KOH as the anolyte and 2 M H_2SO_4 as the catholyte), and (b) galvanostatic polarization at 50 mA/cm^2 with H_2 quantification at the cathode. In-situ electrochemical mass spectrometry of cathodic half-cell of the ARFC ¬in presence and absence of O2 with (c) a MoS_2 and (d) a Pt based cathode electrocatalyst.

-oichiometry (the overall usage of H_2 on the anode vs. H_2 generation at the cathode) significantly lower than 1.[34] The ARFC proposed here can address the issues associated with the solubility of electron donor since most short chain alcohols are highly soluble in aqueous electrolytes. In principle, this should enhance the energy density of the device. However, the sluggish kinetics of alcohol oxidation [41,42] and parallel routes possible during alcohol oxidation on Pt based electrodes [38,39] can noticeably decrease the energy density of the ARFC. The ARFC is also distinctly different from reverse electrodialysis as the former is based on pH gradients and the latter is based on salinity gradients and an entropy driven process. [58,59] The ARFC is both enthalpy as well as entropy driven. Further, the efficiency of the reverse electrodialysis process is low (~30%) due to significant *iR* losses across the saline compartments, [58,59] whereas the conversion efficiency of ARFC is nearly 60% as pH gradients can be achieved over several orders of magnitude without encountering solubility and mass transport limitations. More importantly, the integration of additional functionality of alcohol reformation during electricity generation in ARFC makes it distinctly different from state-of-the-art energy conversion pathways. Although, the ARFC shows a promising way of alcohol reformation along with the electricity generation, there are still various issues and challenges to make it practical. The device works in an asymmetric electrolyte (acid/base) configuration and a reasonably high concentration of acid/base is needed for efficient operation. Hence, the membrane should have high ion selectivity and conductivity, should separate the acid and alkali electrolytes effectively, and should be chemically and thermally stable for long-term operation. Current commercial bipolar membranes, dual-ion exchange membranes and Nafion are quite stable (pH = 0 to 14), but cannot fulfill such practical requirements in the long run. Secondly, developing non-precious electrocatalysts for the HER and alcohol oxidation reaction are crucially important for larger scale expansion of the device. Thirdly, CO_2 in the ambient air can affect the performance at the anodic half-cell due to the

CO_2/CO_3^{2-} equilibrium, being a parasitic reagent that decreases the pH gradients and the electromotive force. Therefore, developing highly stable and efficient functional membranes, durable non-precious electrocatalysts, and CO_2 excluding membranes will be vital for this technology to move from lab scale to industrial scale.

3.4. Conclusions

By harvesting the neutralization energy, we have succeeded in aqueous phase alcohol reformation at room temperature and pressure with simultaneous electric power generation. The ARFC chemistry is unusual because of its distinctly positive entropic heat which allows ~56 % of the total available energy to be harvested from the surroundings leveraging a thermodynamic efficiency as high as 2.67. ARFC inherently captures CO_2 and purifies the hydrogen fuel, thus allowing the usage of the latter directly in a proton exchange membrane fuel cell without any energy intensive purification module. The proposed ARFC is unprecedented because it leads to a hydrogen economy where electric power is harnessed during hydrogen fuel production as well as its utilization. The necessity of pH gradients for the ARFC has indeed cost implications, however, it enables room temperature alcohol reformation to pure hydrogen, CO_2 sequestration and electric power generation in a single device. The pH gradients across the membrane may drive diffusion driven neutralization reactions in the long run which in turn can be delayed by utilizing bipolar membranes as used in water electrolyzers. Similarly, the issue of alcohol cross-over can also be looked at by housing the reactants outside the ARFC and continuously recirculating the half-cell chemicals across respective catalytic chambers akin to flow batteries and (or) by using the alcohol tolerant catalysts like MoS_2 as explained above. Therefore, it is believed that this proof of concept will transcend the horizon of fuel cells in hydrogen economy from simple fuel utilization devices to the overall root of hydrogen economy.

3.5. References

[1] Schuler, T., Kimura, T., Schmidt, T. J. & Büchi, F.N. Towards a generic understanding of oxygen evolution reaction kinetics in polymer electrolyte water electrolysis *Energy Environ. Sci.*, **2020,** *13,* 2153-2166.

[2] White, W., Sanborn, C. D., Fabian, D. M., & Ardo, S. Conversion of Visible Light into Ionic Power Using Photoacid-Dye-Sensitized Bipolar Ion-Exchange Membranes. *Joule,* **2018,** *2* (1), 94–109.

[3] Uddin, A., Dunsmore, L., Zhang, H., Hu, L., Wu, G. & Lister, S. High Power Density Platinum Group Metal-free Cathodes for Polymer Electrolyte Fuel Cells. *ACS Appl. Mater. Interfaces,* **2020,** *12* (2), 2216–2224.

[4] Choi, J. W.; Aurbach, D. Promise and Reality of Post-Lithium-Ion Batteries with High Energy Densities. *Nat. Rev. Mater.* **2016**, *1* (4), 16013.

[5] Chinnam, P. R.; Fall, B.; Dikin, D. A.; Jalil, A. A.; Hamilton, C. R.; Wunder, S. L.; Zdilla, M. J. A Self-Binding, Melt-Castable, Crystalline Organic Electrolyte for Sodium Ion Conduction. *Angew. Chemie - Int. Ed.* **2016**, *55* (49), 15254–15257.

[6] Mourad, E.; Coustan, L.; Lannelongue, P.; Zigah, D.; Mehdi, A.; Vioux, A.; Freunberger, S. A.; Favier, F.; Fontaine, O. Biredox Ionic Liquids with Solid-like Redox Density in the Liquid State for High-Energy Supercapacitors. *Nat. Mater.* **2016,** *16,* 446-453.

[7] Tymoczko, J.; Calle-Vallejo, F.; Schuhmann, W.; Bandarenka, A. S. Making the Hydrogen Evolution Reaction in Polymer Electrolyte Membrane Electrolysers Even Faster. *Nat. Commun.* **2016**, *7* (1), 10990.

[8] Miroshnikov, M.; Divya, K. P.; Babu, G.; Meiyazhagan, A.; Reddy Arava, L. M.; Ajayan, P. M.; John, G. Power from Nature: Designing Green Battery Materials from Electroactive Quinone Derivatives and Organic Polymers. *J. Mater. Chem. A* **2016**, *4* (32), 12370–12386.

[9] Pino, M., Herranz, D., Chacón, J., Fatás, E. & Ocón, P. Carbon treated commercial aluminium alloys as anodes for aluminium-air batteries in sodium chloride electrolyte. *J. Power Sources*, **2016,** *326,* 296–302.

[10] Forsyth, M.; Yoon, H.; Chen, F.; Zhu, H.; MacFarlane, D. R.; Armand, M.; Howlett, P. C. Novel Na^+ Ion Diffusion Mechanism in Mixed Organic-Inorganic Ionic Liquid Electrolyte Leading to High Na^+ Transference Number and Stable, High Rate Electrochemical Cycling of Sodium Cells. *J. Phys. Chem. C* **2016**, *120* (8), 4276–4286.

[11] Anju, V. G., Manjunatha, R., Austeria, P. M. & Sampath, S. Primary and rechargeable zinc – air batteries using ceramic and highly stable TiCN as an oxygen reduction reaction electrocatalyst. *J. Mater. Chem. A*, **2016,** *4,* 5258–5264.

[12] Xie, J., Liang, Z. & Lu, Y., Molecular crowding electrolytes for high-voltage aqueous batteries. *Nat. Mater.* **2020,** *19,* 1006–1011.

[13] Sørensen, B. Hydrogen and Fuel Cells; emerging technologies and applications, (Elsevier Academic Press, London, UK 2018).

[14] Avgouropoulos, G.; Ioannides, T.; Kallitsis, J. K.; Neophytides, S. Development of an Internal Reforming Alcohol Fuel Cell: Concept, Challenges and Opportunities. *Chem. Eng. J.* **2011,** *176–177,* 95–101.

[15] Hou, T.; Zhang, S.; Chen, Y.; Wang, D.; Cai, W. Hydrogen Production from Ethanol Reforming: Catalysts and Reaction Mechanism. *Renew. Sustain. Energy Rev.* **2015,** *44,* 132–148.

[16] Zakaria, K.; Thimmappa, R.; Mamlouk, M.; Scott, K. Hydrogen Generation by Alcohol Reforming in a Tandem Cell Consisting of a Coupled Fuel Cell and Electrolyser. *Int. J. Hydrogen Energy* **2020,** *45* (15), 8107–8117.

[17] Cano, Z. P.; Banham, D.; Ye, S.; Hintennach, A.; Lu, J.; Fowler, M.; Chen, Z. Batteries and Fuel Cells for Emerging Electric Vehicle Markets. *Nat. Energy* **2018**, *3* (4), 279–289.

[18] Ball, M. & Weeda, M. The hydrogen economy: Vision or reality? *Int. J. Hydrogen Energy*, **2015,** *40,* 7903–7919.

[19] Dodds, P. E., Staffell, I., Hawkes, A. D. & Li, F. Hydrogen and fuel cell technologies for heating: A review. *Int. J. Hydrogen Energy*, **2015,** *40,* 2065-2083.

[20] Feng, Y., Liu, H. & Yang, J. A selective electrocatalyst – based direct methanol fuel cell operated at high concentrations of methanol. *Sci. Adv.* **2017,** *3,* e1700580.

[21] Chu, S. & Majumdar, A. Opportunities and challenges for a sustainable energy future. *Nature,* **2012**, *488,* 294–30.

[22] Aricò, A. S., Srinivasan, S. & Antonucci, V. DMFCs: From Fundamental Aspects to Technology Development. *Fuel Cells* **2001,** *1,* 133–161.

[23] Steele, B. C. & Heinzel, A. Materials for fuel-cell technologies. *Nature,* **2001,** *414,* 345–352.

[24] Rodríguez-Lugo, R. E.; Trincado, M.; Vogt, M.; Tewes, F.; Santiso-Quinones, G.; Grützmacher, H. A Homogeneous Transition Metal Complex for Clean Hydrogen Production from Methanol-Water Mixtures. *Nat. Chem.* **2013**, *5* (4), 342–347.

[25] Choi, J., MacArthur, A. H. R., Brookhart, M. & Goldman, A. S. Dehydrogenation and related reactions catalyzed by iridium pincer complexes. *Chem. Rev.* **2011,** *111,* 1761–1779.

[26] Zeng, G., Sakaki, S., Fujita, K. I., Sano, H. & Yamaguchi, R. Efficient catalyst for acceptorless alcohol dehydrogenation: Interplay of theoretical and experimental studies. *ACS Catal.* **2014,** *4,* 1010–1020 (2014).

[27] Balaraman, E., Khaskin, E., Leitus, G. & Milstein, D. Catalytic transformation of alcohols to carboxylic acid salts and H_2 using water as the oxygen atom source. *Nat. Chem.* **2013,** *5,* 122–125.

[28] Trincado, M., Banerjee, D. & Grützmacher, H. Molecular catalysts for hydrogen production from alcohols. *Energy Environ. Sci.* **2014,** *7,* 2464–2503.

[29] Lohr, T. L.; Mouat, A. R.; Schweitzer, N. M.; Stair, P. C.; Delferro, M.; Marks, T. J. Efficient Catalytic Greenhouse Gas-Free Hydrogen and Aldehyde Formation from Aqueous Alcohol Solutions. *Energy Environ. Sci.* **2017**, *10* (7), 1558–1562.

[30] Crabtree, R. H. Homogeneous Transition Metal Catalysis of Acceptorless Dehydrogenative Alcohol Oxidation: Applications in Hydrogen Storage and to Heterocycle Synthesis. *Chem. Rev.* **2017,** 117, 9228–9246.

[31] Alberico, E.; Lennox, A. J. J.; Vogt, L. K.; Jiao, H.; Baumann, W.; Drexler, H. J.; Nielsen, M.; Spannenberg, A.; Checinski, M. P.; Junge, H.; Beller, M. Unravelling the Mechanism of Basic Aqueous Methanol Dehydrogenation Catalyzed by Ru-PNP Pincer Complexes. *J. Am. Chem. Soc.* **2016**, *138* (45), 14890–14904.

[32] Das, U. K., Ben-David, Y., Diskin-Posner, Y. & Milstein, D. N-Substituted Hydrazones by Manganese-Catalyzed Coupling of Alcohols with Hydrazine: Borrowing Hydrogen and Acceptorless Dehydrogenation in One System. *Angew. Chemie - Int. Ed.* **2018**, *57,* 2179–2182.

[33] Jaiswal, G., Landge, V. G., Jagadeesan, D. & Balaraman, E. Iron-based nanocatalyst for the acceptorless dehydrogenation reactions. *Nat. Commun.* **2017,** *8,* 2147.

[34] Manzoor Bhat, Z.; Thimmappa, R.; Devendrachari, M. C.; Kottaichamy, A. R.; Shafi, S. P.; Varhade, S.; Gautam, M.; Thotiyl, M. O. Fuel Exhaling Fuel Cell. *J. Phys. Chem. Lett.* **2018**, *9* (2), 388–392.

[35] Hou, Y.; Zhang, B.; Wen, Z.; Cui, S.; Guo, X.; He, Z.; Chen, J. A 3D Hybrid of Layered MoS_2/Nitrogen-Doped Graphene Nanosheet Aerogels: An Effective Catalyst for Hydrogen Evolution in Microbial Electrolysis Cells. *J. Mater. Chem. A* **2014**, *2* (34), 13795–13800.

[36] Xie, J.; Zhang, J.; Li, S.; Grote, F.; Zhang, X.; Zhang, H.; Wang, R.; Lei, Y.; Pan, B.; Xie, Y. Controllable Disorder Engineering in Oxygen-Incorporated MoS_2 Ultrathin Nanosheets for Efficient Hydrogen Evolution. *J. Am. Chem. Soc.* **2013**, *135* (47), 17881–17888.

[37] Wang, S.; An, C.; Yuan, J. Synthetic Fabrication of Nanoscale MoS2-Based Transition Metal Sulfides. *Materials*. **2010.** *3,* 401–433.

[38] Tripkovi, A. V.; Popovi, K. D.; Grgur, B. N.; Blizanac, B.; Ross, P. N.; Markovi, N. M. Methanol Electrooxidation on Supported Pt and PtRu Catalysts in Acid and Alkaline Solutions. *Electrochim. Acta* **2002**, *47* (22–23), 3707–3714.

[39] Spendelow, J. S., Goodpaster, J. D., Kenis, P. J. A. & Wieckowski, A. Methanol dehydrogenation and oxidation on Pt(111) in alkaline solutions. *Langmuir* **2006,** *22,* 10457–10464.

[40] Zhao, X.; Yin, M.; Ma, L.; Liang, L.; Liu, C.; Liao, J.; Lu, T.; Xing, W. Recent Advances in Catalysts for Direct Methanol Fuel Cells. *Energy Environ. Sci.* **2011**, *4* (8), 2736.

[41] Liu, H.; Song, C.; Zhang, L.; Zhang, J.; Wang, H.; Wilkinson, D. P. A Review of Anode Catalysis in the Direct Methanol Fuel Cell. *J. Power Sources* **2006**, *155* (2), 95–110.

[42] Zadick, A., Dubau, L., Sergent, N., Berthomé, G. & Chatenet, M. Huge Instability of Pt/C Catalysts in Alkaline Medium. *ACS Catal.* **2015,** *5,* 4819–4824.

[43] Huang, L.; Zhang, X.; Wang, Q.; Han, Y.; Fang, Y.; Dong, S. Shape-Control of Pt-Ru Nanocrystals: Tuning Surface Structure for Enhanced Electrocatalytic Methanol Oxidation. *J. Am. Chem. Soc.* **2018**, *140* (3), 1142–1147.

[44] Chen, D. J. & Tong, Y. J. Irrelevance of Carbon Monoxide Poisoning in the Methanol Oxidation Reaction on a PtRu Electrocatalyst. *Angew. Chemie - Int. Ed.* **2015,** *54,* 9394–9398.

[45] Kakati, N.; Maiti, J.; Lee, S. H.; Jee, S. H.; Viswanathan, B.; Yoon, Y. S. Anode Catalysts for Direct Methanol Fuel Cells in Acidic Media: Do We Have Any Alternative for Pt or Pt-Ru? *Chem. Rev.* **2014**, *114* (24), 12397–12429.

[46] Maiyalagan, T., Alaje, T. O. & Scott, K. Highly stable Pt-Ru nanoparticles supported on three-dimensional cubic ordered

mesoporous carbon (Pt-Ru/CMK-8) as promising electrocatalysts for methanol oxidation. *J. Phys. Chem. C* **2012,** *116,* 2630–2638.

[47] Zheng, J., Sheng, W., Zhuang, Z., Xu, B. & Yan, Y. Universal dependence of hydrogen oxidation and evolution reaction activity of platinum-group metals on pH and hydrogen binding energy. *Sci. Adv.* **2016,** *2,* e1501602–e1501602.

[48] Sheng, W., Myint, M., Chen, J. G. & Yan, Y. Correlating the hydrogen evolution reaction activity in alkaline electrolytes with the hydrogen binding energy on monometallic surfaces. *Energy Environ. Sci.* **2013,** *6,* 1509–1512.

[49] Vesborg, P. C. K., Seger, B. & Chorkendorff, I. Recent development in hydrogen evolution reaction catalysts and their practical implementation. *J. Phys. Chem. Lett.* **2015,** *6,* 951–957.

[50] Sheng, W., Gasteiger, H. A. & Shao-Horn, Y. Hydrogen Oxidation and Evolution Reaction Kinetics on Platinum: Acid vs Alkaline Electrolytes. *J. Electrochem. Soc.* **2010,** *157,* B1529.

[51] Kucernak, A. R. & Zalitis, C. General Models for the Electrochemical Hydrogen Oxidation and Hydrogen Evolution Reactions: Theoretical Derivation and Experimental Results under Near Mass-Transport Free Conditions. *J. Phys. Chem. C,* **2016,** *120,* 10721−10745.

[52] Ledezma-Yanez, I.; Wallace, W. D. Z.; Sebastián-Pascual, P.; Climent, V.; Feliu, J. M.; Koper, M. T. M. Interfacial Water Reorganization as a PH-Dependent Descriptor of the Hydrogen Evolution Rate on Platinum Electrodes. *Nat. Energy* **2017**, *2* (4), 17031.

[53] Garcia, A. C., Linares, J. J., Chatenet, M. & Ticianelli, E. A. NiMnOx/C: A Non-noble Ethanol-Tolerant Catalyst for Oxygen Reduction in Alkaline Exchange Membrane DEFC. *Electrocatalysis* **2014,** *5,* 41–49.

[54] Sebastián, D.; Serov, A.; Matanovic, I.; Artyushkova, K.; Atanassov, P.; Aricò, A. S.; Baglio, V. Insights on the Extraordinary Tolerance to Alcohols of Fe-N-C Cathode Catalysts in Highly Performing Direct Alcohol Fuel Cells. *Nano Energy* **2017**, *34*, 195–204.

[55] Guo, J., Zhang, X., Sun, Y., Tang, L. & Zhang, X. $NiMoS_3$ Nanorods as pH-Tolerant Electrocatalyst for Efficient Hydrogen Evolution. *ACS Sustain. Chem. Eng.* **2017,** *5,* 9006–9013.

[56] Ma, K.-B.; Kwak, D.-H.; Han, S.-B.; Park, H.-S.; Kim, D.-H.; Won, J.-E.; Kwon, S.-H.; Kim, M.-C.; Moon, S.-H.; Park, K.-W. Direct Ethanol Fuel Cells with Superior Ethanol-Tolerant Nonprecious Metal Cathode Catalysts for Oxygen Reduction Reaction. *ACS Sustain. Chem. Eng.* **2018**, *6* (6), 7609–7618.

[57] Yang, Y.; Zhang, K.; Lin, H.; Li, X.; Chan, H. C.; Yang, L.; Gao, Q. MoS_2–Ni_3S_2 Heteronanorods as Efficient and Stable Bifunctional Electrocatalysts for Overall Water Splitting. *ACS Catal.* **2017**, *7* (4), 2357–2366.

[58] Veerman, J.; de Jong, R. M.; Saakes, M.; Metz, S. J.; Harmsen, G. J. Reverse Electrodialysis: Comparison of Six Commercial Membrane Pairs on the Thermodynamic Efficiency and Power Density. *J. Memb. Sci.* **2009,** *343* (1–2), 7–15.

[59] Yip, N. Y.; Vermaas, D. A.; Nijmeijer, K.; Elimelech, M. Thermodynamic, Energy Efficiency, and Power Density Analysis of Reverse Electrodialysis Power Generation with Natural Salinity Gradients. *Environ. Sci. Technol.* **2014,** *48* (9), 4925–4936.

Chapter 4

Direct Harvesting of Neutralization Energy as Electrical Driving Force

Abstract: Neutralization energy is the energy released as heat when acid and alkali react to form water which is an entropically as well as an enthalpically favourable spontaneous process. The overall neutralization reaction which involves the formation of water and salt does not lead to change in the oxidation state of the participating species which is a major challenge to perform this reaction electrochemically. In this chapter, we demonstrate an electrochemical neutralization cell for the interconversion of acid-base neutralization energy into electrical energy by employing a reversible H_2/H^+ redox couple. The electrochemical nuetralization cell (ENC) delivered a peak power density of 70 mW/cm^2 at a peak current density of 160 mA/cm^2 with a cathodic H_2 output of ~80 mL in 1 hour. In this Chapter, we also illustrate that the energy benefits from the same fuel stream can be amplified by directing it through ENC prior to PEMFC in a tandem configuration.

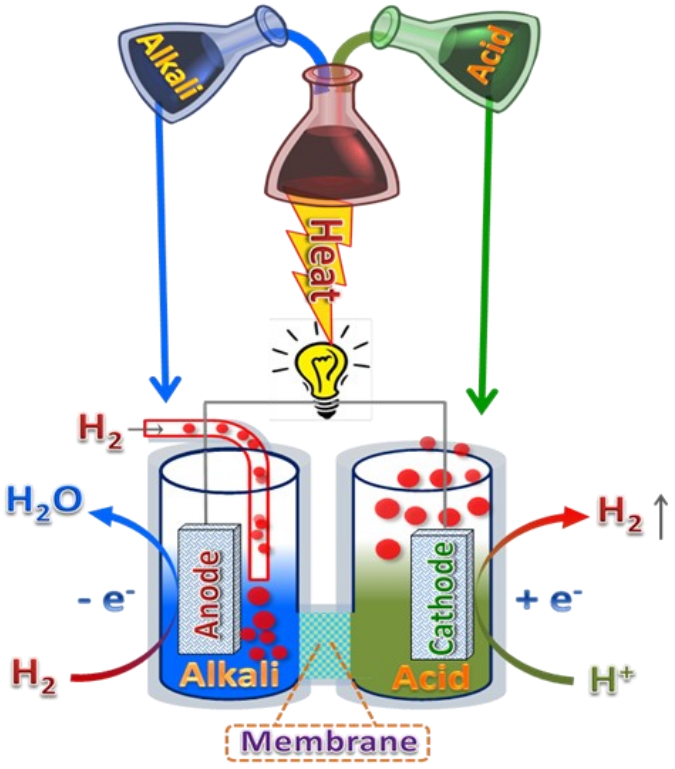

The chapter contains the data taken from my original published work:
Zahid Bhat et.al., J. Phys. Chem. Lett. 2018, 388–392.
Copyright American Chemical Society

4.1. Introduction

21st century is witnessing serious energy crisis and electrochemical energy storage and conversion devices assumed a larger space due to the rapid depletion of the fossil fuels.[1-16] The harvesting of renewable energy sources like wind, solar, geothermal, tidal energy etc., have been the prime interest for routing the energy economy to a sustainable energy economy. However, these renewable energy resources are intermittent and geographic, and heavily dependent on the climate, and thus cannot meet the uninterrupted and long-lasting electricity demand for human activities and industry. Therefore, it is highly desirable to develop reliable energy storage and conversion technologies to take full advantage to meet the growing energy demands of the world. One such energy conversion/storage process which has long been ignored is the acid-alkali neutralization reaction. During the acid–base neutralization process, the standard Gibbs free energy change (ΔG^0) is about −79.9 kJ mol^{-1} and hence it a thermodynamically spontaneous process and the energy is evolved as heat. It is estimated that the global annual acids/alkaline wastes are equivalent to 100 million tons.[17] The disposal process of these waste acid/alkaline solution is the direct neutralization process wherein a lot of heat (~1.11×10^{14} kJ/100 million tons) and salts are expelled to the environment, thus causing serious threats to the environment. If the acid/alkali wastes are neutralized in an electrochemical pathway, energy of about 44 TW h can be harvested in the form of electrical energy which offers a unique platform for the simultaneous treatment of industrial acid and alkaline wastes. Therefore, the development of an electrochemical neutralization device may open a new avenue to design novel aqueous energy storage and conversion devices including fuel cells, supercapacitors and batteries to meet future energy demand. Till date very few studies have been conducted on developing acid–base asymmetric electrolyte systems, asymmetric high voltage supercapacitor, a three-electrolyte ($H_2SO_4|K_2SO_4|KOH$) PbO_2–MH_x battery, an acid–base asymmetric vanadium–MH_x semi-flow battery,

bipolar membrane-based photo electrochemical water electrolysis, and acid–base water electrolysis using a ceramic Li-ion exchange membrane.[18-28] However, in all the cases neutralization energy was used as an additional force for increasing the electrochemical feasibility of the process and to best of our knowledge there are no reports of direct harvesting of neutralization as electric driving force. In this Chapter, we show for the first time the direct conversion of neutralization energy as electric energy without a net redox reaction. To do so, we have coupled a half cell with H_2 as the electron donor in an alkaline pH to an acidic half-cell where hydronium ion served as the electron acceptor, Scheme 4.1, with the net cell reaction being the *electrochemical* acid base neutralization reaction. We further demonstrate that by connecting a PEMFC in series with the ENC, the voltage generation, power and energy output can be at least doubled using the same fuel streams.

4.2. Materials and Methods

Sodium hydroxide (97%), sulphuric acid (98%), potassium hydrogen phosphate (98%), potassium phosphate (99%), acetic acid (99.7%), sodium acetate (99%), potassium sulphate (99%) was bought from Sigma Aldrich India and were used as such. Pt/C was procured from Johnson Matthey India.

All the electrochemical measurements were done with the VMP-300 Electrochemical Work Station (Biologic, France). Electrochemical experiments were carried in standard three electrode set up with platinum (2 mm diameter) as working electrode, Ag/AgCl (3.5 M KCl) as reference and platinum mesh as the counter electrode. Hydrogen evolution and oxidation on platinum electrode was carried out in different pH solutions. pH solutions were made by using H_2SO_4 (pH 0), HSO_4^-/SO_4^{2-} (pH 1 to 2), CH_3COOH/CH_3COONa (pH 3 to 5), $H_2PO_4^-/HPO_4^{2-}$(pH 5 to 8), $HPO_4^{2-}/PO4^{3-}$ (pH 9 to 12), and NaOH (1 M, pH 14). The pH of each solution was adjusted with 1 M H_2SO_4 or 1 M NaOH solutions. Prior to the measurement, the electrode was polished with 0.05 μm alumina powder

and cycled in the respective solution. The solutions were purged with nitrogen followed by hydrogen for 15 minutes before carrying out the hydrogen evolution or oxidation reactions.

For the fuel cell measurements, a closed two compartment cell was made with each compartment having an opening for the gas passage. The two compartments were separated by a pretreated Nafion-117 membrane. The alkaline compartment was fitted with the Pt/C electrode as the anodic electrocatalyst. The electrode was fabricated by coating Pt/C (60 wt% Pt) on Toray carbon paper with a loading of 0.2 mg/cm^2. The cathodic electrode was made by electrochemical deposition of platinum on Pt mesh (loading = ~1 mg/cm^2) by chronoamperometry (4 mA/cm^2 for 2 minutes). Anodic and cathodic half-cells were filled with NaOH (pH =14) and H_2SO_4 (pH=0) respectively. Each measurement was carried out by passing the hydrogen gas into anodic half-cell at 100 ml/min rate and collecting the evolved gas from the cathodic half-cell. For quantification purpose the evolved gas was collected in a calibrated cylinder by water displacement technique. During the long-time polarisation, the gas evolved from the cathodic compartment was passed directly to the commercial air breathing H_2/air fuel cell.

4.3. Results and Discussion

Thermodynamics of Electrochemical Neutralization Cell and H_2-O_2 Fuel Cell

(A) Electrochemical neutralization cell:

The net cell reaction for the neutralization cell can be written as:

$$H^+ + OH^- \rightarrow H_2O \quad \Delta H = ? \quad \Delta S = ?$$

Heat of reaction for the above reaction is;

$$\Delta H^0 = H^0 (H_2O) - H^0 (OH^-) - H^0 (H^+)$$

$$= (-285830\ J) - (-229990\ J) - 0$$

$$= -55830\ J.mol^{-1}$$

Entropy change for the reaction is;

$\Delta S^0 = S^0 (H_2O) - S^0 (OH^-) - S^0 (H^+)$

$= 69.91 - (-10.75) - 0$

$= 80.7\ J.K^{-1}.mol^{-1}$

Therefore, Gibbs free energy for the process is;

$\Delta G^0 = \Delta H^0 - T\Delta S^0$

$= -55830\ J.mol^{-1} - (298\ K \times 80.7\ J.K^{-1}.mol^{-1})$

$= -79878\ J.mol^{-1}$

Thermodynamic Efficiency $= \Delta G^0 / \Delta H^0$

$= -79878\ J.mol^{-1} / - 55830\ J.mol^{-1}$

$= 1.43$

Thermal voltage $= -\Delta H^0 / nF$

$= - 55830\ J.mol^{-1} / 96500\ C.mol^{-1}$

$= 0.579\ V$

The electromotive force generated is;

$e.m.f = \Delta G^o / nF$

$= -79878\ J.mol^{-1} / 96500\ C.mol^{-1}$

$= 0.828\ V$

(B) H_2-O_2 fuel cell:

The net H_2-O_2 fuel cell reaction can be written as:

$H_2 + 1/2(O_2) \rightarrow H_2O \quad \Delta H = ? \ \Delta S = ?$

Heat of reaction for the above reaction is;

$\Delta H^0 = \Delta f^0 (H_2O) - \Delta f^0 (H_2) - \Delta f^0 (O_2)$

where Δf^0 = heat of formation

$= -285800\ J.mol^{-1} - 0 - 0$

$= -285800\ J.mol^{-1}$

Entropy change for the reaction is;

$\Delta S^0 = S^0\ H_2O(l) - S^0\ H_2(g) - S^0\ 1/2O_2(g)$

$= 70\ J.K^{-1}.mol^{-1} - 131\ J.K^{-1}.mol^{-1} - 205/2\ J.K^{-1}.mol^{-1}$

$= -163\ J.K^{-1}.mol^{-1}$

Therefore, Gibbs free energy for the process is;

$\Delta G^0 = \Delta H^0 - T\Delta S^0$

$=-285800\ J.mol^{-1} - (298\ K \times -163\ J.K^{-1}.mol^{-1})$

$=-237226\ J.mol^{-1}$

Thermodynamic Efficiency = $\Delta G^0 / \Delta H^0$

$= -237226\ J.mol^{-1} / -285800\ J.mol^{-1}$

$= 0.83$

Thermal voltage = $-\Delta H^0 / nF$

$= -285800\ J.mol^{-1} / (2 \times 96484\ C.mol^{-1})$

$= 1.481\ V$

The electromotive force generated is;

e.m.f = $-\Delta G^0/nF$

$= 237226\ J.mol^{-1} / (2 \times 96484\ C.mol^{-1})$

$= 1.229\ V$

The proposed electrochemical neutralization fuel cell consists of an anodic half-cell containing H_2 in an alkaline environment (pH=14) with a Pt/C electrocatalyst. The cathodic half-cell constitutes a Pt/C electrocatalyst immersed in an acidic pH (pH=0). Both the half-cells were separated by a Nafion 117 membrane for ionic communication, Scheme 1. The device relies on the proton dependence of the potential for the hydrogen redox reaction (hydrogen oxidation reaction (HOR) and hydrogen evolution reaction (HER)).

The redox potential of these reactions shifts negatively with respect to the pH, as shown by linear sweep voltammograms (LSVs), Figure 4.1a and a Pourbaix diagram, Figure 4.1b, that exhibits a slope of ~60 mV/pH, which is close to the value of 59 mV/pH expected when an equal number of electrons and protons are transferred in a reaction. The Pourbaix diagram, Figure 4.1b, suggests that the hydrogen redox reaction in pH = 14 alkaline solution has a relative negative potential of ~-0.8 V vs. SHE compared to pH = 0 acidic solution (~0 V vs. SHE). This suggests that when an ion selective membrane separates an acidic half-cell where HER is performed (equation 4.1) from an alkaline half-cell where HOR is performed (equation 4.2), a favorable thermodynamic driving force is

developed between the half cells, Figure 4.1c, with the overall reaction being acid–base recombination (equation 4.3). This neutralization reaction is enthalpically and entropically favorable, as shown in the thermodynamic calculations, with ΔH^0 and $T\Delta S^0$ terms (entropic heat) at room temperature of -55.83 kJ/mol and +24.05 kJ/mol (at 298 K), respectively, which together corresponds to an electromotive force of 0.826 V. The entropic heat corresponds to the quantity of heat exchanged between the system and surroundings and hence, a positive $T\Delta S^0$ term represents heat flow to the system from the surroundings.[29,30] While entropic heat is usually negligible in electrochemical systems, for example ~3% of ΔH^0 for a Daniell cell and ~6% of ΔH^0 for a Ni-Cd cell; [31-33], for the electrochemical neutralization cell the entropic heat is almost 43 % of ΔH^0 (Thermodynamic Calculation 4.1a) suggesting that the heat absorbed from the surroundings is quite significant. Therefore, the proposed electro-

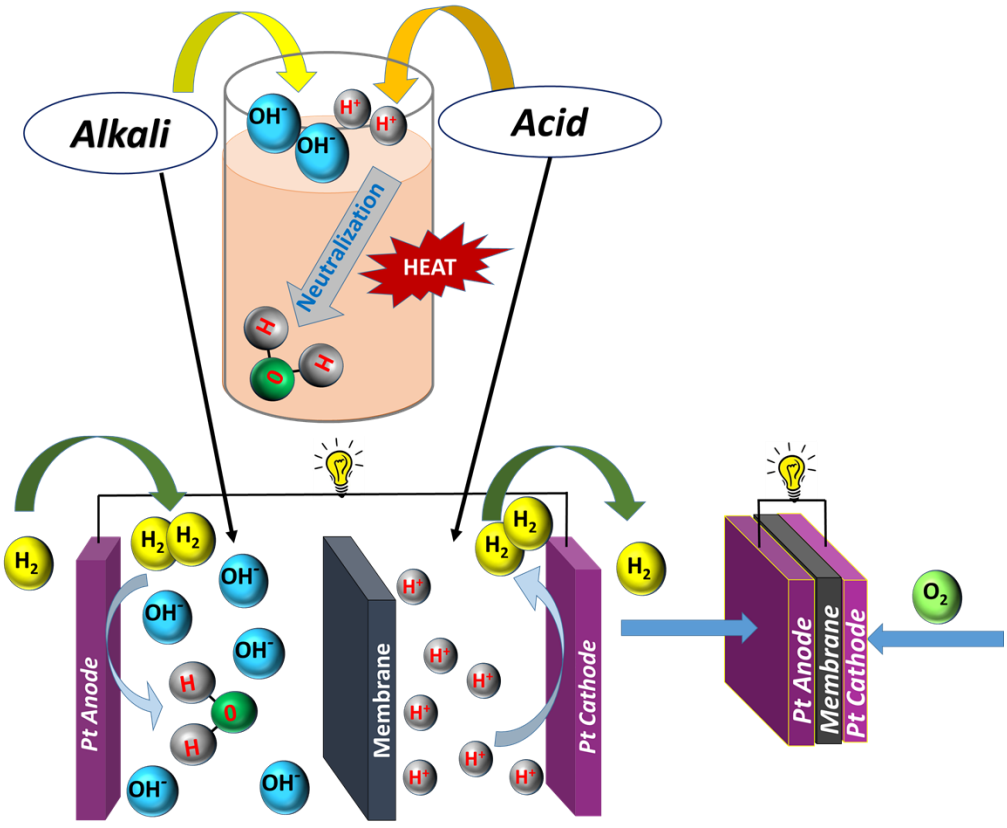

Scheme 4.1. Schematics of electrochemical neutralization cell for harvesting the energy of acid–base neutralization

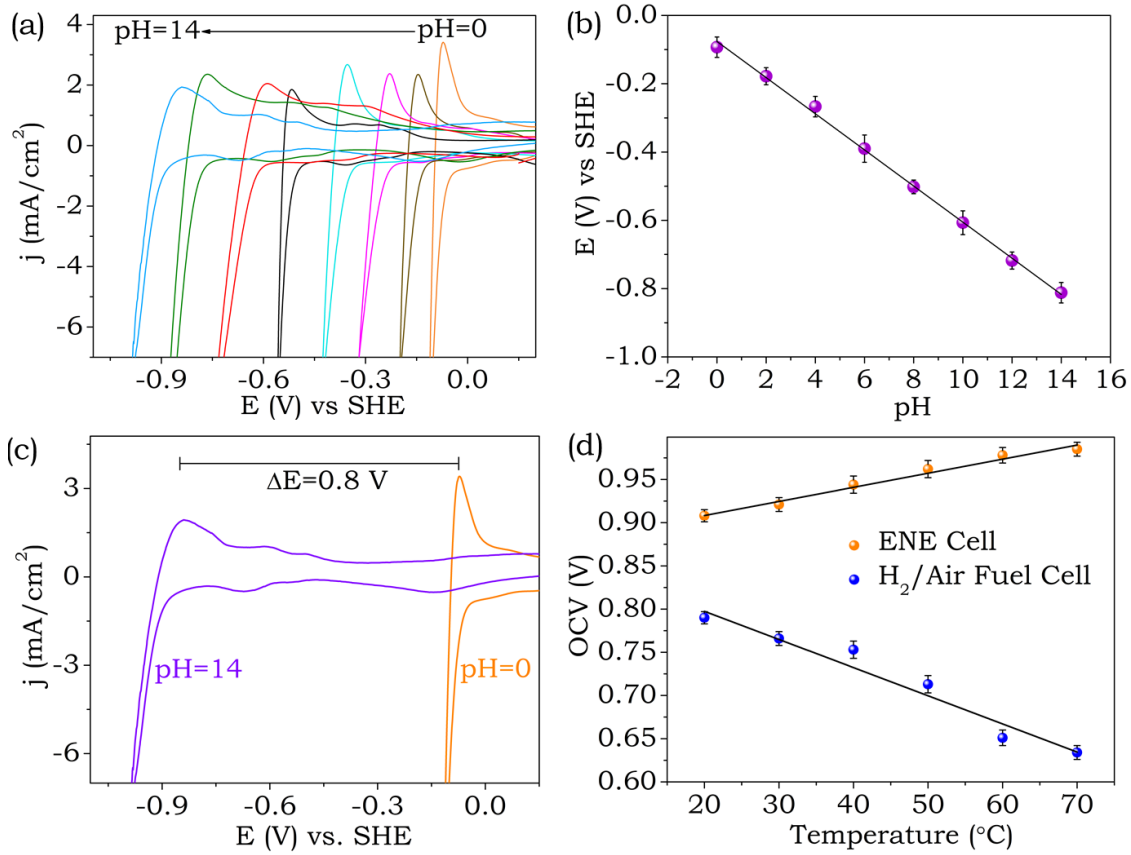

Figure 4.1. Cyclic voltammograms at a scan rate of 20 mV/s for (a) hydrogen redox reactions (hydrogen evolution reaction (HER) and hydrogen oxidation reaction (HOR)) at different pH values on a Pt electrode and (b) Pourbaix diagram for HER/HOR redox reactions. (c) Cyclic voltammograms for HER/HOR redox reactions at pH = 0 and pH = 14 and (d) the plot of open circuit voltage vs. cell temperature for the electrochemical neutralization device (orange trace) and H_2/air fuel cell (blue trace). The lower OCV of H_2-air fuel cell could be due to the lower partial pressure of oxygen in air.

-chemical neutralization cell can harvest the heat of the reaction (ΔH) as well as heat from the surroundings ($T\Delta S$) to perform electrical work. For this reason, the thermodynamic or ideal efficiency ($\Delta G^0/\Delta H^0$) of the electrochemical neutralization cell is more than one (1.43), Calculation 4.1a. For comparative purposes, thermodynamic calculations for a H_2-O_2 fuel cell, Calculation 4.1b, show that the thermodynamic efficiency is less than one (0.83) as entropic heat equivalent to 48 kJ/mol is lost to the

surroundings during cell operation due to the negative TΔS term. Therefore, E^0_{cell} for the electrochemical neutralization cell (0.826 V) is higher than the thermal voltage ($-\Delta H^0/nF$ = 0.579 V) and E^0_{cell} for the H_2-O_2 fuel cell (1.229 V) is lower than the thermal voltage (1.481 V), Calculation 4.1. Since the overall entropy change for the neutralization reaction is positive, Calculation 4.1a, an electrochemical device based on this chemistry should demonstrate a positive temperature coefficient for the open circuit voltage which in turn should allow harvesting of the heat from the surroundings also as electrical driving force. In line with this anticipation, a plot of open circuit voltage vs. temperature for the electrochemical neutralization cell demonstrated a positive slope, Figure 4.1d, which is a rather unique observation. For example, in state-of-the-art H_2-O_2 fuel cells this entropic heat (corresponding to TΔS = 48 kJ/mol) is lost to the surroundings in the form of heat due to the negative entropy change of water formation, Calculation 4.1b. This is clearly visible from the plot of open circuit voltage vs. temperature for a H_2-air fuel cell, Figure 4.1d. Most fuel cells have a negative entropic heat with ideal efficiency less than one, except for notable exceptions of the formic acid fuel cell and the carbon/carbon monoxide fuel cell.[34,35]

Cathodic half-cell redox reaction:

$$2H^+ \text{ (catholyte)} + 2e^- \rightleftharpoons H_2 \text{ (g)} \quad E^0_{SHE} = 0 \text{ V} \quad (4.1)$$

Anodic half-cell redox reaction:

$$2H_2O \text{ (anolyte)} + 2e^- \rightleftharpoons H_2 \text{ (g)} + 2OH^- \text{ (anolyte)} \quad E^0_{SHE} = -0.826 \text{ V} \quad (4.2)$$

Total cell reaction:

$$2H^+ \text{ (catholyte)} + 2OH^- \text{ (anolyte)} \rightleftharpoons 2H_2O \text{ (anolyte)} \quad E^0_{Cell} = +0.826 \text{ V} \quad (4.3)$$

The proposed electrochemical neutralization fuel cell yielded an open circuit voltage of ~900 mV, Figure 4.2b, which is close to the value expected based on Figure 4.1. Slightly higher OCV than that expected based on Nernstian equilibrium of H_2/H^+ could be due to the higher concentrations of H^+ and OH^- above the standard concentrations. The

polarization curve demonstrates a peak power density of ~70 mW/cm^2 at ~160 mA/cm^2 peak current, Figure 4.2c. The galvanostatic discharge curve at the peak rate (160 mA/cm^2) demonstrate a steady state voltage of ~375 mV resulting in the production of ~80 mL of H_2 gas from the cathodic compartment in 1 h time, Figure 4.2d. The experimental and theoretical values matched quite closely indicating the near absence of parasitic chemistry. H_2 consumption in the anodic half-cell (Eq 4.2) and its evolution (Eq 4.1) in the cathodic half-cell is further confirmed by in-situ electrochemical mass spectrometry, Figure 4.2d.

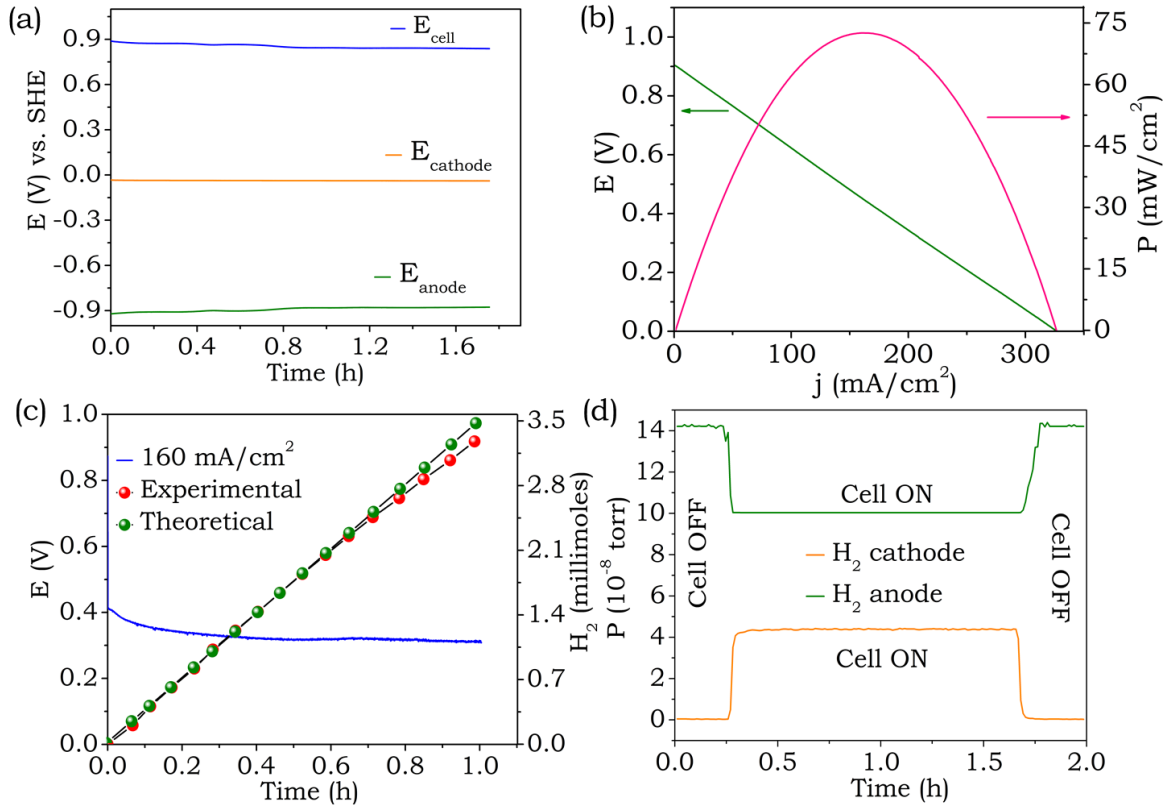

Figure 4.2. (a) Open circuit voltage profiles for ENC with a H_2 flow rate of 100 mL/minute to the anode, (b) polarization curve for ENC with a H_2 flow rate of 100 mL/minute and (c) galvanostatic polarization of ENC at the peak current density (~160 mA/cm^2) with H_2 quantification at the cathode and (d) in-situ electrochemical mass spectrometry for the anodic and cathodic half-cells.

When the resulting H_2 produced at the cathode of ENC is pumped to a PEMFC in an air breathing configuration, it delivered an OCV of ~900

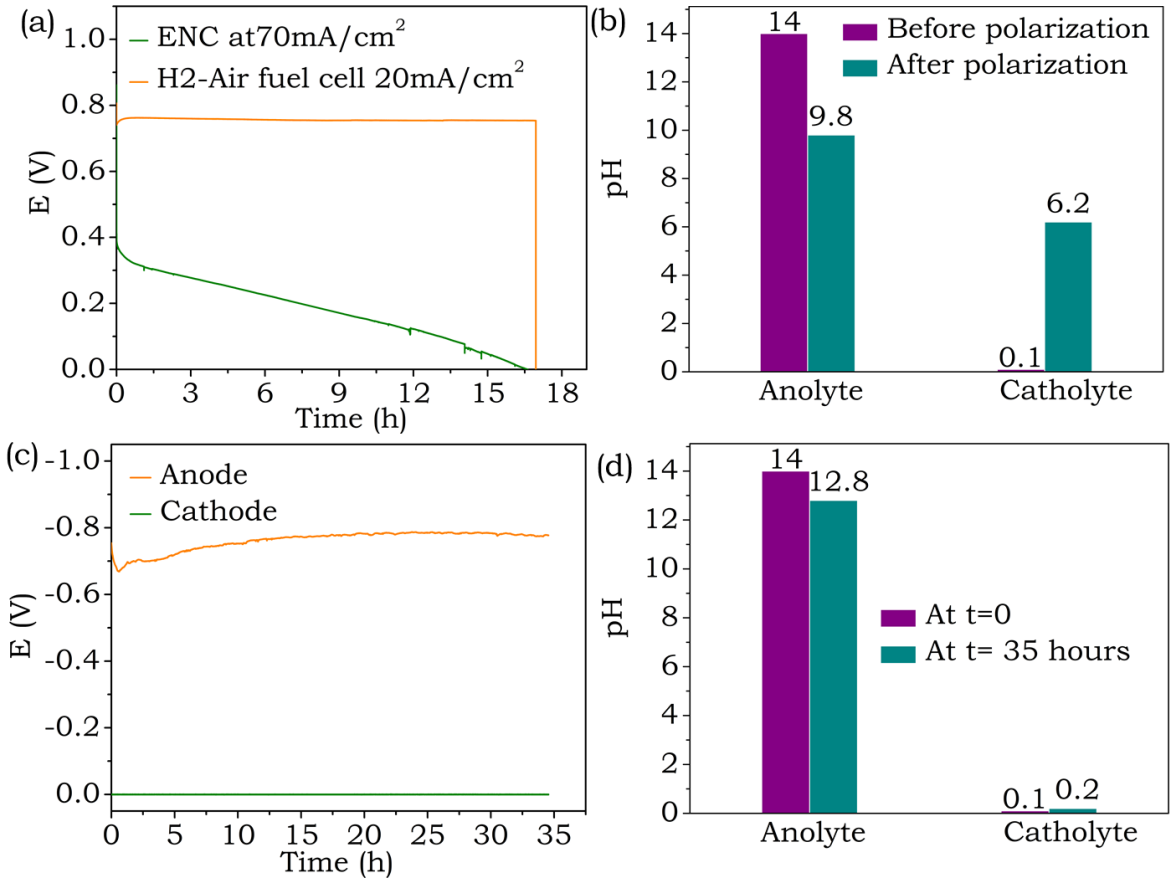

Figure 4.3. (a) Galvanostatic polarization of electrochemical neutralization ell at 160 mA/cm^2 when it is connected to an air-breathing PEMFC (discharged at 30 mA/cm^2) and (b) corresponding pH measurements at anodic and cathodic half-cells before and after galvanostatic polarization. (c) Open circuit voltage profile for electrochemical neutralization cell without purging H_2 to the anodic side and (d) corresponding pH changes in the anodic and cathodic half-cell.

-mV, and a galvanostatic discharge at 30 mA/cm^2 demonstrated a steady state voltage close to 750 mV, Figure 4.3a. It should be noted that the PEMFC discharge lasted for nearly 18 hours by which the cell voltage of ENC dropped to zero due to the neutralization reactions, Figure 4.3a and equation 4.3, confirming that H_2 produced at the cathode of ENC dropped to zero due to the neutralization reactions, Figure 4.3a and equation 4.3, confirming that H_2 produced at the cathode of electrochemical neutralization cell is the fuel for air breathing PEMFC. This further

suggest that energy benefits from same fuel stream can at least be doubled by directing it through the neutralization cell in a tandem configuration with a PEMFC. The pH of the anolyte decreased and the pH of the catholyte increased during the discharge chemistry, Figure 4.3b, confirming that hydronium ion is the electron acceptor and the reaction is driven by the energy of neutralization reaction. All these suggest the anodic chemistry, cathodic chemistry and complete cell chemistry as shown in equation 4.1-4.3 with salt formation (Na_2SO_4) at the cathode. The pH decrease observed in Figure 4.3b is not due to diffusion driven chemical reactions of H^+ and OH^- when they are separated by an ion conductor. This is confirmed by monitoring the pH of anodic and cathodic compartments at the open circuit as a function of time, Figure 4.3c,d. No significant decrease in pH and voltage was observed even after 35 hours suggesting the pH change observed in Figure 4.3b is the result of electrochemical neutralization reactions as shown in equations 4.1-4.3.

Individual half-cell polarization studies demonstrate that anodic part limit the overall performance, Figure 4.4a, which is due to sluggish electrode kinetics of HOR in alkaline medium as explained earlier.[36-44] When a fixed amount of H_2 is supplied to the anode (40 mL), almost 20 mL was collected at the cathode by the time the cell voltage fell to zero during galvanostatic discharge at 160 mA/cm^2, Figure 4.4b). This indicates that the stoichiometry of H_2 gas supplied and reacted is close to 0.5 which is typical of any PEMFC,[45,46] and the conversion efficiency is close to 50%. The lower discharge time in Figure 4.4b compared to Figure 4.2c could be due to limited supply of H_2 and associated concentration polarization at a current of 160 mA/cm^2. This could be due to lower solubility of H_2 in aquatic environment, trapping of H_2 in the head space, supplier tube space etc. In order to prove this concentration polarization effect, discharge experiments were carried out with respect H_2 fuel amount, Figures 4.4c. The discharge profiles at the same rate with different amounts of hydrogen demonstrated a monotonic relation between discharge time and the amount of hydrogen, Figure 4.4c. This confirm

that the lower discharge time in Figure 4.4b is due to the limited supply of hydrogen fuel. The interfacial stability of ENC is further investigated by galvanostatic pulse discharge, Figure 4.4d. On increasing the rate, the cell voltage dropped, however on decreasing the rate the cell voltage regained to approximately the same level for each rate suggesting decent interfacial stability.

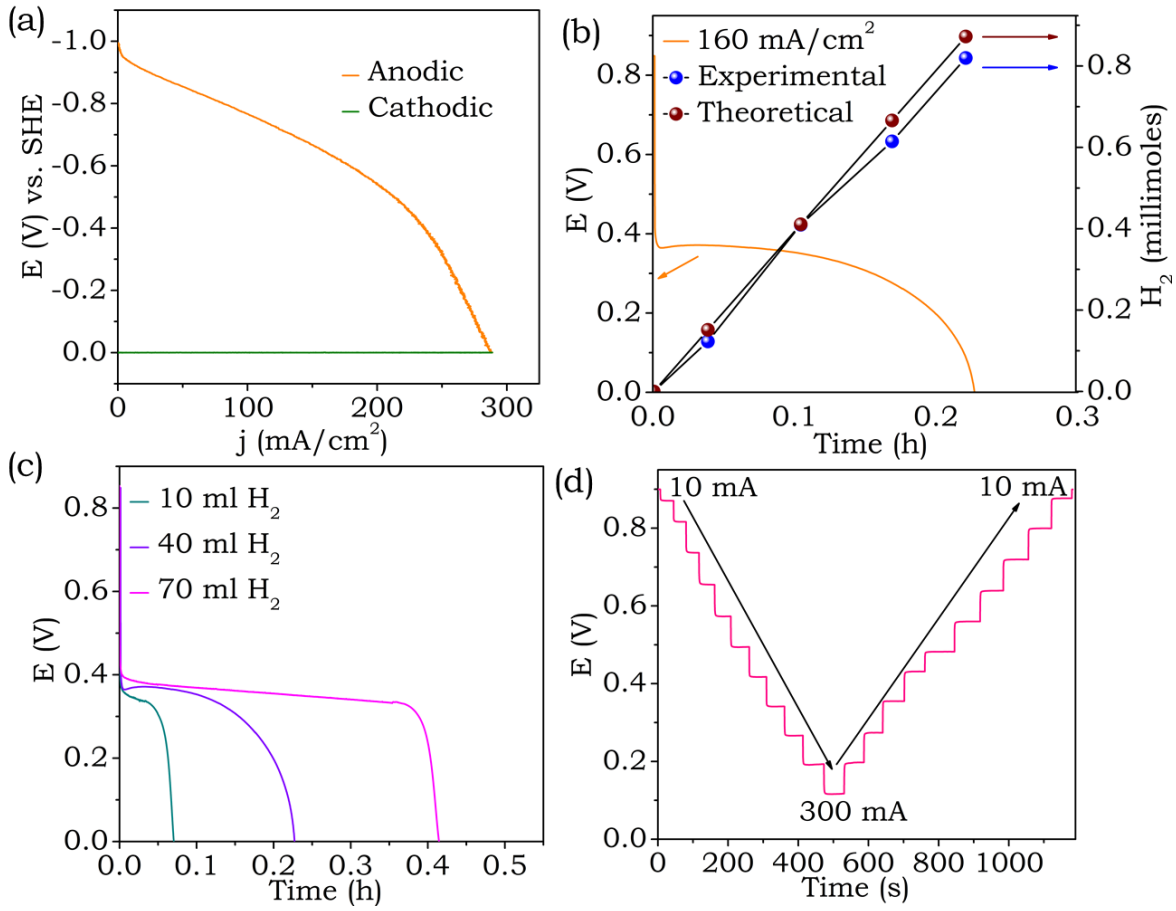

Figure 4.4. (a) Individual electrode polarization and (b) H_2 quantification from the cathode when anode is supplied with fixed amounts of hydrogen (40 mL) at 160 mA/cm^2. (c) Discharge profiles at a constant rate (160 mA/cm^2) with varying amounts of H_2 fuel. (d) Step current discharge of ENC.

4.4. Conclusions

In this Chapter, we have demonstrated an electrochemical neutralization cell by harnessing the free energy of acid base neutralization reaction as electromotive force. Proposed architecture

constitutes H_2 as an electron donor in an alkaline pH and hydronium ion playing the crucial role of cathodic electron acceptor so as to exhale the fuel inhaled at the anode. ENC directly harvest the neutralization energy as electric energy without a net redox reaction. We also illustrate that the electrical energy benefits from the same fuel stream can at least be doubled by linking the neutralization electrochemical cell in a tandem configuration with a PEMFC.

4.5. References

[1] Mourad, E.; Coustan, L.; Lannelongue, P.; Zigah, D.; Mehdi, A.; Vioux, A.; Freunberger, S. A.; Favier, F.; Fontaine, O. Biredox Ionic Liquids with Solid-like Redox Density in the Liquid State for High-Energy Supercapacitors. *Nat. Mater.* **2016**, *1*,446-454

[2] Schafzahl, L.; Mahne, N.; Schafzahl, B.; Wilkening, M.; Slugovc, C.; Borisov, S. M.; Freunberger, S. A. Singlet Oxygen during Cycling of the Aprotic Na-O2 Battery. *Angew. Chemie Int. Ed.* **2017**,*56,* 1–6.

[3] Miroshnikov, M.; Divya, K. P.; Babu, G.; Meiyazhagan, A.; Reddy Arava, L. M.; Ajayan, P. M.; John, G. Power from Nature: Designing Green Battery Materials from Electroactive Quinone Derivatives and Organic Polymers. *J. Mater. Chem. A* **2016**, *4* (32), 12370–12386.

[4] Kannan, R.; Kakade, B. A.; Pillai, V. K. Polymer Electrolyte Fuel Cells Using Nafion-Based Composite Membranes with Functionalized Carbon Nanotubes ** Zuschriften. *Angew. Chem. Int. Ed. Engl.* **2008**, *47*, 2693–2696.

[5] Forsyth, M.; Yoon, H.; Chen, F.; Zhu, H.; MacFarlane, D. R.; Armand, M.; Howlett, P. C. Novel Na+ Ion Diffusion Mechanism in Mixed Organic-Inorganic Ionic Liquid Electrolyte Leading to High Na+ Transference Number and Stable, High Rate Electrochemical Cycling of Sodium Cells. *J. Phys. Chem. C* **2016**, *120* (8), 4276–4286.

[6] Hassoun, J.; Lee, K. S.; Sun, Y. K.; Scrosati, B. An Advanced Lithium Ion Battery Based on High Performance Electrode Materials. *J. Am. Chem. Soc.* **2011**, *133* (9), 3139–3143.

[7] Sood, R.; Cavaliere, S.; Jones, D. J.; Rozière, J. Electrospun Nanofibre Composite Polymer Electrolyte Fuel Cell and Electrolysis Membranes. *Nano Energy* **2016**, *26*, 729–745.

[8] Gao, J.; Li, L.; Tan, J.; Sun, H.; Li, B.; Idrobo, J. C.; Singh, C. V.; Lu, T. M.; Koratkar, N. Vertically Oriented Arrays of ReS2 Nanosheets for Electrochemical Energy Storage and Electrocatalysis. *Nano Lett.* **2016**, *16* (6), 3780–3787.

[9] Nagarathinam, M.; Saravanan, K.; Phua, E. J. H.; Reddy, M. V.; Chowdari, B. V. R.; Vittal, J. J. Redox-Active Metal-Centered Oxalato Phosphate Open Framework Cathode Materials for Lithium Ion Batteries. *Angew. Chemie - Int. Ed.* **2012**, *51* (24), 5866–5870.

[10] Kamat, P. V.; Bisquert, J.; Buriak, J. Lead-Free Perovskite Solar Cells. *ACS Energy Lett.* **2017**, *2* (4), 904–905.

[11] Kreuer, K. D. On the Development of Proton Conducting Polymer Membranes for Hydrogen and Methanol Fuel Cells. *J. Memb. Sci.* **2001**, *185* (1), 29–39.

[12] Hassoun, J.; Lee, K. S.; Sun, Y. K.; Scrosati, B. An Advanced Lithium Ion Battery Based on High Performance Electrode Materials. *J. Am. Chem. Soc.* **2011**, *133* (9), 3139–3143.

[13] Maiyalagan, T.; Alaje, T. O.; Scott, K. Highly Stable Pt À Ru Nanoparticles Supported on Three-Dimensional Cubic Ordered Mesoporous Carbon (Pt À Ru / CMK-8) as Promising Electrocatalysts for Methanol Oxidation. *J. Phys. Chem. C* **2012**, 2630–2638.

[14] Abraham, K. M. Prospects and Limits of Energy Storage in Batteries. *J. Phys. Chem. Lett.* **2015**, *6* (5), 830–844.

[15] Aricò, A. S.; Srinivasan, S.; Antonucci, V. DMFCs: From Fundamental Aspects to Technology Development. *Fuel Cells* **2001**, *1* (2), 133–161.

[16] Bashyam, R.; Zelenay, P. A Class of Non-Precious Metal Composite Catalysts for Fuel Cells. *Nature* **2006**, *443* (7107), 63–66.

[17] Ding, Y.; Cai, P.; Wen, Z. Electrochemical Neutralization Energy: From Concept to Devices. *Chem. Soc. Rev.* **2021**, *50* (3), 1495–1511.

[18] Cai, P.; Li, Y.; Wang, G.; Wen, Z. Alkaline–Acid Zn–H_2O Fuel Cell for the Simultaneous Generation of Hydrogen and Electricity. *Angew. Chemie - Int. Ed.* **2018**, *57* (15), 3910–3915.

[19] Cai, P.; Wang, G.; Chen, K.; Wen, Z. Reversible Zn-Quinone Battery with Harvesting Electrochemical Neutralization Energy. *J. Power Sources* **2019**, *428*, 37–43.

[20] D'Ambrose, M. J.; Turney, D. E.; Yadav, G. G.; Nyce, M.; Banerjee, S. Material Failure Mechanisms of Alkaline Zn Rechargeable Conversion Electrodes. *ACS Appl. Energy Mater.* **2021**. *4* (4), 3381-3392.

[21] Li, Y.; Chen, J.; Cai, P.; Wen, Z. An Electrochemically Neutralized Energy-Assisted Low-Cost Acid-Alkaline Electrolyzer for Energy-Saving Electrolysis Hydrogen Generation. *J. Mater. Chem. A* **2018**, *6* (12), 4948–4954.

[22] Liu, C.; Chi, X.; Han, Q.; Liu, Y. A High Energy Density Aqueous Battery Achieved by Dual Dissolution/Deposition Reactions Separated in Acid-Alkaline Electrolyte. *Adv. Energy Mater.* **2020**, *10* (12), 1–7.

[23] Schreier, M.; Héroguel, F.; Steier, L.; Ahmad, S.; Luterbacher, J. S.; Mayer, M. T.; Luo, J.; Grätzel, M. Solar Conversion of Co2 to CO Using Earth-Abundant Electrocatalysts Prepared by Atomic Layer Modification of CuO. *Nat. Energy* **2017**, *2* (7), 1–9.

[24] Wang, G.; Chen, J.; Cai, P.; Jia, J.; Wen, Z. A Self-Supported Ni-Co Perselenide Nanorod Array as a High-Activity Bifunctional Electrode for a Hydrogen-Producing Hydrazine Fuel Cell. *J. Mater. Chem. A* **2018**, *6* (36), 17763–17770.

[25] Wang, G.; Chen, J.; Li, Y.; Jia, J.; Cai, P.; Wen, Z. Energy-Efficient Electrolytic Hydrogen Production Assisted by Coupling Urea Oxidation with a PH-Gradient Concentration Cell. *Chem. Commun.* **2018**, *54* (21), 2603–2606.

[26] Weng, S. X.; Chen, X. A Hybrid Electrolyzer Splits Water at 0.8V at Room Temperature. *Nano Energy* **2016**, *19* (3), 138–144.

[27] Yadav, G. G.; Turney, D.; Huang, J.; Wei, X.; Banerjee, S. Breaking the 2 v Barrier in Aqueous Zinc Chemistry: Creating 2.45 and 2.8 v MnO2-Zn Aqueous Batteries. *ACS Energy Lett.* **2019**, *4* (9), 2144–2146.

[28] Zhong, C.; Liu, B.; Ding, J.; Liu, X.; Zhong, Y.; Li, Y.; Sun, C.; Han, X.; Deng, Y.; Zhao, N.; Hu, W. Decoupling Electrolytes towards Stable and High-Energy Rechargeable Aqueous Zinc–Manganese Dioxide Batteries. *Nat. Energy* **2020**, *5* (6), 440–449.

[29] Madani, S.S., Schaltz, E., and Kær, S.K. An experimental analysis of entropic coefficient of a lithium titanate oxide battery. *Energies* **2019,** *12*(14), 2685.

[30] Winter, M., and Brodd, R.J. What are batteries, fuel cells, and supercapacitors? *Chem. Rev.* **2004,** *104*, 4245–4269.

[31] Schmidt-Rohr, K. How Batteries Store and Release Energy: Explaining Basic Electrochemistry. *J. Chem. Educ.* **2018,** *95,* 1801–1810.

[32] Claus Daniel and Jurgen O. Besenhard. Fundamentals and General Aspects of Electrochemical Energy Storage:Thermodynamics and Mechanistics. Handbook of Battery Materials, 2nd edition WileyVCH, Weinheim, Germany, **2011,** Ch. 1, 1–26.

[33] Winterbone, D.E., Turan, A., Winterbone, D.E., and Turan, A. Advanced Thermodynamics for Engineers, Elsevier Ltd. **2015,** Chapter 21, *1*, 497–526.

[34] B. Sørensen, Hydrogen and Fuel Cells Emerging Technologies and Applications, Elsevier Academic Press, New York, **2005,** ch. 3 p. 104

[35] Debe, M. K. Handbook of Fuel Cells—Fundamentals, Technology and Applications Vol. 3 (eds Vielstich, W., Gasteiger, H. A. & Lamm, A.) (Wiley, Chichester, UK,). **2003,** Ch. 4.

[36] Kucernak, A. R.; Zalitis, C. General Models for the Electrochemical Hydrogen Oxidation and Hydrogen Evolution Reactions: Theoretical Derivation and Experimental Results under Near Mass-Transport Free Conditions. *J. Phys. Chem. C* **2016,** *120,* 10721−10745.

[37] Sheng, W.; Zhuang, Z.; Gao, M.; Zheng, J.; Chen, J. G.; Yan, Y. Correlating hydrogen oxidation and evolution activity on platinum at different pH with measured hydrogen binding energy. *Nat. Commun.* **2015,** *6,* 5848.

[38] Strmcnik, D.; Uchimura, M.; Wang, C.; Subbaraman, R.; Danilovic, N.; van der Vliet, D.; Paulikas, A. P.; Stamenkovic, V. R.; Markovic, N. M. Promotion of Hydroxyl Adsorption. *Nat. Chem.* **2013,** *5,* 300–306.

[39] Li, J.; Ghoshal, S.; Bates, M. K.; Miller, T. E.; Davies, V.; Stavitski, E.; Attenkofer, K.; Mukerjee, S.; Ma, Z. F.; Jia, Q. Experimental Proof of the Bifunctional Mechanism for the Hydrogen Oxidation in Alkaline Media. *Angew. Chem., Int. Ed.* **2017,** *56 (49),* 15594–15598.

[40] Zheng, J.; Sheng, W.; Zhuang, Z.; Xu, B.; Yan, Y. Universal Dependence of Hydrogen Oxidation and Evolution Reaction Activity of Platinum-Group Metals on pH and Hydrogen Binding Energy. *Sci. Adv.* **2016,** *2 (3),* e1501602–e1501602.

[41] Schmidt, T. J.; Ross, P. N.; Markovic, N. M. Temperature Dependent Surface Electrochemistry on Pt Single Crystals in Alkaline Electrolytes: Part 2. The Hydrogen Evolution/oxidation Reaction. *J. Electroanal. Chem.* **2002,** 524–525.

[42] Jervis, R.; Mansor, N.; Gibbs, C.; Murray, C. a.; Tang, C. C.; Shearing, P. R.; Brett, D. J. L. Hydrogen Oxidation on PdIr/C Catalysts in Alkaline Media. *J. Electrochem. Soc.* **2014,** *161 (4),* F458–F463.

[43] Ledezma-Yanez, I.; Wallace, W. D. Z.; Sebastian-Pascual, P.;́ Climent, V.; Feliu, J. M.; Koper, M. T. M. Interfacial Water Reorganization as a pH-Dependent Descriptor of the Hydrogen Evolution Rate on Platinum Electrodes. *Nat. Energy* **2017,** *2 (4),* 17031.

[44] Rheinlander, P. J.; Herranz, J.; Durst, J.; Gasteiger, H. A. Kinetics of the Hydrogen Oxidation/Evolution Reaction on Polycrystalline Platinum in Alkaline Electrolyte Reaction Order with Respect to Hydrogen Pressure. *J. Electrochem. Soc.* **2014**, *161 (14)*, F1448–f1457.

[45] Barbir, F.; Gomez, T. Efficiency and Economics of Proton´ Exchange Membrane (PEM) Fuel Cells. *Int. J. Hydrogen Energy* **1997**, *22 (10),* 1027–1037.

[46] Edwards, P. P.; Kuznetsov, V. L.; David, W. I. F.; Brandon, N. P. Hydrogen and Fuel Cells: Towards a Sustainable Energy Future. *Energy Policy* **2008,** *36 (12),* 4356–4362.

Chapter 5

An Electrochemical Neutralization Cell for Spontaneous Water Desalination

Abstract: An entropically favoured electrochemical reaction sequence can interconvert external heat as electrical energy, since its temperature coefficient is directly related to entropy change. This account shows that an electrochemically driven neutralization pathway exhibits a positive temperature coefficient for the open circuit voltage (1.63 ± 0.11 mV/K), which in turn can harvest ~24 kJ/mol of entropic heat, at room temperature, from the surroundings as electrical driving force. We show that the inter-conversion of neutralization energy as electrical energy can spontaneously desalinate saline water during electric power generation by consuming ~13.6 kJ for the removal of 1 mole of NaCl. Desalination without the aid of an external power supply by performing reversible redox reactions involving only gases, water, H^+ and OH^- such that the products and reactants of the reaction will not contaminate the desalinated water opens up an unprecedented pathway for addressing potable water crises looming over the 21st century.

The chapter contains the data taken from my original published work:
Zahid Bhat et.al., Joule 2020, 4 (8), 1730–1742.
Copyright © 2020 Elsevier Inc.

5.1. Introduction

Even though ~71% of the earth's surface is covered with water, availability of potable water has alarmingly shrunk with explosive rise in global population.[1,2] The ultimate source of water to alleviate this problem is seawater, however its high salinity of ~35 g/L makes it unfit for drinking or irrigation purposes.[3-5] Therefore, desalination methods for the removal of salt from sea water play a crucial role in providing a sustainable, rainfall-independent water supply.[6-9] The state of the art processes for water desalination such as seawater reverse osmosis and thermal distillation are more energy demanding than alternative freshwater supplies from rivers and streams, ground water, recycled waste water etc.[10-12] Other alternative methods such as capacitive deionization, electro-dialysis, shock electro-dialysis and concentration polarization also consume a large amount of energy per unit volume of water making them less attractive for sustainable, long-term management of growing water demand.[13-17]

Electrodialytic process for desalination have two major shortcomings: (i) ohmic iR losses and (ii) losses due to redox reactions that typically generate chemical species that can poison the desalinated water. [18-20] Here we demonstrate spontaneous desalination of saline water during electric power generation by interconverting neutralization energy and electrical driving force. This represents an innovative design to overcome the shortcomings of electrodialysis process (especially the shortcoming (ii)) by performing reversible redox reactions involving only gases, water, H^+ and OH^- such that the products and reactants of the redox reactions will not poison the desalinated water. Recently, desalination is reported in metal ion batteries and supercapacitors during electric power generation.[21-24] Though this integrates an additional dimension to batteries which are otherwise confined in the domain of energy storage,[25-33] desalination requires irreversible consumption of the free energy of active metallic anode.[34,35] Secondly, a part of the electrical

energy stored in the batteries due to the charging redox reactions is utilized for desalination during the discharge.[36,37] The desalination chemistry we offer is distinctly different from the desalination in metal ion batteries and flow batteries because, the electron donor consumed in the anodic half-cell is regenerated in the cathodic half-cell with the net result being spontaneous water desalination without a net redox reaction and without any water contamination by the discharge products.

5.2. Materials and Methods

H_2SO_4 (96%), NaOH (97%), NaCl (99%), K_2HPO_4 (98%), KH_2PO_4 (99%), H_3PO_4 (83%), CH_3COOH (99.7%), $KHSO_4$ (99%), $KHCO_3$ (99.7%), K_2CO_3 (99%) and oxalic acid (99%) were obtained from Sigma-Aldrich India. Pt/C with 40 wt% of Pt on carbon (Pt/C), Nafion 117 and Fumasep membranes were obtained from Fuel Cell Store (USA).

Electrochemical measurements were carried out using a Biologic potentiostat/galvanostat (VMP-300). In-situ electrochemical mass spectrometry was carried out with HPR-20 R&D (Hiden analytical) Quadruple mass analyzer. Microwave plasma atomic emission spectroscopy (MP-AES) was carried out with MP-AES-4200 System (Agilent technologies) and conductivity was measured with μ controller-based conductivity meter (Type 306, Systronics India).

Linear sweep voltammetry (LSV) and cyclic voltammetry (CV) experiments were carried out in a 3-electrode setup. Platinum disk (2 mm diameter) and platinum flag electrodes were used as a working electrode and counter electrode, respectively. $Hg/HgSO_4/SO_4^{2-}$ and $Hg/HgO/OH^-$ were used as reference electrodes in acidic and alkaline media, respectively. The working electrodes were cleaned by polishing with 0.05-micron alumina powder followed by cycling in 0.5 M H_2SO_4 until reproducible platinum features were obtained in the cyclic voltammograms. Prior to each measurement the solutions were saturated by purging with hydrogen gas for 15 minutes. 0.5 M sulphuric acid (pH = 0), sulphate buffer (pH = 2), acetate buffer (pH = 4), phosphate buffer (pH =

5 to 12) and 1 M sodium hydroxide (pH = 14) were used to prepare the respective pH solutions.

A three-compartment homemade cell was used for the desalination experiments (Scheme 1). The anodic compartment was separated from the middle saline compartment (saline compartment) by an anion exchange membrane (Fumasep) and the cathodic compartment was separated from the middle saline compartment by a cation exchange membrane (Nafion 117). The anodic and cathodic compartments were filled with 40 mL solutions of H_2SO_4 (1 M) and NaOH (2 M), respectively. Pt/C (0.5 mg/cm^2) and Pt mesh were used as electrodes in anodic and cathodic compartments respectively. The stagnant middle saline compartment was filled with 13 mL saline solution of 4 M NaCl. During device operation, H_2 was bubbled into the anodic half-cell at flow rate of 100 mL/min. The amount of hydrogen consumed and evolved during the discharge studies was monitored by in-situ electrochemical mass spectrometry. Quantification of the hydrogen gas coming out of the cathodic compartment was carried out with the help of the water displacement technique. The concentration of sulphuric acid and sodium hydroxide before and after discharge was estimated by acid-base titration. 1 M oxalic acid was used as the primary standard and phenolphthalein was used as the indicator. The concentration of sodium ion in the saline compartment was monitored by the Microwave Plasma Atomic Emission Spectroscopy (MPAES) technique. Mohr's method was used to determine the chloride ions concentration in the saline solution by titrating against silver nitrate using potassium chromate as the indicator. The decrease in the concentration of the salt in saline compartment was also monitored using a conductivity meter. EIS measurements were carried out using two Pt/C electrodes in the frequency range of 100 kHz to 10 mHz with a 10 mV AC (peak to peak) amplitude. EIS measurements were carried out between the anode and middle saline compartment, cathode and middle saline compartment and finally between the anode and cathode compartments to find the individual iR drops across each of the compartments. For

desalination using the H_2-O_2 fuel cell, all three compartments were filled with 4 M NaCl solution and the architectural configuration remained the same as for the electrochemical neutralization cell. For the hydrogen oxidation reaction in the anodic half-cell and the oxygen reduction reaction in the cathodic half-cell Pt/C (0.5 mg/cm^2 loading) was used as the electrocatalysts. Hydrogen and oxygen were bubbled continuously through the anodic and cathodic compartments respectively at 100 mL/min flow rates. The cell was kept short circuited for 30 hours for desalination.

5.3. Results and Discussion

The architecture of the water desalination device driven by electrochemical neutralization is shown in Scheme 5.1 and it possesses a three-compartment architectural configuration: an alkaline anodic compartment (top), a saline compartment (middle) and an acidic cathodic compartment (bottom). The anodic and cathodic compartments were separated from the middle compartment by an anion exchange membrane (AEM) and a cation exchange membrane (CEM), respectively. The middle compartment houses saline water for desalination consisting of an aqueous salt solution at a concentration of 4 M NaCl (13 mL feed). The anodic half-cell compartment contains an aqueous alkaline solution at pH = 14 (NaOH; 40 mL) and the cathodic half-cell compartment contains an aqueous acidic solution at pH = 0 (H_2SO_4; 40 mL). The device relies on the proton dependence of the potential for the hydrogen redox reaction (hydrogen oxidation reaction (HOR) and hydrogen evolution reaction (HER)), Scheme 5.1. As discussed in detail in chapter 4, the redox potential of these reactions shifts negatively with respect to the pH, as shown by linear sweep voltammograms (LSVs) and Pourbaix diagram suggests that the hydrogen redox reaction in pH = 14 alkaline solution has a relative negative potential of ~-0.8 V vs. SHE compared to pH = 0 acidic solution (~0 V vs. SHE) (refer Figure 4.1, chapter 4). This suggests that when an ion selective membrane separate an acidic half-cell where

HER is performed (equation 5.1) from an alkaline half-cell where HOR is performed (equation 5.2), a favorable thermodynamic driving force is developed between the half cells, Figure 5.1c, with the overall reaction being acid–base recombination (equation 5.3). During the overall process, the decrease in the anions and cations in the anolyte and catholyte will be taken care by the movement of ions from the middle compartments to the respective compartment as suggested by equations 5.4 and 5.5. Overall, the total cell reaction shows the desalination of the saline water in the middle compartment during electricity production by using electrochemical neutralization as the driving force, equation 5.6. The neutralization reaction is enthalpically and entropically favorable with important implications in harvesting energy also from the surroundings as electrical driving force as discussed in chapter 4.

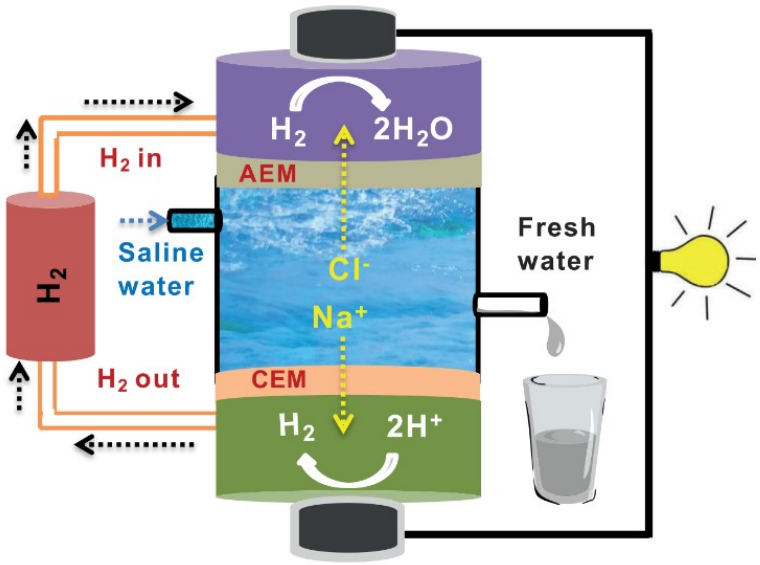

Scheme 5.1. Schematic representation of the electrochemical neutralization cell for spontaneous water desalination. AEM and CEM stand for anion exchange membrane and cation exchange membranes, respectively.

Cathodic half-cell redox reaction:

$$2H^+ \text{ (catholyte)} + 2e^- \rightleftharpoons H_2 \text{ (g)} \quad E^0_{SHE} = 0 \text{ V} \quad (5.1)$$

Anodic half-cell redox reaction:

$$2H_2O\ (anolyte) + 2e^- \rightleftharpoons H_2\ (g) + 2OH^-\ (anolyte) \quad E^0_{SHE} = -0.826\ V \quad (5.2)$$

Full cell redox reaction (Reaction 1 – Reaction 2):

$$2H^+\ (catholyte) + 2OH^-\ (anolyte) \rightleftharpoons 2H_2O\ (anolyte) \quad E^0_{Cell} = +0.826\ V \quad (5.3)$$

Catholyte half-cell ionic reaction:

$$2Na^+\ (middle\ saline) + SO_4^{2-}\ (catholyte) \rightleftharpoons Na_2SO_4\ (catholyte) \quad (5.4)$$

Anolyte half-cell ionic reaction:

$$2Cl^-\ (middle\ saline) + 2Na^+\ (anolyte) \rightleftharpoons 2NaCl\ (anolyte) \quad (5.5)$$

Total cell reaction (Reaction 3 + Reaction 4 + Reaction 5):

$$H_2SO_4\ (catholyte) + 2NaOH\ (anolyte) + 2NaCl\ (middle\ saline) \rightleftharpoons$$

$$Na_2SO_4\ (catholyte) + 2NaCl\ (anolyte) + 2H_2O\ (anolyte) \quad (5.6)$$

Single electrode potentials of the electrochemical neutralization cell when H_2 is bubbled into the alkaline half-cell and decoupled from the acidic half-cell by an ion selective membrane (Nafion 117) show that the former has a relative negative potential (anode) compared to the latter (cathode), Figure 5.2a. In line with this, the electrochemical neutralization cell for water desalination with hydrogen fuel as the electron donor shows an open circuit voltage (OCV) of nearly 900 mV, a power density of ~27 mW/cm^2 and a peak current density of ~150 mA/cm^2, Figure 5.2b. The galvanostatic discharge of the device at 50 mA/cm^2 shows a stable voltage plateau at ~0.55 V with the generation of molecular hydrogen (~23 mL/hr) at the cathode, Figure 5.2c, which is nearly equal to the theoretical Faradaic efficiency. The consumption of hydrogen in the anodic half-cell and the corresponding evolution of hydrogen in the cathodic half-cell during the discharge chemistry is confirmed by in-situ electrochemical mass spectrometry, Figure 5.2d. These confirm equation 1 as the cathodic half-cell chemistry and equation 2 as the anodic half-cell chemistry.

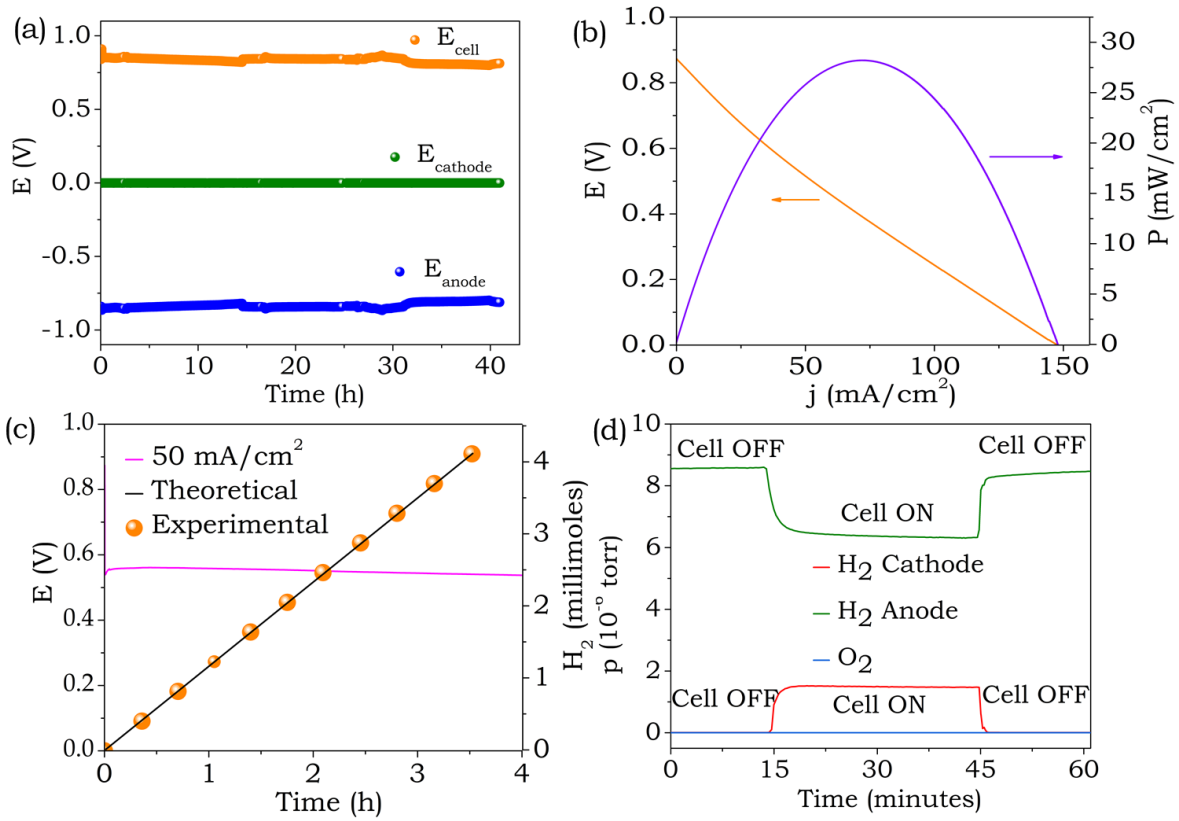

Figure 5.2. (a) Single electrode potentials for the anodic and cathodic half-cells of the electrochemical neutralization cell with hydrogen fuel as the electron donor, (b) polarization curve for the electrochemical neutralization cell for water desalination with hydrogen as the electron donor, (c) galvanostatic polarization of the device at a current density of 50 mA/cm^2 with H_2 quantification at the cathode and (d) in-situ electrochemical mass spectrometry for the anodic and cathodic half-cells.

In order to understand water desalination in the middle saline chamber of a three-compartment cell, the cell was discharged at 50 mA/cm^2 until the driving force at that current density dropped to zero, which required about 22 hours, Figure 5.3a. The desalination of the middle saline compartment was monitored by conductivity and Microwave Plasma Atomic Emission Spectroscopy (MP-AES) before and after discharge of the cell. The conductance of the middle saline compartment decreased from 156.5 mS (before discharge) to 57.8 mS (after discharge) confirming the desalination process during electric power generation, Figure 5.3b. The MP-AES measurement of the middle saline compartment

was used to monitor the Na^+ ion concentration which confirmed a noticeable decrease in the sodium ion concentration after sustained polarization, Figure 5.3c. The Cl^- ion concentration before and after discharge was followed by Mohr's titration method and it further evidenced a decrease in Cl^- concentration in the middle saline compartment after the discharge chemistry, Figure 5.3c. The decrease in the concentration of Cl^- ions from 4 M to ~1 M is commensurate to the decrease in concentration of Na^+ ions, which corresponds to ~0.4 moles of salt removal in 21.29 hours and a flux of 18.79 mmol/hr/cm^2. The concentration of H^+ and OH^- in the acidic and alkaline half-cells before and after discharge was monitored by titration techniques. The titration data showed that the concentration of NaOH decreased in the alkaline half-cell from 2 M to ~1 M and the concentration of H_2SO_4 in the acidic half-cell decreased from 1 M to ~0.5 M, Figure 5.3d. This decrease in the acid and alkali concentration during discharge confirms that electrochemical neutralization energy is responsible for water desalination (equation 5.3). It should be noted that when the electrical circuit is at open circuit, slight alterations in H^+ and OH^- concentrations were detected after almost 50 hours, Figure 5.3e. The concentration of the salt in the saline compartment decreased to a lesser extent, as almost 3.9 millimoles of salt was removed in 50 hours, which corresponds to a flux of 78 μmol/hr/cm^2. Comparing this flux to the 240-fold larger flux that occurred concomitant with H_2 redox (18.79 mmol/hr/cm^2), further substantiates the utility of the electrochemical neutralization cell for desalination. The slow decrease in the salt concentration in the saline compartment and H^+ and OH^- concentration in the respective half-cells (Figure 5.4e) when the electrical circuit is at open circuit is mostly due to diffusion driven transport of ions across the ion exchange membranes, resulting in desalination together with water formation in the saline compartment. This salt leakage phenomenon is also responsible for the lack of fully formed built-in Donnan electric potentials across the

membranes and thus observation of an open circuit potential between the half-cell electrodes. Without H_2 redox the leaky membrane performed desalination by concerted opposing transport of two ions across each membrane driven mostly by diffusion, H^+/Na^+ through the CEM and Cl^-/OH^- through the AEM. Notably, the rate of H^+/Na^+ exchange was independent of the rate of Cl^-/OH^- exchange, meaning that the pH of the saline compartment likely changed over time at electrical open circuit. However, with H_2 redox the electrochemical shunt provides an alternative mechanism to desalination where only a single Na^+ or Cl^- ion is transported across each membrane by drift due to concerted electron transport through the external circuit. In this case, Na^+ and Cl^- are transported, with a small amount of SO_4^{2-} and Na^+ co-ion transport, meaning that the pH of the saline compartment remained almost unchanged as desired for a desalination application. Therefore, hydrogen allows faster neutralization and desalination to be performed than the passive transport when the electrical circuit is at open circuit (Figure 5.3c vs. Figure 5.3e), which is clear from larger flux rate in the former compared to the latter. In fact, the presence of hydrogen in the anodic half-cell (by bubbling) provides an extra handle to control the net rate of neutralization and the desalination process via the rate at which electric current is produced. Taken together, it can be concluded that the pH changes observed (Figure 5.3d) in the time scale of the measurement (~22 hours) when current is drawn (Figure 5.3a) from the electrochemical neutralization cell is primarily due to the electrochemical neutralization reaction occurring via hydrogen redox reactions in the half cells. Supporting this, the amount of charge passed in Figure 5.3a is close to the observed consumption of H^+ ions in the cathodic half-cell and OH^- ions in anodic half-cell and changes in the number of moles of Na^+ and Cl^- in the middle saline compartment, Figure 5.33 and Calculation 5.2.

Calculation 5.1: Comparison of charge passed vs. moles of OH^- consumed in the anolyte, H^+ consumed in the catholyte, and Na^+ and Cl^- removed from the saline compartment.

Time of discharge = 21.29 hours

Discharge current = 50 mA

Total charge passed = 0.05 A × (21.29 h x 3600 s/h) = 3832.2 Coulombs

Number of moles of charge passed = 3832.2 C / 96484 C/mol = **0.0397 moles**

Change in concentration of H_2SO_4 in cathodic compartment = 0.5 M

Number of moles of H^+ consumed (40 mL catholyte) = (0.5 M × 2/1000) × 40 mL = **0.04 moles**

Change in concentration of NaOH in anodic compartment = 1 M

Number of moles of OH^- consumed (40 mL anolyte) = (1 M x 1/1000) × 40 mL = **0.04 moles**

Change in concentration of Na^+ in the middle compartment = 3.1 M

Number of moles of Na^+ removed (13 mL feed) = (3.1 M x 1/1000) × 13 mL = **0.0403 moles**

Change in concentration of Cl^- in the middle compartment = 2.9 M

Number of moles of Cl^- removed (13 mL feed) = (2.9 M x 1/1000) × 13 mL = **0.0377 moles**

Therefore, the change in number of moles of H^+, OH^-, Na^+ and Cl^- are approximately equal to the charge passed.

One of the important parameters in the desalination process is the amount of energy consumed for salt removal. In order to determine this, we carried out long term polarization of the electrochemical neutralization cell with and without the saline compartment, Figure 5.4a. The shaded portion represents the amount of energy consumed during the desalination process, which corresponds to ~13.6 kJ/mole of NaCl (13 mL of saline feed), Calculation 5.2. A comparison with state of the art desalin-

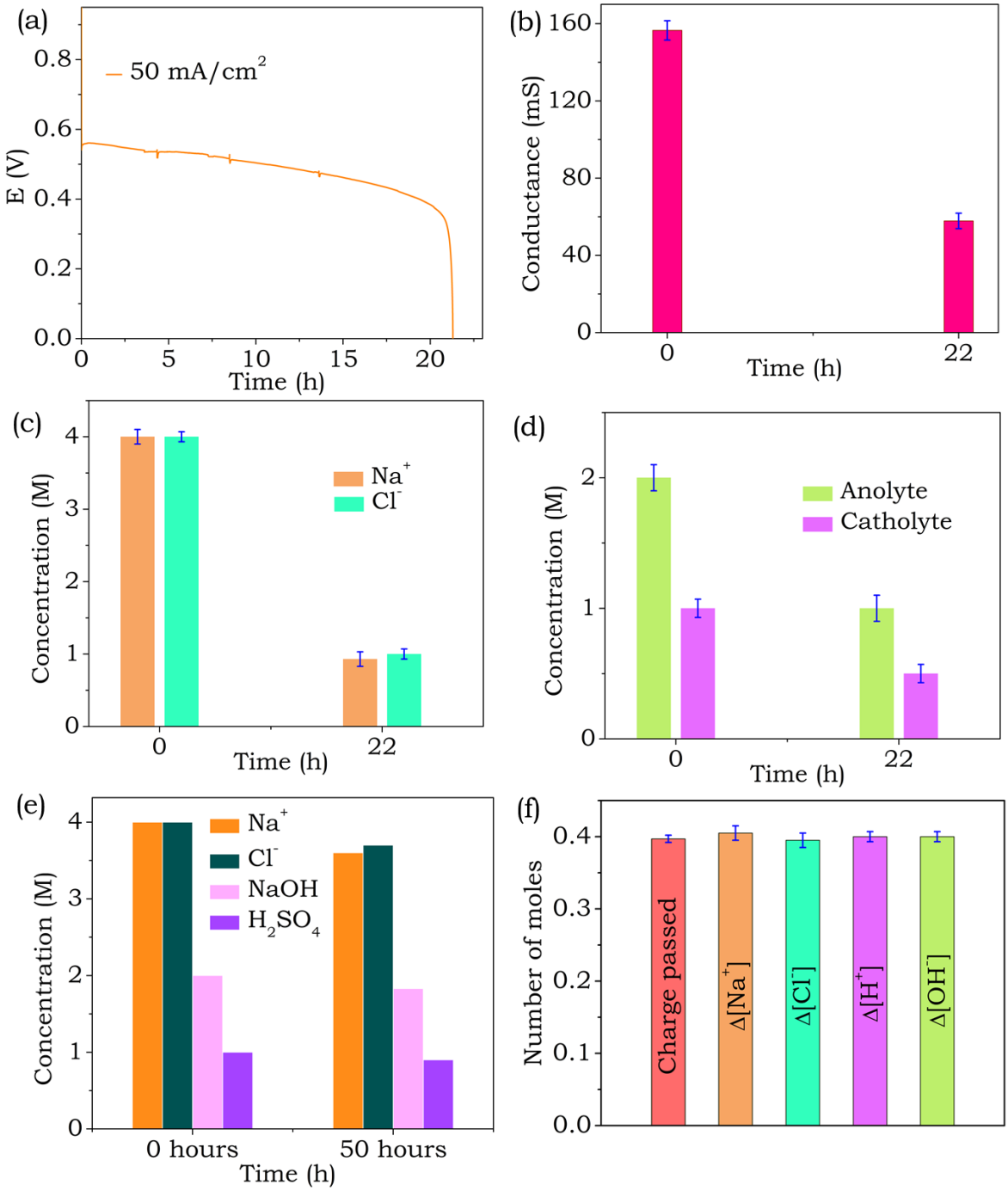

Figure 5.3. (a) Galvanostatic discharge of the electrochemical neutralization cell for water desalination at a current density of 50 mA/cm^2, (b) conductance measurements of the middle saline compartment before and after long term polarization, (c) concentration of Na^+ ions measured by Microwave Plasma Atomic Emission Spectroscopy (MP-AES), and concentration of Cl^- ions measured by Mohr's titration method before and after long term discharge, (d) concentration of anolyte

(NaOH) and catholyte (H_2SO_4) before and after long term polarization, (e) concentration of Na^+ ions measured by Microwave Plasma Atomic Emission Spectroscopy (MP-AES), concentration of Cl^- ions measured by Mohr's titration method, concentration of anolyte (NaOH) and the concentration of catholyte (H_2SO_4) before and after keeping the electrical circuit at open circuit for 50 hours and (f) amount of charge passed (from Figure 5.3a) vs. consumption of H^+ ions in the cathodic half-cell and OH^- ions in anodic half-cell and change in the number of moles of Na^+ and Cl^- ions in the middle saline compartment.

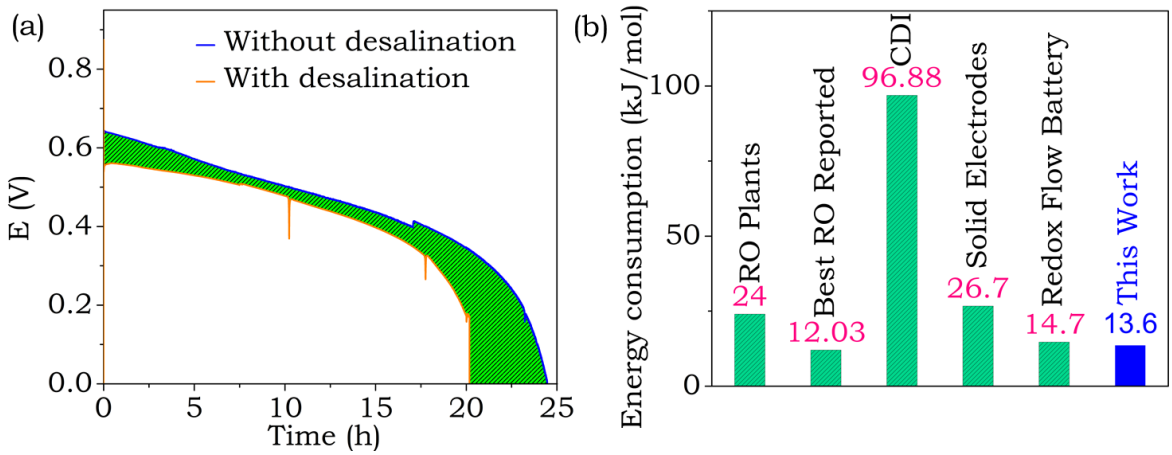

Figure 5.4. (a) Galvanostatic discharge of the electrochemical neutralization cell at a current density of 50 mA/cm^2 with (orange trace) and without (blue trace) middle saline compartment. (b) Comparison of the energy efficiency of desalination in the electrochemical neutralization cell with reverse osmosis, metal ion batteries and capacitive deionization. [45, 46, 47, 48, 34]

-ation processes such as reverse osmosis (RO), desalination using metal ion batteries and capacitive desalination (CDI) suggest that the energy efficiency of desalination in the electrochemical neutralization cell is comparable to the best RO process reported in the literature, Figure 5.4b.[45-48] It should be noted that since currents are carried by the ions and electrolytic conductance (reciprocal of electrolyte resistance) is directly proportional to the quantity of electricity carried by them, the middle

saline compartment is analogous to a resistor connecting the two half cells. Thus, the *iR* drop of the device increases with the progress of desalination due to the obvious decrease in the salt concentration in the middle saline compartment, Figure 5.4a. That is why the energy consumption is more towards the end of the discharge, Figure 5.4a, albeit the sharp drop in potential at the end of the experiment that included the middle saline compartment is likely due at least in part to local concentration gradients from lack of mixing.

Calculation 5.2: Energy calculations for the electrochemical neutralization device.

The amount of energy consumed was calculated from the galvanostatic discharge curve, Figure 5.4a.

Amount of electrical energy produced = I × E × t = area under E vs t curve × discharge current

Discharge current used = 0.05 A

Electricity produced without desalination = area under blue trace × 0.05 A

Electricity produced with desalination = area under red trace × 0.05 A

Area under blue trace = 12.09 Vh

Area under red trace = 9.07 Vh

Conversion of Wh to Joules (1 Wh = 3600 J)

Amount of salt removed from the middle compartment (see Calculation S2) ≈ 0.04 moles

Therefore, Energy output to perform useful work at 50 mA/cm^2 = 0.6045 VAh = 0.6045 Wh = 2176.2 Joules = **54.41 kJ/mol**

Therefore, Excess energy output to perform useful work (in addition to desalination) at 50 mA/cm^2 = 0.4535 VAh = 0.4535 Wh = 1632.6 Joules = **40.82 kJ/mol**

Energy invested for desalination at 50 mA/cm^2 = 2176.2 Joules – 1632.6 Joules = 543.6 Joules = **13.59 kJ/mol**

Calculation 5.3: Energy conversion efficiency calculations for the electrochemical neutralization device.

To remove one mole of salt, one mole of H^+ and one mole of OH^- will be consumed.

Assuming standard-state conditions, total free energy available = 79.88 kJ/mol

Assuming non-standard-state conditions and including the driving force for transfer of salt species, each over time, the total free energy available is calculated as follows,

Time = 21.29 h x 3600 s/h = 76644 s

Total free energy available = integral with respect to time from 0 to 76644 s for -(-79878 J/mol + RT ln [(t/76644)^2 / ((2 – (t/76644))^2 x (4 – ((40/13) x (t/76644)))^2)]) / 96500 C/mol x 0.05 A

= -6.96243×10^9 J-s/mol / 96500 C/mol x 0.05 A

= 3607.5 Joules = **90.19 kJ/mol**

Therefore, parasitic losses at 50 mA/cm^2 = 90.19 kJ/mol – 54.41 kJ/mol = **35.78 kJ/mol**

Overall energy conversion efficiency at 50 mA/cm^2 = 54.41 kJ/mol / 90.19 kJ/mol = **60.3%**

To understand individual *iR* drop contributions in each compartment, we performed electrochemical impedance spectroscopy (EIS). EIS measurements were carried out with Pt electrodes between the anode and middle saline compartment, cathode and middle saline compartment and finally between the anode and cathode, Figure 5.5a and Figure 5.5b. Solution resistances were determined from the Nyquist plots and *iR* drops

were calculated by multiplying the area specific solution resistance by the current density used (50 mA/cm^2). EIS measurements were also carried out after the complete discharge of the electrochemical neutralization device, Figure 5.5a and Figure 5.5b. As can be seen the solution resistances show clear increase after the discharge, Figure 5.5c, due to decrease in the concentration of ions in the middle saline compartment which are in line with our conductance data (Figure 5.3b) and ICP-MS (Figure 5.3c) measurements in the middle saline compartment. In either case, *iR* drop between the anode and the cathode is the sum of the *iR* drops between anode and middle saline compartment and cathode and middle saline compartment, Figure 5.5c and Figure 5.5d. It is worth noting that the half-cell resistances (anolyte and catholyte) are expected not to change noticeably in the electrochemical neutralization device with and without the middle saline compartment, however, the middle saline compartment resistance will increase with the progress of desalination. Hence, the energy consumed for desalination ($\Delta V \times i \times t$, where ΔV is the *iR* drop across the middle saline compartment, i is the current density and t is the time of discharge) = i^2Rt can be calculated from the product of current density and area under the shaded portion in Figure 5.4a where saline compartment resistance (R) is the variable factor and the half-cell resistances are inherently considered when energy efficiency is estimated from the difference between the discharge curves as shown in Figure 5.4a. Therefore, the shaded region in Figure 5.4a primarily reflects the energy efficiency of the desalination process. The extent of desalination demonstrated here is on par with state of art desalination processes, yet is achieved without irreversibly consuming the free energy of expensive metal ions as in redox flow batteries and metal ion batteries and instead only interconverts the neutralization energy into electrical driving force without a net redox reaction and without any water contamination by the discharge products. This electrochemical neutralization device does have parasitic losses that include *iR* drops in the anodic and cathodic half-cells along with kinetic losses for the hydrogen oxidation/evolution reactions

that in total amount to ~35.78 kJ/mol, Calculation 5.3. Therefore, the overall energy efficiency of the electrochemical neutralization device during desalination at the current density used for the discharge (50 mA/cm^2) is ~60 %, Calculation 5.3. Notably, this calculation includes the time-dependent driving force for both acid–base neutralization and transfer of salt species (Calculation 5.3). While the driving force for salt transfer was small compared to that for acid–base neutralization, it was also thermodynamically favoured for Na^+ and Cl^- to migrate out of the middle saline compartment, because H_2SO_4 without Na^+ and NaOH without Cl^- were used as the fuel. Taking into consideration all available free energies, the average Gibbs free energy and average potential available to perform useful work were 90.19 kJ/mol and ~0.93 V, respectively, consistent with the open circuit voltage observed in Figure 5.2a.

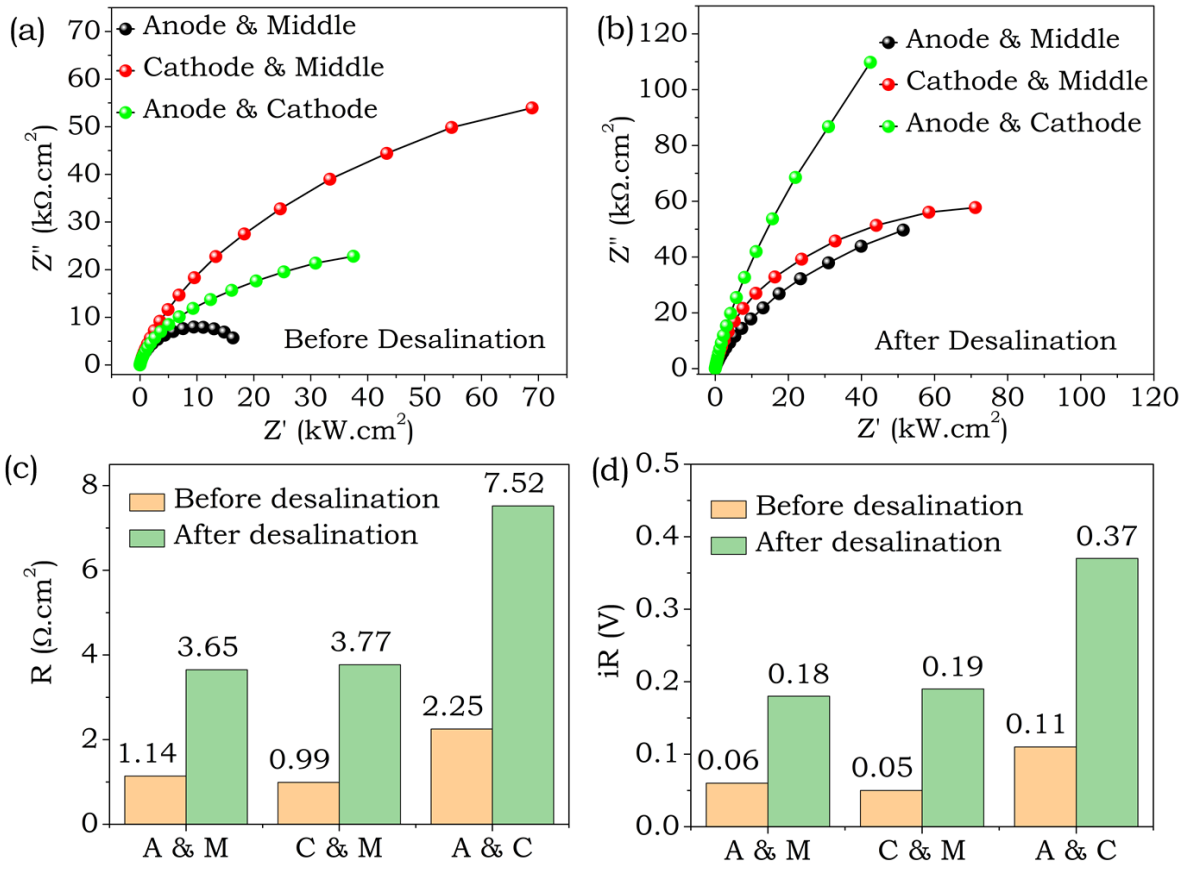

Figure 5.5. Nyquist plots for the electrochemical neutralization cell (a) before desalination and (b) after desalination. (c) Comparison of solution resistance before and after desalination and (d) comparison of *iR* drops

before and after desalination (A, M and C represent anodic, middle and cathodic compartments, respectively). In panel d, *iR* drop is calculated by multiplying the area specific resistance with the current density of 50 mA/cm^2.

For comparative purposes, we also carried out desalination using a H_2-O_2 fuel cell operating under neutral conditions equipped with the same architectural configurations as in the electrochemical neutralization cell. All the three compartments were filled with same salt solutions (4 M NaCl) without any pH gradients. The cell was kept short circuited for nearly 30 hours and the extent of desalination was measured by monitoring the concentration of salt in the saline compartment before and after the experiment. The MP-AES/titration data suggest that even after 30 hours only ~0.5 M salt was removed from the middle saline compartment, Figure 5.6a and Figure 5.6b, which is nearly 6 times less than that achieved with the electrochemical neutralization device (Figure 5.3c) at 50 mA/cm^2. Since the rate of desalination is directly related to the quantity of charge passed, the net rate of desalination is expected to be ~4.5 times higher in the case of the electrochemical neutralization cell compared to the neutral H_2-O_2 fuel cell even under short circuit conditions because the short circuit current for the former is ~4.5 times higher than that of the latter (Figure 5.3a and Figure 5.6). We further note that based on power performance metrics of the electrochemical neutralization cell vs. the neutral H_2-O_2 fuel cell (Figure 5.3a and Figure 5.6), even if desalination rates are the same (when identical current densities are drawn) the power metrics will be substantially higher for the former compared to the latter. This clearly shows the advantages of performing desalination using an electrochemical neutralization cell over a design based on a H_2-O_2 fuel cell.

The low performance of the H_2-O_2 based fuel cell design may be because of the neutral-pH operating conditions which impart sluggish kinetics for the hydrogen oxidation reaction and the oxygen reduction reactions.[49-52] Further, the respective formation of hydronium and hyd-

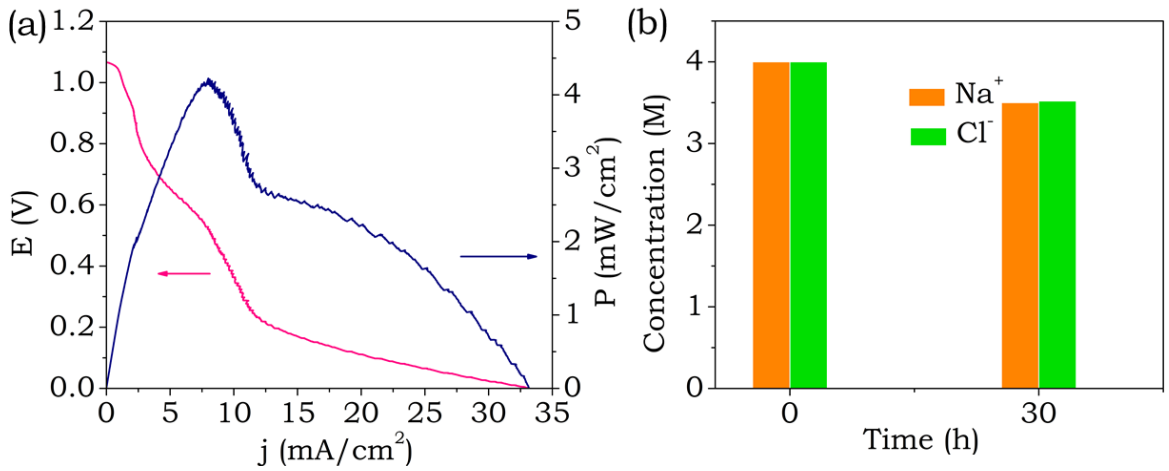

Figure 5.6. (a) Polarization curve for a H_2-O_2 fuel cell for water desalination with hydrogen fuel as the electron donor and oxygen as the electron acceptor and (b) concentration of Na^+ ions measured by Microwave Plasma Atomic Emission Spectroscopy (MP-AES) and concentration of Cl^- ions measured by Mohr's titration method before and after keeping the electrical circuit at short circuit for 30 hours. All the three compartments contained an aqueous 4 M NaCl solution. H_2 and O_2 were supplied to anodic and cathodic half-cells respectively at 100 mL/min flow rate. Pt/C was used as electrocatalysts for the hydrogen oxidation reaction and the oxygen reduction reaction in the anodic and the cathodic half-cells respectively.

-roxyl ions in the anodic and cathodic compartments will eventually contribute to the shifting of the half-cell potentials. The half-cell potentials should shift by 59 mV/pH with the anodic potential drifting towards the positive direction and the cathodic potential drifting towards the negative direction. This will result in further decrease of cell potential equivalent to ~120 mV/pH change. Moreover, in the overall process hydrogen fuel is consumed. Taken together, the electrochemical neutralization cell represents a novel chemistry to perform desalination during electric power production. As demonstrated, the electrochemical neutralization cell generates electric power by the inter-conversion of the neutralization energy. A part of this neutralization energy is utilized for electricity production while the remaining part is invested to perform desalination by

driving the movement of ions from the middle saline compartment. This neutralization chemistry harvests nearly 30% ($T\Delta S^0$ = 24.05 kJ/mol) of the total free energy (ΔG^0 = -79.88 kJ/mol) from the surroundings and desalination is achieved by performing reversible redox reactions involving only gases, water, H^+ and OH^- such that the products and reactants of the redox reactions do not poison the desalinated water. Desalination using the electrochemical neutralization device provides opportunities to neutralize acid and alkaline wastes from industries, which can be achieved by designing stable and durable membranes suiting those specific conditions and will open up new directions in the science of desalination and waste water treatment.

5.4. Conclusions

In this Chapter, we have shown an electrochemical neutralization cell where desalination of saline water can be spontaneously driven during electric power production without a net redox reaction by interconverting neutralization energy as electrical driving force. A comparative energy efficiency evaluation with state-of-the-art desalination processes suggests that the energy efficiency in terms of desalination is ~13.6 kJ/mol of NaCl which is comparable to the best reverse osmosis process reported in the literature. This pathway is unprecedented because desalination is achieved in the electrochemical neutralization cell without irreversibly consuming free energy stored in expensive metals as in redox flow batteries and metal ion batteries but by just interconverting the energy of neutralization as an electrical driving force. The device uses acid and alkali as fuels for desalination by performing reversible redox reactions involving only gases, water, H^+ and OH^- such that the products and reactants of the redox reactions do not poison the desalinated water as in the state-of-the-art electrodialysis process. The electrochemical neutralization cell offers a plethora of opportunities in energy conversion/storage like electro organic synthesis, fuel reforming, fuel

separation, water purification etc., during electric power production which are ongoing in our laboratory.

5.5. References

[1] Ghaffour, N., Missimer, T.M., and Amy, G.L. Technical review and evaluation of the economics of water desalination: Current and future challenges for better water supply sustainability. *Desalination* **2013,** *309*, 197–207.

[2] Shannon, M.A., Bohn, P.W., Elimelech, M., Georgiadis, J.G., Marĩas, B.J., and Mayes, A.M. Science and technology for water purification in the coming decades. *Nature* **2008,** *452*, 301–310.

[3] Elimelech, M., and Phillip, W.A. The future of seawater desalination: Energy, technology, and the environment. *Science* **2011,** (80) *333*, 712–717.

[4] Shannon, M.A., Bohn, P.W., Elimelech, M., Georgiadis, J.G., Marĩas, B.J., and Mayes, A.M. Science and technology for water purification in the coming decades. *Nature* **2008,** *452*, 301–310.

[5] Lee, J., Srimuk, P., Zwingelstein, R., Zornitta, R.L., Choi, J., Kim, C., and Presser, V. Sodium ion removal by hydrated vanadyl phosphate for electrochemical water desalination. *J. Mater. Chem. A* **2019**, *7*, 4175–4184.

[6] Chen, W., Chen, S., Liang, T., Zhang, Q., Fan, Z., Yin, H., Huang, K.W., Zhang, X., Lai, Z., and Sheng, P. High-flux water desalination with interfacial salt sieving effect in nanoporous carbon composite membranes. *Nat. Nanotechnol.* **2018,** *13*, 345–350.

[7] Suss, M.E., and Presser, V. Water Desalination with Energy Storage Electrode Materials. *Joule* **2018,** *2*, 10–15.

[8] Subramani, A., and Jacangelo, J.G. Emerging desalination technologies for water treatment: A critical review. *Water Res.* **2015**,*75*, 164–187.

[9] Ghaffour, N., Missimer, T.M., and Amy, G.L. Technical review and evaluation of the economics of water desalination: Current and future

challenges for better water supply sustainability. *Desalination* **2013,** *309*, 197–207.

[10] Lee, K.P., Arnot, T.C., and Mattia, D. A review of reverse osmosis membrane materials for desalination-Development to date and future potential. *J. Memb. Sci.* ***2011,*** *370*, 1–22.

[11] Mito, M.T., Ma, X., Albuflasa, H., and Davies, P.A. Reverse osmosis (RO) membrane desalination driven by wind and solar photovoltaic (PV) energy: State of the art and challenges for large-scale implementation. *Renew. Sustain. Energy Rev.* **2019,***112*, 669–685.

[12] Henthorne, L., and Boysen, B. State-of-the-art of reverse osmosis desalination pretreatment. *Desalination* **2015,** *356*, 129–139. Environ. Sci. Technol. Lett. *2*, 367–372.

[13] Arulrajan, A.C., Ramasamy, D.L., Sillanpää, M., van der Wal, A., Biesheuvel, P.M., Porada, S., and Dykstra, J.E. Exceptional Water Desalination Performance with Anion-Selective Electrodes. Adv. Mater. **2019,** *31*, 1–5.

[14] Kim, S.J., Ko, S.H., Kang, K.H., and Han, J. Direct seawater desalination by ion concentration polarization. *Nat. Nanotechnol.* **2010,** *5*, 297–301.

[15] Nam, D.H., Lumley, M.A., and Choi, K.S. A Desalination Battery Combining Cu 3 [Fe(CN) 6] 2 as a Na-Storage Electrode and Bi as a Cl-Storage Electrode Enabling Membrane-Free Desalination. *Chem. Mater.* **2019,** *31*, 1460–1468.

[16] Schlumpberger, S., Lu, N.B., Suss, M.E., and Bazant, M.Z. (2015). Scalable and Continuous Water Deionization by Shock Electrodialysis. *Environ. Sci. Technol. Lett.* **2015,** *2*, 367–372.

[17] Strathmann, H. Electrodialysis, a mature technology with a multitude of new applications. *Desalination,* **2010,** *264*, 268–288.

[18] Vermaas, D.A., Veerman, J., Yip, N.Y., Elimelech, M., Saakes, M., and Nijmeijer, K. High efficiency in energy generation from salinity gradients with reverse electrodialysis. *ACS Sustain. Chem. Eng.* **2013,***1*, 1295–1302.

[19] Moreno, J., Grasman, S., Van Engelen, R., and Nijmeijer, K. Upscaling Reverse Electrodialysis. *Environ. Sci. Technol.* **2018,** *52*, 10856–10863.

[20] Kim, D., Amy, G.L., and Karanfil, T. Disinfection by-product formation during seawater desalination: A review. *Water Res.* **2015,** *81*, 343–355.

[21] Beh, E.S., Benedict, M.A., Desai, D., and Rivest, J.B. A redox-shuttled electrochemical method for energy-efficient separation of salt from water. *ACS Sustain. Chem. Eng.* **2019,** *7*, 13411–13417.

[22] Kim, T., Gorski, C.A., and Logan, B.E. Low Energy Desalination Using Battery Electrode Deionization. *Environ. Sci. Technol. Lett.* **2017,** *4*, 444–449.

[23] Lee, J., Jo, K., Lee, J., Hong, S.P., Kim, S., and Yoon, J. Rocking-Chair Capacitive Deionization for Continuous Brackish Water Desalination. *ACS Sustain. Chem. Eng.* **2018,** *6*, 10815–10822.

[24] Liang, Q., Chen, F., Wang, S., Ru, Q., He, Q., Hou, X., Su, C. yuan, and Shi, Y. An organic flow desalination battery. *Energy Storage Mater.* **2019,** *20*, 203–207.

[25] Mourad, E.; Coustan, L.; Lannelongue, P.; Zigah, D.; Mehdi, A.; Vioux, A.; Freunberger, S. A.; Favier, F.; Fontaine, O. Biredox Ionic Liquids with Solid-like Redox Density in the Liquid State for High-Energy Supercapacitors. *Nat. Mater.* **2016**, *16*, 446-453.

[26] Choi, N.-S.; Chen, Z.; Freunberger, S. A.; Ji, X.; Sun, Y.-K.; Amine, K.; Yushin, G.; Nazar, L. F.; Cho, J.; Bruce, P. G. Challenges Facing Lithium Batteries and Electrical Double-Layer Capacitors. *Angew. Chem. Int. Ed.* **2012,** *51* (40), 9994–10024.

[27] Maiyalagan, T., Alaje, T.O., and Scott, K. Highly stable Pt-Ru nanoparticles supported on three-dimensional cubic ordered mesoporous carbon (Pt-Ru/CMK-8) as promising electrocatalysts for methanol oxidation. *J. Phys. Chem. C* **2012,** *116*, 2630–2638.

[28] Chinnam, P. R.; Fall, B.; Dikin, D. A.; Jalil, A.; Hamilton, C. R.; Wunder, S. L.; Zdilla, M. J. A Self-Binding, Melt-Castable, Crystalline

Organic Electrolyte for Sodium Ion Conduction. *Angew. Chem. Int. Ed.* **2016,** *128* (49), 15480–15483.

[29] Wang, Z., Tam, L.Y.S., and Lu, Y.C. Flexible Solid Flow Electrodes for High-Energy Scalable Energy Storage. *Joule* **2019,** *3*, 1677–1688.

[30] Nugent, J. M.; Santhanam, K. S. V; Rubio, A.; Ajayan, P. M. Fast Electron Transfer Kinetics on Multiwalled Carbon Nanotube Microbundle Electrodes. *Nano Lett.* **2001,** *1* (2), 87–91.

[31] Wallace, A.G., and Symes, M.D. Decoupling Strategies in Electrochemical Water Splitting and Beyond. *Joule* **2018,** *2*, 1390–1395.

[32] Zhao, F., Wang, P., Ruff, A., Hartmann, V., Zacarias, S., Pereira, I.A.C., Nowaczyk, M.M., Rögner, M., Conzuelo, F., and Schuhmann, W. A photosystem i monolayer with anisotropic electron flow enables Z-scheme like photosynthetic water splitting. *Energy Environ. Sci.* **2019,** *12*, 3133–3143.

[33] Mukherjee, D., Muthu Austeria, P., and Sampath, S. Few-Layer Iron Selenophosphate, FePSe 3 : Efficient Electrocatalyst toward Water Splitting and Oxygen Reduction Reactions. *ACS Appl. Energy Mater.* **2018,** *1*, 220–231.

[34] Desai, D., Beh, E.S., Sahu, S., Vedharathinam, V., Van Overmeere, Q., De Lannoy, C.F., Jose, A.P., Völkel, A.R., and Rivest, J.B. Electrochemical Desalination of Seawater and Hypersaline Brines with Coupled Electricity Storage. *ACS Energy Lett.* **2018,** *3*, 375–379.

[35] Hou, X., Liang, Q., Hu, X., Zhou, Y., Ru, Q., Chen, F., and Hu, S. Coupling desalination and energy storage with redox flow electrodes. *Nanoscale* **2018,** *10*, 1s2308–12314.

[36] La Mantia, F., Pasta, M., Deshazer, H.D., Logan, B.E., and Cui, Y. Batteries for efficient energy extraction from a water salinity difference. *Nano Lett.* **2011,** *11*, 1810–1813.

[37] Pasta, M., Wessells, C.D., Cui, Y., and La Mantia, F. A desalination battery. *Nano Lett.* **2012,** *12*, 839–843.

[38] Madani, S.S., Schaltz, E., and Kær, S.K. An experimental analysis of entropic coefficient of a lithium titanate oxide battery. *Energies* **2019**, *12*(14), 2685

[39] Winter, M., and Brodd, R.J. What are batteries, fuel cells, and supercapacitors? *Chem. Rev.* **2004,** 104, 4245–4269.

[40] Schmidt-Rohr, K. How Batteries Store and Release Energy: Explaining Basic Electrochemistry. *J. Chem. Educ.* **2018,** *95*, 1801–1810.

[41] Claus Daniel and Jurgen O. Besenhard. Fundamentals and General Aspects of Electrochemical Energy Storage:Thermodynamics and Mechanistics. Handbook of Battery Materials, 2nd edition *WileyVCH , Weinheim, Germany,* **2011,** Ch. 1, p1–26.

[42] Winterbone, D.E., Turan, A., Winterbone, D.E., and Turan, A. Advanced Thermodynamics for Engineers, *Elsevier Ltd.* **2015,** Chapter 21, *1*, p497–526.

[43] B. Sørensen, Hydrogen and Fuel Cells Emerging Technologies and Applications, *Elsevier Academic Press, New York,* **2005**, ch. 3 p. 104

[44] Debe, M. K. Handbook of Fuel Cells—Fundamentals, Technology and Applications Vol. 3 (eds Vielstich, W., Gasteiger, H. A. & Lamm, A.) *Wiley, Chichester, UK.* **2003,** Ch. 4.

[45] Chen, F., Huang, Y., Guo, L., Sun, L., Wang, Y., and Yang, H.Y. Dual-ions electrochemical deionization: A desalination generator. *Energy Environ. Sci.* **2017,***10*, 2081–2089.

[46] Choi, S., Chang, B., Kang, J.H., Diallo, M.S., and Choi, J.W. Energy-efficient hybrid FCDI-NF desalination process with tunable salt rejection and high-water recovery. *J. Memb. Sci.* **2017,** *541*, 580–586.

[47] Huang, Y., Chen, F., Guo, L., Zhang, J., Chen, T., and Yang, H.Y. (2019). Low energy consumption dual-ion electrochemical deionization system using $NaTi_2(PO_4)_3$-AgNPs electrodes. *Desalination* **2019,** *451*, 241–247.

[48] Zhao, R., Porada, S., Biesheuvel, P.M., and Van der Wal, A. Energy consumption in membrane capacitive deionization for different water

recoveries and flow rates, and comparison with reverse osmosis. *Desalination* **2013,** *330*, 35–41.

[49] Zhong, K., Lu, X., Dai, Y., Yang, S., Li, J., Zhang, H., Wang, Y., Zuo, J., Tang, J., and Su, M. UiO66-NH_2 as self-sacrificing template for Fe/N-doped hierarchically porous carbon with high electrochemical performance for oxygen reduction in microbial fuel cells. *Electrochim. Acta* **2019,** 323, 134777.

[50] Yu, E.H., Cheng, S., Logan, B.E., and Scott, K. Electrochemical reduction of oxygen with iron phthalocyanine in neutral media. *J. Appl. Electrochem.* **2009,** 39, 705–711.

[51] Wang, Y., Zhong, K., Huang, Z., Chen, L., Dai, Y., Zhang, H., Su, M., Yan, J., Yang, S., Li, M., et al. Novel g-C_3N_4 assisted metal organic frameworks derived high efficiency oxygen reduction catalyst in microbial fuel cells. *J. Power Sources* **2020,** 450, 227681.

[52] Santoro, C., Serov, A., Stariha, L., Kodali, M., Gordon, J., Babanova, S., Bretschger, O., Artyushkova, K., and Atanassov, P. Iron based catalysts from novel low-cost organic precursors for enhanced oxygen reduction reaction in neutral media microbial fuel cells. *Energy Environ. Sci.* **2016,** 9, 2346–2353.

Chapter 6

Summary and Outlook

Summary and future outlook of the thesis entitled "Design and Development of Unconventional pH Differential Fuel Cells"

The work in this thesis reports the design and development of unconventional fuel cells by interfacial modification of the cathodic interface by pH dependent and pH independent redox couples. By employing a pH independent outer sphere redox couple at the cathodic interface, issues like alcohol crossover, carbon corrosion and depolarization losses were addressed and the performance metrics were improved by nearly 8 times compared to the state of art Pt based DAFC-O_2. By modifying the cathodic interface with a pH dependent redox couple, additional functionality (reforming) was introduced in a DAFC's reaction pathway. This led to the design of an alcohol reforming fuel cell (ARFC) which can reform alcohols to pure hydrogen at room temperature and pressure during electricity production. As alcohol reformation is an energy intensive process, ARFC basically utilizes energy of neutralization as the driving force to make the overall process spontaneous. The idea of harvesting the neutralization energy directly into electrical energy led to the designing of an electrochemical neutralization cell (ENC). The major challenge to make this direct inter-conversion viable was the non-redox nature of the neutralization reaction which was overcome by utilizing a pH dependent H^+/H_2 redox couple, Scheme 1. ENC demonstrated a positive temperature coefficient of electromotive force and as such nearly 30 % of the total electricity output was harvested from the surroundings which makes it different from the state of art fuel cells where nearly 24 % of energy is lost to surroundings.

ENC offers plethora of opportunities in the domain of energy storage and conversion devices. The Nernst equation for ENC is $\boldsymbol{E_{cell} = E^{\emptyset}_{[OX]1/[Red]1} - E^{\emptyset}_{[OX]2/[Red]2} + 0.0591 \times (pH_a - pH_c)}$ which implies that by exploiting proper redox couples ($[Ox]_1/[Red]_1$ & $[Ox]_2/[Red]_2$) and pH differences in the half-

cells ($pH_a - pH_c$), it is possible to design various energy storage and conversion devices with tremendous possibilities. Few examples include, high voltage aqueous fuel cells (~2 V), low voltage electrolyzers (<0.5 V), high energy density supercapacitors, electro-organic synthesis coupled with fuel production, fuel separation etc. It was demonstrated that ENC in a three-compartment design can cause spontaneous water desalination during electricity production by utilization energy of neutralization as driving force. Although the electrochemical neutralization has many promising applications, it is still in the early stages of development. As discussed, the device works on the principle of asymmetric electrolyte configuration and as such the low-cost membranes which are stable in highly acidic and alkaline PHs have to be designed for sustainable operation. Different redox couples have to be identified to explore new possibilities and stable and durable electrocatalysts have to be developed to drive the reaction efficiently in respective pH solutions.

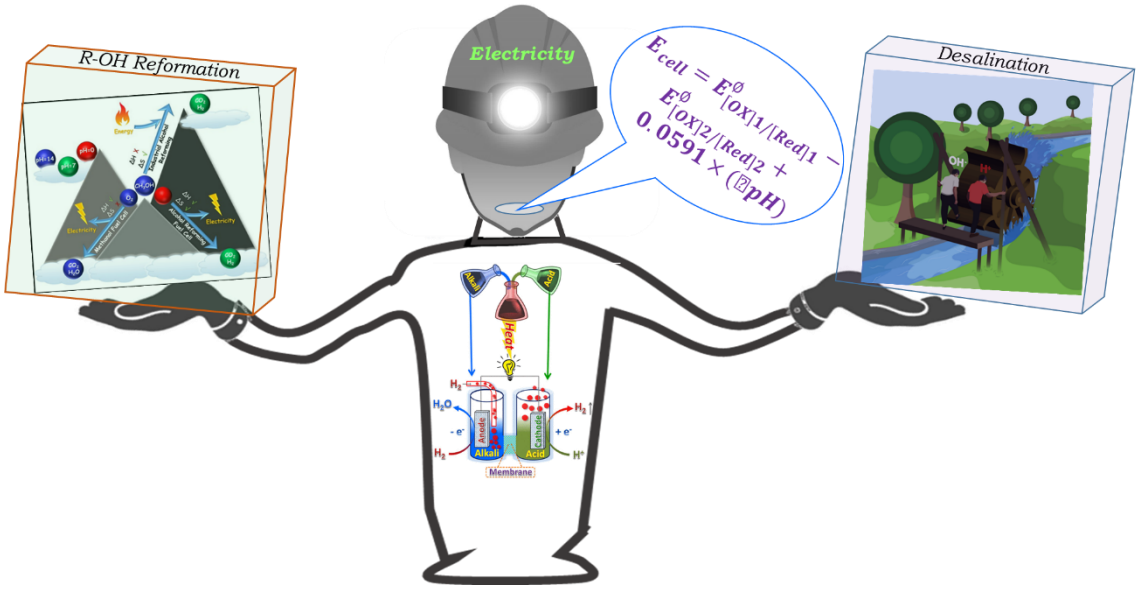

Scheme 1. Application of electrochemical neutralization for the development of unconventional fuel cells.

List of Publications

List of Publications

[1] **Bhat, Z. M.;** Thimmappa, R.; Dargily, N. C.; Raafik, A.; Kottaichamy, A. R.; Devendrachari, M. C.; Itagi, M.; Makri Nimbegondi Kotresh, H.; Freunberger Stefan A.; Thotiyl, M. O. Ambient Condition Alcohol Reforming to Hydrogen with Electricity Output. *ACS Sustain. Chem. Eng.* 2021, 9, *8, 3104–3111.*

[2] **Bhat, Z. M.;** Pandit, D.; Ardo, S.; Thimmappa, R.; Kottaichamy, A. R.; Christudas Dargily, N.; Devendrachari, M. C.; Ottakam Thotiyl, M. An Electrochemical Neutralization Cell for Spontaneous Water Desalination. *Joule* 2020, *4 (8), 1730–1742.*

[3] **Manzoor Bhat, Z.**; Thimmappa, R.; Devendrachari, M. C.; Kottaichamy, A. R.; Shafi, S. P.; Varhade, S.; Gautam, M.; Thotiyl, M. O. Fuel Exhaling Fuel Cell. *J. Phys. Chem. Lett. 2018, 388–392.* **(Nature India highlight)**

[4] **Manzoor Bhat, Z.;** Thimmappa, R.; Devendrachari, M. C.; Shafi, S. P.; Aralekallu, S.; Kottaichamy, A. R.; Gautam, M.; Thotiyl, M. O. A direct alcohol fuel cell driven by an outer sphere positive electrode, *J. Phys. Chem. Lett. 2017, 8, 3523-3529.* ***(JPCL Spotlights Article)***

[5] Gautam, M.; **Bhat, Z. M.;** Raafik, A.; Le Vot, S.; Devendrachari, M. C.; Kottaichamy, A. R.; Dargily, N. C.; Thimmappa, R.; Fontaine, O.; Thotiyl, M. O. Coulombic Force Gated Molecular Transport in Redox Flow Batteries. *J. Phys. Chem. Lett.* **2021**, 1374–1383. **(Equal first author)**

[6] Itagi, M.; **Bhat, Z. M.;** Thimmappa, R.; Pandit, D.; Devendrachari, M. C.; Sannegowda, L. K.; Thotiyl, M. O. An Electrochemical Valorization Fuel Cell for Simultaneous Electroorganic and Hydrogen Fuel Syntheses. *J. Phys. Chem. C* 2020, *124* (21), 11284–11292. **(Equal first author)**

[7] Sudhakara, S. M.; **Bhat, Z. M.;** Devendrachari, M. C.; Kottaichamy, A. R.; Itagi, M.; Thimmappa, R.; Khan, F.; Kotresh, H. M. N.; Thotiyl, M. O. A Zinc-Quinone Battery for Paired Hydrogen Peroxide

Electrosynthesis. *J. Colloid Interface Sci.* 2020, *559*, 324–330. **(Equal first author)**

[8] Marichelvam, T.; **Manzoor Bhat, Z.;** Thimmappa, R.; Devendrachari, M. C.; Kottaichamy, A. R.; Naranammalpuram Sundaram, V. N.; Thotiyl, M. O. Hydrogen Fuel Exhaling Zn-Ferricyanide Redox Flow Battery. *ACS Sustain. Chem. Eng.* 2019, *7* (19), 16241–16246. **(Equal first author)**

[9] Swapnil V., **Manzoor Bhat, Z.;** Devendrachari, M. C.; Kottaichamy, A. R.; Gautam M.; Shafi, S. P.; Kalegowda Y.; Thotiyl, M. O. A Hybrid Hydrazine Redox Flow Battery with a Reversible Electron Acceptor, *Phys. Chem. Chem. Phys., 2018, 20, 21724.* **(Equal first author)**

[10] Swapnil V., **Manzoor Bhat, Z.;** Devendrachari, M. C.; Kottaichamy, A. R.; Khiare, S.; Shafi, S. P.; Thotiyl, M. O. An Inherent Heat Driven Fuel Exhaling Hydrazine Fuel Cell, *Chem. Phys. Lett., 2018, 706, 553–557.* **(Equal first author)**

[11] Kottaichamy, A. R.; Begum, S.; Nazrulla, M. A.; Dargily, N. C.; Devendrachari, M. C.; **Manzoor Bhat, Z.;** Thimmappa, R.; Makri Nimbegondi Kotresh, H.; Vinod, C. P.; Thotiyl, M. O. Unprecedented Isomerism-Activity Relation in Molecular Electrocatalysis. *J. Phys. Chem. Lett.* 2020, *11* (1), 263–271.

[12] Kottaichamy, A. R.; Begum, S.; Devendrachari, M. C.; **Bhat, Z. M.;** Thimmappa, R.; Nimbegondi Kotresh, H. M.; Vinod, C. P.; Thotiyl, M. O. Geometrical Isomerism Directed Electrochemical Sensing. *Anal. Chem.* 2020, *92* (6), 4541–4547.

[13] Neethu C. D., Thimmappa, R.; **Manzoor Bhat, Z.;** Devendrachari, M. C.; Kottaichamy, A. R.; Gautam M.; Shafi, S. P.; Thotiyl, M. O. A Rechargeable Hydrogen Battery, *J. Phys. Chem. Lett. 2018, 9 (10), 2492–2497. [JPCL Spotlights Article].*

[14] Battu S.; Itagi M.; **Manzoor Bhat, Z.;** Khiare, S.; Kottaichamy, A. R.; Lokesh K. S.; Thimmappa, R.; Thotiyl, M. O. Metal Coordination Polymer Framework Governed by Heat of Hydration for Noninvasive

Differentiation of Alkali Metal Series, *Anal. Chem. 2018, 90 (21), 12917–12922.*

[15] Itagi M.; Battu S.; Devendrachari, M. C.; **Manzoor Bhat, Z.;** Kottaichamy, A. R.; Pandit D.; Gautam M.; Thimmappa, R.; Lokesh K. S.; Thotiyl, M. O. A Zinc Battery Driven by an Electro-organic Reactor Cathode, *ACS Sustainable Chem. Eng., 2018. 6 (11), 15007–15014.*

[16] Sur S.; Kottaichamy, A. R.; **Manzoor Bhat, Z.;** Devendrachari, M. C.; Thimmappa, R.; Thotiyl, M. O. A pH dependent high voltage aqueous supercapacitor with dual electrolytes, *Chem. Phys. Lett. 2018, 712, 160–164.*

[17] Devendrachari, M. C.; Thimmappa, R.; **Manzoor Bhat, Z.;** Shafi, S. P.; Harish M. N. K., Kottaichamy, A. R.; Kallam R. V. Reddy and Thotiyl, M. O. A Vitamin C Fuel Cell with a Non-Bonded Cathodic Interface, *Sustainable Energy Fuels 2018, 2, 1813.*

[18] Devendrachari, M. C.; Chidananda B., **Zahid M. Bhat,** Kotresh, H. M.; Kottaichamy, A. R.;Swapnil V., Khiare, S.; Kallam R. V. Reddy and Thotiyl, M. O. An All Solid-State Zinc−Air Battery with a Corrosion-Resistant Air Electrode, *ChemElectroChem 2018, 5, 1–6.*

[19] Khiare, S.; Gaikwad, P.; Devendrachari, M. C.; Kottaichamy, A. R.; **Manzoor Bhat, Z.;** Varhade, S.; Shafi, S. P.; Thimmappa, R.; Thotiyl, M. O. An Electrochemical Wind Velocity Sensor , *Anal. Chem. 2018, 90 (7), 4501–4506.*

[20] Gaikwad, P.; Misal, M.; Khiare, S.; Raafik, A.; Aralekallu, S.; Varhade, S.; **Manzoor Bhat, Z.;** Kottaichamy, A. R.; Devendrachari, M. C.; Gautam, M.; Thotiyl, M. O. A redox-active electrochemical decoder, *Adv. Mat.Technol. 2018, 3, 1700337 (1-6).*

[21] Khaire, S.; Gaikwad, P.; Aralekallu, S.; **Manzoor Bhat, Z.;** Kottaichamy, A. R.; Devendrachari, M. C.; Thimmappa, R.; Shafi, S. P.; Gautam, M.; Thotiyl, M. O. An interface-controlled redox switch for wastewater remediation, *ChemElectroChem. 2018, 5, 362–366.*

[22] Gaikwad, P.; Kadlag, K.; Nambiar, M.; Devendrachari, M. C.; Aralekallu, S.; Kottaichamy, A. R.; **Manzoor Bhat, Z.;** Thimmappa, R.;

Shafi, S. P.; Thotiyl, M. O. Redox active binary logic gate circuit for homeland security, *Anal. Chem. 2017, 89, 7893-7899.*

[23] R.; Aralekallu, S.; Devendrachari, M. C.; Kottaichamy, A. R.; **Manzoor Bhat, Z**.; Shafi, S. P.; Lokesh, K. S.; Thotiyl, M. O. A single chamber direct methanol fuel cell. Thimmappa, *Adv. Mater. Interfaces 2017, 4, 1700321.*

AWARDS

2020 TIFR Platinum Jubilee Award for the best oral presentation at Conference on Advances in Catalysis, Energy, and Environmental Research (CACEE) 2020.

2019 Commendation Prize at New Generation Ideation Contest by HPCL, India.

2018 Young Scholar award by Indian Association for Hydrogen Energy and Advanced Materials.